



---

# SEMICONDUCTOR DISK LASER-BASED FREQUENCY COMBS

---

Thesis presented to the *Faculty of Science* for the degree of  
*Doctor of Science*

**Nayara Jornod**

M. Sc. in Physics

submitted on 13.04.2018 to the jury:

Prof. Thomas Südmeyer	Director
Prof. Majid Ebrahim-Zadeh	Examiner
Dr. Keith G. Wilcox	Examiner
Dr. Stéphane Schilt	Examiner
Dr. Valentin J. Wittwer	Examiner

Neuchâtel, 2018



## IMPRIMATUR POUR THESE DE DOCTORAT

---

La Faculté des sciences de l'Université de Neuchâtel  
autorise l'impression de la présente thèse soutenue par

**Madame Nayara JORNOD**

Titre:

**“Semiconductor Disk Laser-Based  
Frequency Combs”**

**sur le rapport des membres du jury composé comme suit:**

- Prof. Thomas Südmeyer, directeur de thèse, Université de Neuchâtel, Suisse
- Prof. Majid Ebrahim-Zadeh, ICFO-The Institute of Photonic Sciences, Barcelone, Espagne
- Dr Keith G. Wilcox, University of Dundee, Royaume-Uni
- Dr Stéphane Schilt, Université de Neuchâtel, Suisse
- Dr Valentin J. Wittwer, Université de Neuchâtel, Suisse

Neuchâtel, le 25 juin 2018

Le Doyen, Prof. R. Bshary





# Keywords – Mots-clés

## **Keywords**

Semiconductor disk laser (SDL), vertical external-cavity surface-emitting laser (VECSEL), modelocked laser, optical frequency comb, optical amplifier, waveguide, supercontinuum generation, carrier-envelope offset (CEO), self-referencing, laser stabilization, metrology, frequency noise, phase noise, optical parametric oscillator (OPO)

## **Mots-clés**

Laser à disque semi-conducteur (SDL), laser à cavité verticale externe à émission de surface (VECSEL), laser à verrouillage de modes, peigne de fréquences optique, amplificateur optique, guide d'onde, génération de supercontinuum, décalage de phase entre porteuse en enveloppe (CEO), auto-référencement, stabilisation de laser, métrologie, bruit de fréquence, bruit de phase, oscillateur paramétrique optique (OPO)



# Abstract

This thesis studies the first self-referenced frequency combs based on modelocked semiconductor disk lasers (SDLs).

The generation of stabilized frequency combs based on ultrafast lasers has been a significant breakthrough for many applications in various fields of physics, spectroscopy and metrology. Optical frequency combs can serve as a frequency ruler that provides a direct and phase-coherent link between optical and microwave frequencies. Despite the fact that optical frequency combs revolutionized numerous scientific areas, so far, they have not entered large-scale markets. For this, comb laser sources have to be improved, targeting high reliability, while keeping the source compact and cost-efficient.

Ultrafast SDLs, also referred to as vertical external-cavity surface-emitting lasers (VECSELs), are a very promising technology for this purpose as they are based on the semiconductor technology, allowing for low-cost wafer-scale mass-production. They enable very compact laser setups and have large emission wavelengths flexibility inherited from the band-gap engineering. In addition, they do not suffer from Q-switching instabilities and stable fundamental modelocking was demonstrated at repetition rates ranging from 100 MHz to 100 GHz. High repetition rate frequency combs have an increased power per comb line that is beneficial for applications such as astronomy or low-noise microwave generation.

The stabilization of the two degrees of freedom of the modelocked laser, the repetition frequency and the carrier-envelope offset (CEO) frequency is required for most comb applications. However, the detection of the CEO frequency is challenging and no stabilization was achieved before for any ultrafast semiconductor laser. The CEO detection is usually done using a self-referencing scheme that requires a coherent octave-spanning spectrum, which can be generated using highly nonlinear fibers such as photonic crystal fibers (PCFs). In order to maintain the coherence in the spectral broadening process, ultrashort femtosecond pulses (typically <200 fs) with kilowatt peak power are required. However, even though peak powers up to 6.3 kW and pulse durations down to 96 fs have been demonstrated in SDLs, the combination of both has still not been reached. Therefore, the octave-spanning spectrum generation in a PCF directly from the output of the laser could not be demonstrated until now and additional amplification and compression stages are necessary.

In this work, an efficient fiber amplifier has been developed, which led to the first demonstration of the CEO frequency stabilization of an ultrafast SDL. The amplified pulses were temporally compressed and sent to a commercially available PCF for the coherent octave-spanning supercontinuum spectrum generation. A self-referencing scheme enabled the CEO detection and stabilization via a modulation of the pump power. This result demonstrates the feasibility of a frequency comb based on the SDL technology and constitutes an important step in the further development of compact frequency combs.

Finally, wavelength conversion in an optical parametric oscillator is studied to overcome the current limitations in the emission wavelength of ultrafast SDLs. Emission in the mid-infrared is highly attractive since a large number of molecules have strong rotational-vibrational transitions in this spectral range and the development of mid-infrared frequency combs enables simple, fast and highly sensitive molecular spectroscopy sensing methods.

# Résumé

Cette thèse présente une étude des premiers peignes de fréquences auto-référencés basés sur des lasers à disques semi-conducteurs (SDLs) à modes verrouillés en phase.

L'avènement des peignes de fréquences stabilisés basés sur des lasers à impulsions ultra-courtes a permis une avancée significative et de nombreuses applications dans divers domaines de la physique, de la spectroscopie et de la métrologie. Les peignes de fréquences optiques peuvent être utilisés comme une règle de mesure dans le domaine des fréquences fournissant un lien direct et cohérent entre les fréquences optiques et micro-ondes. Bien que les peignes de fréquences optiques aient révolutionné de nombreux domaines scientifiques, ils n'ont pas encore pénétré les marchés à grande échelle. Pour cela, les sources laser doivent être améliorées, en ciblant une haute fiabilité tout en gardant la source compacte et économiquement attractive.

Les SDLs à impulsions ultra-courtes, également appelés lasers à cavité verticale externe à émission de surface ou VECSELS (de l'anglais *vertical external-cavity surface-emitting lasers*), constituent une source laser très prometteuse à cet égard de par la technologie des semi-conducteurs qui permet une production de masse à faible coût. Ils rendent possibles des configurations de lasers très compactes et présentent une grande flexibilité dans leur longueur d'onde d'émission grâce à l'ingénierie de bandes. En outre, ils ne souffrent pas d'instabilités de mode déclenché (Q-

*switching*) et un fonctionnement stable en verrouillage de mode a été démontré à des taux de répétition allant de 100 MHz à 100 GHz. Les peignes de fréquences à taux de répétition élevés ont une puissance accrue par mode, ce qui est bénéfique pour des applications telles que l'astronomie ou la génération de signaux micro-ondes à faible bruit.

La stabilisation des deux degrés de liberté du laser à verrouillage de mode, la fréquence de répétition et la fréquence du décalage de phase entre la porteuse et l'enveloppe (*carrier-envelope offset* en anglais, CEO) est nécessaire pour la plupart des applications. Cependant, la détection de la fréquence CEO est difficile et aucune stabilisation n'avait été obtenue auparavant pour un laser à semi-conducteur à impulsions ultra-courtes. La détection de la fréquence CEO est généralement effectuée à l'aide d'une méthode d'auto-référencement qui nécessite un spectre cohérent couvrant une octave de fréquence. Ce dernier peut être généré en utilisant des fibres optiques hautement non linéaires telles que des fibres à cristaux photoniques (*photonic crystal fibers* en anglais, PCFs). Afin de maintenir la cohérence durant le processus d'élargissement spectral, des impulsions ultra-courtes dans le domaine des femtosecondes (typiquement <200 fs) avec une puissance de crête de l'ordre du kilowatt sont nécessaires. Cependant, même si des puissances maximales allant jusqu'à 6.3 kW et des durées d'impulsion allant jusqu'à 96 fs ont été démontrées pour des SDLs, la combinaison des deux n'a pas encore été atteinte. Par conséquent, la génération d'un spectre d'une octave utilisant une PCF directement à partir de la sortie du laser n'a pas pu être démontrée jusqu'à présent et des étapes supplémentaires d'amplification et de compression des impulsions sont nécessaires.

Dans ce travail, un amplificateur à fibre a été développé permettant la première démonstration de stabilisation de la fréquence CEO d'un SDL à impulsions ultra-courtes. Les impulsions amplifiées ont été comprimées temporellement et couplées dans une PCF pour la génération cohérente d'un spectre supercontinuum couvrant une octave. Une technique d'auto-

---

référencement permet la détection et la stabilisation de la fréquence CEO via une modulation de la puissance de la diode de pompe du laser. Ce résultat démontre la faisabilité d'un peigne de fréquences basé sur la technologie SDL et constitue une étape importante dans le développement des peignes de fréquences compacts.

Enfin, une conversion de longueur d'onde à l'aide d'un oscillateur paramétrique optique a été étudiée, permettant de surmonter les limites actuelles de la longueur d'onde d'émission atteignable avec des SDL à impulsions ultra-courtes. L'émission dans l'infrarouge moyen est très intéressante car un grand nombre de molécules ont de fortes transitions rotationnelles-vibrationnelles dans cette gamme spectrale et le développement de peignes de fréquences dans l'infrarouge moyen permet l'accès à des méthodes de détection de spectroscopie moléculaire simples, rapides et très sensibles.



# Contents

Abstract.....	v
Résumé.....	vii
Contents .....	xi
List of symbols and acronyms .....	xv
Publications .....	xix
Journal publications .....	xix
Conference presentations .....	xx
Chapter 1 Introduction.....	1
Chapter 2 Noise analysis of an ultrafast SDL .....	9
2.1 Noise in lasers .....	10
2.1.1 CW laser noise and linewidth.....	11
2.1.2 Noise of modelocked lasers.....	14
2.2 Repetition rate frequency noise characterization and stabilization of an ultrafast SDL .....	20
2.2.1 Repetition rate transfer function.....	22
2.2.2 Repetition rate frequency stabilization.....	24

## Contents

---

2.3	Theoretical principle for the characterization of the CEO frequency noise without $f$ -to- $2f$ interferometry.....	25
2.4	First investigation of the noise and modulation properties of the carrier-envelope offset in a modelocked semiconductor laser.....	28
2.4.1	References .....	38
Chapter 3	Amplification of an ultrafast SDL .....	43
3.1	High-power amplification of a femtosecond vertical external-cavity surface-emitting laser in an Yb:YAG waveguide.....	44
3.1.1	Introduction.....	45
3.1.2	Experimental setup.....	47
3.1.3	Results and discussion.....	50
3.1.4	Conclusion.....	53
3.1.5	References and links.....	54
Chapter 4	CEO frequency stabilization of an ultrafast SDL .....	59
4.1	Carrier-envelope offset frequency stabilization of a gigahertz semiconductor disk laser .....	62
4.1.1	Introduction.....	63
4.1.2	Experiment and results .....	65
4.1.3	Conclusion .....	74
4.1.4	References .....	75
Chapter 5	Towards longer wavelengths.....	81
5.1	Basic principle of OPOs .....	83
5.1.1	Energy conservation.....	83
5.1.2	Phase matching and conservation of momentum.....	84
5.1.3	Quasi-phase matching .....	85
5.1.4	Parametric gain .....	87
5.1.5	Synchronous pumping.....	88

---

5.2	Ultrafast optical parametric oscillator pumped by a vertical external-cavity surface-emitting laser .....	89
5.2.1	Introduction.....	89
5.2.2	Experiment.....	91
5.2.3	Results .....	95
5.2.4	Conclusion .....	98
5.2.5	References and links.....	98
Chapter 6	Conclusion and Outlook.....	103
	Bibliography.....	107



# List of symbols and acronyms

## Symbols

$d_{\text{eff}}$	nonlinear coefficient (pm/V)
$\epsilon_0$	vacuum permittivity (J/V <sup>2</sup> /m)
$E_S$	signal electric field (V/m)
$f_{\text{CEO}}$	carrier-envelope offset frequency (Hz)
$f_{\text{rep}}$	repetition frequency (Hz)
$h$	Planck constant (J/Hz)
$I_p$	pump intensity (W/m <sup>2</sup> )
$k$	wavenumber (m <sup>-1</sup> )
$L_{\text{cr}}$	crystal length (m)
$\lambda$	wavelength (m)
$\Lambda$	poling period (m)
$n(\lambda)$	refractive index
$P_{\text{av}}$	average power (W)
$S$	power spectral density
$\sigma_{\text{amp}}$	RMS amplitude noise (%)
$\sigma_{\text{jitter}}$	RMS timing jitter (s)

*List of symbols and acronyms*

---

$T$	time period between two pulses (s)
$T_{\text{meas}}$	measurement time (s)
$\delta\nu$	optical linewidth (Hz)
$\nu_N$	frequency of the $N^{\text{th}}$ line of the spectrum of a comb (Hz)
$\chi^{(2)}$	second order nonlinearity
$\nu$	optical frequency (Hz)
$w_P$	pump beam waist $1/e$ field amplitude (m)
$\Gamma$	gain factor (% or dB)
$Z_R$	Rayleigh range (m)

## **Acronyms**

CEO	carrier-envelope offset
CW	continuous wave
DPSSL	diode-pumped solid-state laser
FN	frequency noise
FWHM	full width at half maximum
HVA	high voltage amplifier
LBO	lithium triborate
Mid-IR	mid-infrared
MIXSEL	modelocked integrated external-cavity surface-emitting laser
OC	output coupler
OPO	optical parametric oscillator

---

PCF	photonic crystal fiber
PI	proportional integral
PLL	phase-locked loop
PPLN	periodically poled lithium niobate
PSD	power spectral density
PZT	piezo-electric transducer
QCL	quantum cascade laser
QPM	quasi-phase matching
RIN	relative intensity noise
RMS	root-mean-square
SC	supercontinuum
SDL	semiconductor disk laser
SESAM	semiconductor saturable absorber mirror
SNR	signal-to-noise ratio
SSB	single sideband
VCSEL	vertical cavity surface-emitting lasers
VECSEL	vertical external-cavity surface-emitting laser



# Publications

Parts of this thesis are published in the following journal papers and conference proceedings. The text and figures are printed as published, only the format of the text, the numbering and the size of figures were adapted to the style of this thesis. All papers are reprinted with permission from the corresponding publishers. The copyright of the original publications are held by the respective copyright holders.

## Journal publications

1. N. Jornod, K. Gürel, V. J. Wittwer, P. Brochard, S. Hakobyan, S. Schilt, D. Waldburger, U. Keller, and T. Südmeyer, "*Carrier-envelope offset frequency stabilization of a gigahertz semiconductor disk laser*," *Optica* 4, 1482-1487 (2017).
2. N. Jornod, V. J. Wittwer, C. Kränkel, D. Waldburger, U. Keller, T. Südmeyer, and T. Calmano, "*High-power amplification of a femtosecond vertical external-cavity surface-emitting laser in an Yb:YAG waveguide*," *Opt. Express* 25, 16527-16533 (2017).
3. N. Jornod, V. J. Wittwer, M. Gaponenko, M. Hoffmann, N. Hempler, G. P. A. Malcolm, G. T. Maker, and T. Südmeyer, "*Ultrafast optical parametric oscillator pumped by a vertical external-cavity surface-emitting laser (VECSEL)*", *Opt. Express* 25, 28983-28989 (2017).

4. P. Brochard, N. Jornod, S. Schilt, V. J. Wittwer, S. Hakobyan, D. Waldburger, S. M. Link, C. G. E. Alfieri, M. Golling, L. Devenoges, J. Morel, U. Keller, and T. Südmeyer, "First investigation of the noise and modulation properties of the carrier-envelope offset in a modelocked semiconductor laser," *Opt. Lett.* 41, 3165–3168 (2016).
5. K. Balskus, S. Schilt, V. J. Wittwer, P. Brochard, T. Ploetzing, N. Jornod, R. A. McCracken, Z. Zhang, A. Bartels, D. T. Reid, and T. Südmeyer, "Frequency comb metrology with an optical parametric oscillator," *Opt. Express* 24, 8370-8381 (2016).

## Conference presentations

1. N. Modsching, C. Paradis, P. Brochard, N. Jornod, K. Gürel, C. Kränkel, S. Schilt, V. J. Wittwer, T. Südmeyer, "Frequency Comb Stabilization of a 50-fs Thin-Disk Laser Oscillator Operating in a Strongly SPM-broadened Regime", *CLEO*, San Jose, May 2018, oral, p. SM4L.6.
2. N. Modsching, C. Paradis, P. Brochard, N. Jornod, K. Gürel, C. Kränkel, S. Schilt, V. J. Wittwer, T. Südmeyer, "Frequency Comb Stabilization of a 4 W, 50-fs Thin-Disk Laser Oscillator", *EFTF*, Torino, April 2018, oral, p. B2L-A-6.
3. K. Gürel, S. Hakobyan, V. J. Wittwer, N. Jornod, S. Schilt, T. Südmeyer, "Novel Methods for CEO Stabilization in Fiber Laser Frequency Combs", *EFTF*, Torino, April 2018, oral, p. B2L-A-3.
4. N. Jornod, K. Gürel, V. J. Wittwer, P. Brochard, S. Hakobyan, S. Schilt, D. Waldburger, U. Keller, T. Südmeyer, "Carrier-envelope offset frequency stabilization of an ultrafast semiconductor laser", *Photonics West*, San Francisco, CA, February 2018, oral, p. 10515-18.

- 
5. K. Gürel, V. J. Wittwer, S. Hakobyan, N. Jornod, S. Schilt, T. Südmeyer, *"Novel techniques for stabilizing fiber laser frequency combs"*, Photonics West, San Francisco, CA, February 2018, oral, p. 10512-58.
  6. K. Gürel, S. Hakobyan, V. J. Wittwer, N. Jornod, S. Schilt, T. Südmeyer, *"CEO frequency stabilization of an ultrafast fiber laser by opto-optical modulation (OOM) of a semiconductor absorber"*, UFO, Jackson Hole, WY, October 2017, oral.
  7. N. Jornod, K. Gürel, V. J. Wittwer, P. Brochard, S. Hakobyan, S. Schilt, D. Waldburger, U. Keller, T. Südmeyer, *"Carrier-envelope offset frequency stabilization of a mode-locked semiconductor disk laser"*, ASSL, Nagoya, September 2017, oral, p. AW1A.6.
  8. N. Jornod, K. Gürel, V. J. Wittwer, P. Brochard, S. Hakobyan, S. Schilt, D. Waldburger, U. Keller, T. Südmeyer, *"Towards Self-Referencing of a VECSEL Frequency Comb"*, CLEO EU, Munich, June 2017, oral, p. CF-1.4.
  9. N. Jornod, V. J. Wittwer, M. Gaponenko, M. Hoffmann, N. Hempler, G. P. Malcolm, G. T. Maker, T. Südmeyer, *"First Ultrafast Optical Parametric Oscillator (OPO) Pumped by a Vertical External Cavity Surface Emitting Laser (VECSEL)"*, Europhoton, Vienna, August 2016, oral, p. SSI-2.3.
  10. N. Jornod, V. J. Wittwer, T. Südmeyer, C. Kränkel, T. Calmano, *"High Power Yb:YAG Waveguide Amplification of a Femtosecond Semiconductor Disk Laser"*, CLEO, San Jose, June 2016, oral, p. SF2I.1.
  11. N. Jornod, P. Brochard, V. J. Wittwer, S. Schilt, S. Hakobyan, D. Waldburger, S. M. Link, C. G. E. Alfieri, M. Golling, L. Devenoges, J. Morel, U. Keller, T. Südmeyer, *"First Investigation of the Noise and Modulation Properties of the Carrier Envelope Offset Frequency in a Modelocked Semiconductor Laser"*, CLEO, San Jose, June 2016, oral, p. SM2H.5.

12. K. Balskus, S. Schilt, V. J. Wittwer, P. Brochard, T. Ploetzing, N. Jornod, R. A. McCracken, Z. Zhang, A. Bartels, D. T. Reid, T. Südmeyer, “*Frequency comb metrology with a near-infrared optical parametric oscillator*”, CLEO, San Jose, June 2016, oral, p. SM1H.6.
13. P. Brochard, N. Jornod, V. J. Wittwer, S. Schilt, D. Waldburger, S. M. Link, C. G. E. Alfieri, M. Golling, L. Devenoges, J. Morel, U. Keller, T. Südmeyer, “*Carrier-envelope offset characterization in a semiconductor modelocked laser without  $f$ -to- $2f$  interferometry*”, EFTF, York, April 2016, oral, p. 1070.
14. S. Schilt, K. Balskus, V.J. Wittwer, P. Brochard, T. Ploetzing, N. Jornod, R. A. McCracken, Z. Zhang, A. Bartels, D. T. Reid, T. Südmeyer, “*Noise characterization and optical frequency measurement with an optical parametric oscillator frequency comb*”, 8<sup>th</sup> Frequency Standard and Metrology Symposium, Potsdam, October 2015, poster.

# Chapter 1

## Introduction

Time and frequency are the physical quantities that can be measured with the highest precision. Since the prehistoric era, humankind has been trying to keep track on time. The first reference was the primary source of light on Earth, the apparent motion of the Sun. Later, new methods were developed to reach a finer division of the day. An example is the sundial that consists of a plate and a stick that cast the shadow of the Sun onto a dial divided into the 12 hours of a daytime. The precision of this device strongly depends on its configuration, but cannot be better than a few minutes in one day. In comparison, the optical clocks based on the laser technology developed nowadays can demonstrate stability that corresponds to a clock running with a precision of 4 seconds in the lifetime of the universe<sup>1</sup>. Throughout the ages, the study of light has played an important role and has become a physical science called photonics.

A key milestone in the development of photonics was the demonstration of the first laser in 1960 by Maiman<sup>2</sup>. Since then, lasers have invaded our world, becoming essential worldwide via laser-based data communications and in the all-day life in nearly all electronic devices such as printers, bar-code scanners, Blu-Ray players or computer mice.

A laser can emit light continuously in time or as a train of pulses with durations ranging from microseconds down to few femtoseconds. If one looks at the spectrum of a pulse train generated by a modelocked laser in the frequency domain, it corresponds to a comb of lines evenly spaced (Figure 1.1). Two radio frequencies characterize the frequency position in the optical spectrum: the repetition frequency, which is the spacing between two lines and corresponds to the inverse of the time between two consecutive pulses; and the carrier-envelope offset (CEO) frequency, which is the offset of the comb spectrum from the origin of the frequency axis. If these frequencies are known or stabilized, the optical spectrum of the modelocked laser is called a frequency comb. A fully-stabilized frequency comb is a precious tool which can be used as a ruler to measure optical frequencies with high precision. Its discovery was awarded by the Nobel Prize in Physics in 2005<sup>3,4</sup>. Since then, frequency combs have enabled huge progress and exciting new applications in many domains such as spectroscopy, medicine and fundamental science.

A crucial point for most applications is the stabilization of both the repetition and CEO frequencies. The stabilization of the repetition frequency has been demonstrated in 1986<sup>5</sup> by simply detecting the pulse train with a fast photodetector at the output of the laser and applying a feedback to the cavity length, usually via a piezo-electric transducer (PZT). The detection of the CEO frequency was much more challenging as it is not directly measurable from the laser spectrum. Innovative techniques had to be invented to propose a detection scheme. The most commonly used method is based on a nonlinear interferometric detection<sup>6</sup> which beats the blue part of the spectrum with the frequency-doubled red part. The resulting beat note corresponds to the CEO frequency, which can be stabilized using a modulation of the intracavity dispersion or the nonlinearity, in most cases performed by modulation of the optical pump power. However, this technique requires an octave-spanning spectrum that is typically not directly available from the modelocked laser. In 2000,

the development of nonlinear fibers for the generation of a supercontinuum (SC) spectrum<sup>7</sup> was the key milestone that enabled the demonstration of stabilized frequency combs<sup>8,9</sup>.

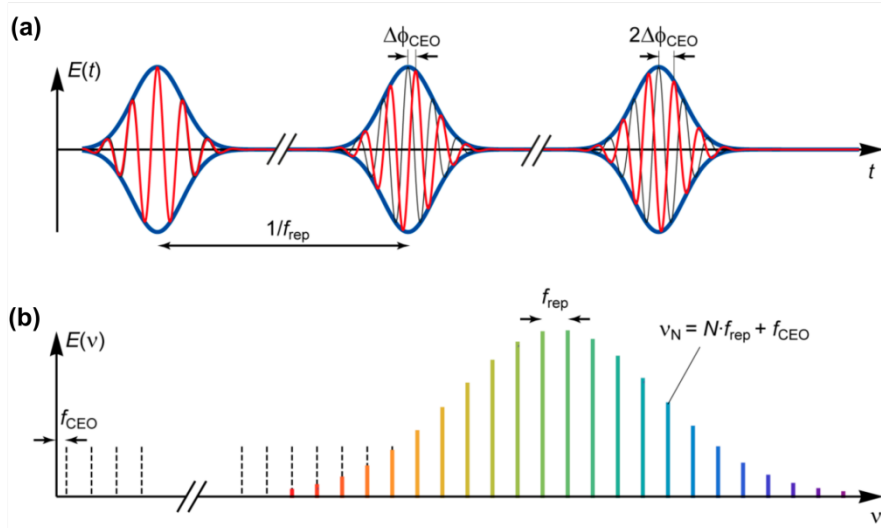


Figure 1.1: Time (a) and frequency (b) domain representation of the frequency comb from a modelocked laser. Figure taken from Schilt and Südmeyer<sup>10</sup>.

The first frequency comb systems were based on Ti:sapphire lasers. Ti:sapphire lasers enable extremely short pulses and repetition frequencies that can go up to multi-GHz in a low noise setup, but need to be pumped in the green, which requires bulky and complex pumping schemes. Fiber-based frequency combs can operate at the very interesting telecom wavelength spectral range at  $1.5 \mu\text{m}$  and are very reliable. They demonstrated extremely low noise operation<sup>11</sup> and were even operated outside the lab in a moving car<sup>12</sup>. Their typical operation regime is at repetition frequencies in the range of several tens to a few hundreds of MHz. Even though a fs diode-pumped fiber laser-based frequency comb operated at 1 GHz<sup>13</sup>, it is difficult to reach higher repetition frequencies. Another promising technology relies on diode-pumped solid-state lasers (DPSSLs) which also demonstrated GHz frequency combs without the

need of external amplification and compression stages<sup>14-16</sup>. This was an important breakthrough since there were initially concerns of feasibility of generating stabilized frequency combs due to the noise of the multi-mode pump source. Finally, the development of green laser diodes recently enabled the demonstration of the first diode-pumped Ti:sapphire CEO stabilization<sup>17</sup>.

The development of frequency combs follows a trend towards less complex laser setups, cheaper fabrication costs and a high flexibility in the generated repetition as well as optical frequency. It is in this framework that this thesis investigates frequency combs based on GHz modelocked semiconductor lasers. These lasers, called semiconductor disk lasers (SDLs) or vertical external-cavity surface-emitting lasers (VECSELs) gather the potential of very compact sources with cost-efficient wafer-scale mass production. However, the CEO frequency stabilization of an SDL could not be demonstrated in the beginning of this thesis, mainly due to the limited lasers peak power and too long pulse duration.

Lasers based on a semiconductor gain material have a long history as they were demonstrated only two years after the invention of the laser<sup>18</sup>. Nowadays they are the most common lasers in the market. In addition to the numerous applications in the multimedia and telecommunication sectors, they are a key building block of the modelocked laser technology, implemented as most of their pump sources as continuous wave (CW) laser diodes. The two most common diode types are the electrically-pumped edge-emitter diodes and the vertical cavity surface-emitting lasers (VCSELs), restricted to CW operation. The call for an external cavity to facilitate the addition of cavity elements such as saturable absorber for passive modelocking operation or wavelength filters for wavelength tuning and the demand for higher output powers led to the development of the first CW-optically-pumped VECSEL in 1997<sup>19</sup>. The modelocking operation was obtained with the implementation of a semiconductor saturable absorber mirror (SESAM) in the external cavity and was first

---

demonstrated in 2000 with a modelocked VECSEL emitting pulses of 22-ps duration and 22 mW of output power<sup>20</sup>.

Since then, a lot of work has been done to improve VECSELs properties in terms of output power and pulse duration. Today, the record output power from a fs-VECSEL is 5.1 W demonstrated in 2012<sup>21</sup>. More recently, pulse duration down to 96 fs were demonstrated at 100-mW average output power and 560-W peak power<sup>22</sup>, as well as 6.3 kW of peak power, which was obtained from a different system in 410-fs pulses<sup>23</sup>.

The short upper state lifetime of the semiconductor gain enables the demonstration of high repetition frequencies without the problem of Q-switching instabilities. Typically, VECSELs operate in the multi-GHz repetition rate, with a record of 50 GHz<sup>24</sup> in fundamentally modelocked operation. Even higher repetition rates of 175 GHz were obtained using harmonic modelocking<sup>25</sup>. Another advantage of the semiconductor gain is the possibility to integrate both the gain and saturable absorber into the same chip, leading to the so-called modelocked integrated external-cavity surface-emitting laser (MIXSEL)<sup>26</sup>. This type of lasers constitutes the ultimate step towards compactness and enabled modelocked repetition frequencies up to 100 GHz<sup>27</sup>. Figure 1.2 presents an overview of the published results of modelocked lasers with a repetition frequency in the GHz-regime. It shows that semiconductor lasers are well present in the picture and start competing with other technologies. Some results even have sufficient peak power for the demonstration of direct SC generation<sup>28</sup>. However, the octave-spanning SC generation has not yet been demonstrated from a direct launch of the laser pulse train into a nonlinear fiber. Tentative with compressed pulse duration of 150 fs and 1015 W of peak power were also not sufficient for the generation of the octave-spanning SC<sup>29</sup>.

A solution to increase the power is the implementation of external amplification. This was demonstrated with a VECSEL emitting at 1.5  $\mu\text{m}$ . The amplified pulses reached 4.5 W of average power in 15.5-ps duration

and enabled the generation of a broad supercontinuum extending from 1320 nm to 2000 nm<sup>30</sup>. However this SC did not cover the requested octave and was most likely incoherent. In 2014, Zaugg *et al.* demonstrated the coherent octave-spanning SC generation of a fiber-amplified VECSEL emitting in the 1- $\mu$ m region<sup>31</sup>. A standard  $f$ -to- $2f$  interferometer enabled the first detection of the CEO frequency of a SDL. Unfortunately, the signal-to-noise ratio (SNR) of the beat note was not sufficient for a noise characterization or a stabilization.

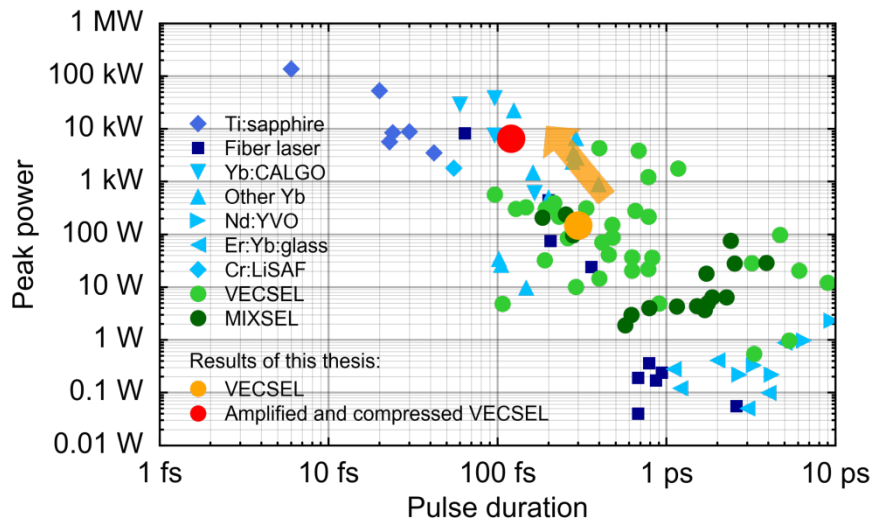


Figure 1.2: Selected overview of the achieved peak power of different modelocked laser technologies with pulse repetition rates from and above 1 GHz<sup>20-22,24,26-28,31-96</sup>. The light green dots represent results based on optically pumped VECSELs. The orange circle represents the ultrafast SDL used in this thesis for the demonstration of CEO stabilization and the red point is the generated peak power after amplification and compression.

In addition the different studies of the timing jitter and amplitude noise performed on VECSELs<sup>97-100</sup> and MIXSELs<sup>101</sup> demonstrated comparable performances to DPSSLs<sup>15,102,103</sup>. These noise properties place these laser sources in a very promising situation in the world of frequency combs.

---

This thesis follows the three main steps towards the demonstration of a SDL-based frequency comb that are

- The characterization of the noise of a SDL to determine the CEO frequency stabilization feasibility;
- The investigation of a proper amplifier and pulse compression stage for the generation of higher peak power and shorter pulse durations;
- The demonstration of the stabilization of the CEO frequency.

Chapter 2 focuses on the noise characterization of a 1.8-GHz SDL (orange point in Figure 1.2). The main noise sources in continuous-wave and modelocked lasers are presented. A noise characterization and stabilization of the repetition frequency are shown followed by the description of an indirect method for the measurement of the CEO frequency noise. Using this setup, the frequency noise of the CEO frequency is measured, showing the feasibility of a future stabilization by feedback to the pump current.

In chapter 3, a compact crystalline waveguide-based amplifier is investigated and demonstrates the efficient laser amplification from 60 mW to 2.9 W.

Chapter 4 presents the main result of this thesis that is the CEO frequency stabilization of an ultrafast SDL. To do so, efficient power amplification and spectral broadening are performed in an Yb-doped fiber amplifier developed in our institute. The compressed pulses (red point in Figure 1.2) enable the coherent octave-spanning supercontinuum generation in a photonic crystal fiber (PCF) followed by the CEO frequency detection in a standard  $f$ -to- $2f$  interferometer. The CEO frequency stabilization and an investigation on the origin of the free-running noise are presented.

Another advantage of the semiconductor technology is the possibility of engineering the emission wavelength of the semiconductor

gain medium. In CW operation, VECSELS cover emission wavelengths ranging from 391 nm<sup>104</sup> to 5.3 μm<sup>105</sup>. However, the range is limited between 665 nm<sup>106</sup> and 2 μm<sup>107</sup> in pulsed regime.

In chapter, 5 the development of an optical parametric oscillator pumped by an ultrafast SDL is presented. The parametric process enables the conversion of the SDL properties towards longer wavelengths. It is a first step in the development of SDL-based frequency combs emitting in the mid-infrared.

Finally, chapter 6 concludes the thesis and provides an outlook on the future improvements, developments and applications of the SDL technology.

# Chapter 2

## Noise analysis of an ultrafast SDL

The reduction of the noise of a laser is a key point for many applications in optical metrology or optical communications. In a pulsed laser, random fluctuations of the pulse power, of the timing between two consecutive pulses or of the phase of the carrier wave relative to the pulse envelope are noise sources that influence the frequency stability and linewidth of optical lines of the frequency comb. Therefore, the origin of the noise in the laser has first to be investigated and its level and spectral distribution need to be characterized. A careful design of the cavity to make it mechanically- and thermally-stable and the optimization of the pump source and its current driver in terms of noise levels are key parameters that will generally reduce the laser noise. The further reduction of the noise can then be implemented using an active stabilization loop applying a feedback signal to the laser.

In this chapter, the noise characterization of a GHz modelocked SDL is presented. Section 2.1 summarizes the theoretical definitions and possible origins of different types of noise that are present in CW and modelocked lasers. In section 2.2, the noise characterization and stabilization of the repetition frequency of the ultrafast SDL are presented.

After a brief description of an indirect CEO frequency noise detection scheme that does not require the traditional  $f$ -to- $2f$  interferometry presented in section 2.3, the noise of the CEO frequency of the ultrafast SDL is characterized using this method and presented in section 2.4.

## **2.1 Noise in lasers**

Every laser system output suffers from some noise due to fluctuations of the global system. The origin of this noise can be separated in two main categories. The first one is called quantum noise and results from spontaneous emission in the gain medium. The second is the noise arising from technical origins. The main sources of technical noise are a noisy pump source, vibrations of mechanical components of the resonator or temperature fluctuations. As quantum noise is mainly dependent on the laser operation mode, it can be reduced by reducing the optical losses, increasing the intracavity power or implementing active stabilization setup. On the other hand, technical noise is mainly controlled by careful cavity design, shielding and damping from ambient noise sources and implementation of active stabilization setups.

The following section 2.1.1 describes the intensity and frequency noise that occur in CW lasers and their relation to the laser linewidth. In section 2.1.2, the three main types of noise encountered in modelocked lasers are presented, i.e.:

- the amplitude noise,
- the timing phase noise,
- and the CEO phase noise.

## 2.1.1 CW laser noise and linewidth

### Intensity noise

Intensity noise represents the fluctuations of the laser output power around its average value. Note that this term may also refer to optical intensity, that is the optical power per unit area, but which will not be treated here. The time-dependent optical power of the laser can be expressed as

$$P(t) = P_{\text{av}} + \delta P(t), \quad (2.1)$$

where  $P_{\text{av}}$  is the average power and  $\delta P(t)$  a fluctuating quantity with zero mean value. In most cases, it is more common to consider the relative intensity noise (RIN) of the laser, which is the noise of the optical power normalized to the average power  $P_{\text{av}}$ :

$$I(t) = \frac{\delta P(t)}{P_{\text{av}}}. \quad (2.2)$$

The single sideband (SSB) power spectral density (PSD) of the RIN describes the distribution of the normalized power fluctuations as a function of the Fourier frequency  $f$ . Using the Wiener-Khinchin theorem, it is defined as

$$S_I(f) = \int_{-\infty}^{+\infty} G_I(\tau) \cdot e^{-i2\pi f\tau} d\tau, \quad (2.3)$$

where  $G_I(\tau)$  is the autocorrelation function of  $I(t)$  defined as

$$G_I(\tau) = \lim_{\Delta \rightarrow \infty} \frac{1}{\Delta} \int_{-\Delta/2}^{\Delta/2} I(t + \tau) I(t) dt. \quad (2.4)$$

The RIN PSD can be integrated over a given frequency range to provide a single number root-mean-square (RMS) value of the RIN, that is

$$\sigma_I|_{[f_{\text{low}}, f_{\text{high}}]} = \sqrt{2 \cdot \int_{f_{\text{low}}}^{f_{\text{high}}} S_I(f) df}, \quad (2.5)$$

which is usually specified in percent. The factor 2 before the integral comes from the fact that the SSB-PSD of the relative power fluctuations  $S_I(f)$  is considered here. Note that the specification of the integration bandwidth is essential and is typically determined by the inverse of the measurement time  $T_{\text{meas}}$  for the lower frequency limit ( $f_{\text{low}} = \frac{1}{T_{\text{meas}}}$ ) and the bandwidth of the measurement setup for the higher frequency limit  $f_{\text{high}}$ .

### Frequency noise and linewidth

Any laser, even a single-frequency laser, is not perfectly monochromatic and its power spectrum (optical spectrum as a function of its wavelength  $\lambda$  or frequency  $\nu$ ) has a finite full width at half maximum (FWHM) linewidth. The linewidth partially results from the quantum noise inherent to the lasing process that causes the intrinsic linewidth, which corresponds to the Schawlow-Townes limit<sup>108</sup>. Additional technical noise gives rise to a broadening of the linewidth.

The linewidth of lasers is generally too narrow to be resolved by standard optical spectrum analyzers. Other measurement techniques have thus been developed. An example used in this thesis is to perform a heterodyne beat with another independent laser which has a significantly lower frequency noise than the laser under study and is used as reference oscillator. The characterization of the beat note signal can be assumed to be a good estimate of the frequency noise properties of the laser under test.

The linewidth constitutes a single number that characterizes the spectral properties of a laser. It is useful for a simple comparison with other lasers, but generally a deeper characterization of the spectral behavior of the laser is necessary. This is obtained with the measurement of the frequency noise PSD  $S_{\delta\nu}(f)$ , where  $\delta\nu$  is the fluctuation around the central emission frequency  $\nu$  and  $S_{\delta\nu}(f)$  is defined from the autocorrelation function  $G_{\delta\nu}(\tau)$  of the frequency fluctuations by

$$S_{\delta\nu}(f) = \int_{-\infty}^{+\infty} G_{\delta\nu}(\tau) \cdot e^{-i2\pi f\tau} d\tau. \quad (2.6)$$

### **$\beta$ -separation line**

The optical lineshape and resulting linewidth of a laser can be directly computed from the frequency noise PSD  $S_{\delta\nu}(f)$  (see Elliott *et al.*<sup>109</sup>). However it is not always straightforward and may take a long computational time. A simple approximation method has been developed by Di Domenico *et al.*<sup>110</sup> to straightforwardly estimate the linewidth of a laser from its frequency noise PSD.

The basic idea is to introduce the so-called  $\beta$ -separation line in the frequency noise PSD

$$\beta(f) = \frac{8\ln 2}{\pi^2} \cdot f. \quad (2.7)$$

This line separates the frequency noise spectrum into two regions: frequencies which have a noise above the line contribute to the linewidth while those with a noise below the line do not affect the linewidth but only contribute to the wings of the line shape function. The linewidth can be simply approximated by the surface  $A$  below the frequency noise PSD for the frequency components for which the noise is above the  $\beta$ -separation line (see Figure 2.1). The FWHM linewidth is then computed as

$$FWHM = \sqrt{(8\ln 2)A}. \quad (2.8)$$

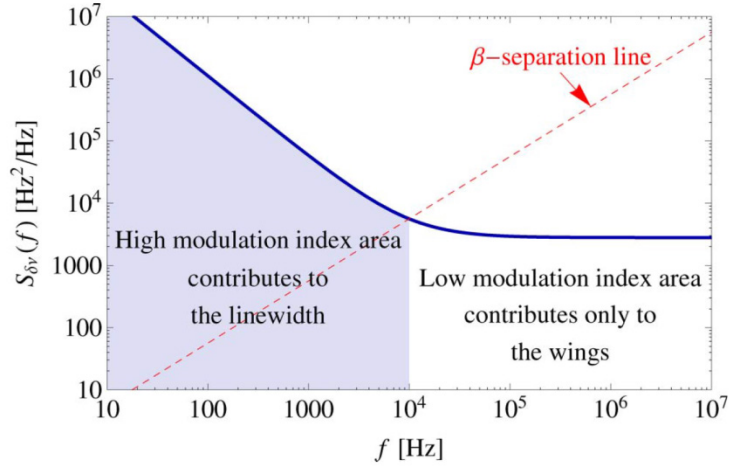


Figure 2.1: Figure taken from Di Domenico *et al.*<sup>110</sup>. A typical laser frequency noise PSD made of  $1/f$  noise at low Fourier frequencies and white frequency noise at high Fourier frequencies. The red dashed line is the  $\beta$ -separation line which separates the spectrum into the two regions: the violet area contributes to the linewidth, the white one contributes only to the wings of the line shape function.

## 2.1.2 Noise of modelocked lasers

The following section summarizes the theoretical description of the different types of noise occurring in a modelocked laser. It is mainly based on the work developed in Von der Linde<sup>111</sup> and adapted with the notations from Wittwer<sup>112</sup>.

### Ideal pulse train

A modelocked laser emits a train of pulses, where two subsequent pulses are separated by the time period  $T = \frac{1}{f_{\text{rep}}}$ . For most lasers, this time period is much larger than the pulse duration, and therefore the pulse shape can be approximated by a Dirac delta function  $\delta(t)$ . The time-dependent optical power of an ideal noise-free modelocked laser is then described by a sum of equally-spaced delta functions, called a Dirac comb

$$P(t) = P_{\text{av}} \cdot T \cdot \sum_{n=-\infty}^{+\infty} \delta(t - n \cdot T). \quad (2.9)$$

The corresponding PSD in the frequency domain is also a Dirac comb of equidistant lines given by

$$S_{P,\text{ideal}}(f) = (P_{\text{av}})^2 \cdot \sum_{n=-\infty}^{+\infty} \delta(f - n \cdot f_{\text{rep}}). \quad (2.10)$$

### Amplitude noise

As for the CW lasers described in the previous section, modelocked lasers suffer from amplitude fluctuations which can be expressed as

$$P(t) = (1 + I(t)) \cdot P_{\text{av}} \cdot T \cdot \sum_{n=-\infty}^{+\infty} \delta(t - n \cdot T), \quad (2.11)$$

where  $I(t)$  represents the normalized power fluctuations as introduced in equation (2.2). Going to the frequency domain with the help of the Wiener-Khinchin theorem, the PSD becomes

$$\begin{aligned} S_{P,\text{amp}}(f) &= (P_{\text{av}})^2 \cdot \sum_{n=-\infty}^{+\infty} [\delta(f - n \cdot f_{\text{rep}}) + S_I(f - n \cdot f_{\text{rep}})] \\ &= S_{P,\text{ideal}}(f) + (P_{\text{av}})^2 \cdot \sum_{n=-\infty}^{+\infty} S_I(f - n \cdot f_{\text{rep}}), \end{aligned} \quad (2.12)$$

where  $S_I$  is the power spectral density of the relative power fluctuations. This equation demonstrates that amplitude fluctuations in the time domain correspond to the emergence of sidebands in the frequency domain as depicted in Figure 2.2. The amplitude of these sidebands is identical for all harmonics.

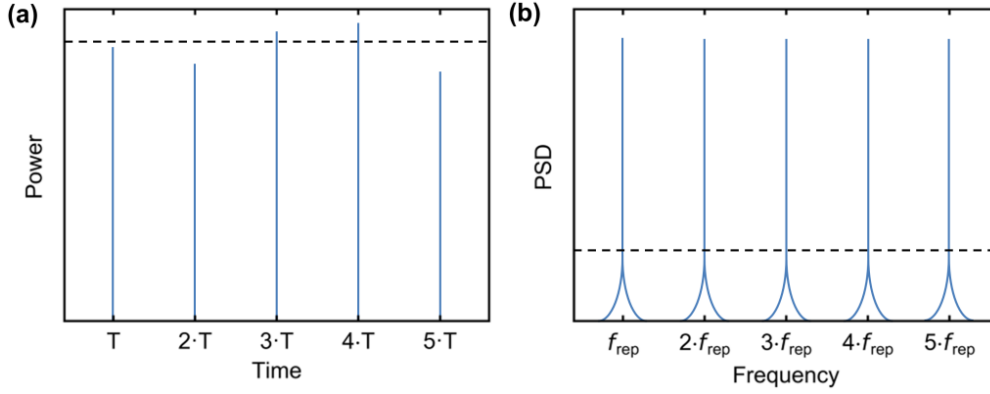


Figure 2.2: Power representation in the time domain (a) and frequency domain (b) of a modelocked laser pulse train that is affected by amplitude noise.

When characterizing the amplitude noise of a modelocked laser, one is typically interested in the noise contained in the sidebands of one harmonic  $m$

$$S_{m,\text{amp}}(f) = S_I(f - m \cdot f_{\text{rep}}). \quad (2.13)$$

This corresponds to the PSD of  $I(t)$  and can be integrated over a given frequency range to provide the integrated RMS amplitude noise

$$\sigma_{\text{amp}}|_{[f_{\text{low}}, f_{\text{high}}]} = \sqrt{2 \cdot \int_{f_{\text{low}}}^{f_{\text{high}}} S_{m,\text{amp}}(f) df}. \quad (2.14)$$

### Timing phase noise

In addition to amplitude noise, the repetition frequency  $f_{\text{rep}}$ , i.e., the inverse of the time interval  $T$  between pulses, also fluctuates. This is described in the time domain by the following expression

$$P(t) = P_{\text{av}} \cdot T \cdot \sum_{n=-\infty}^{+\infty} \delta(t - n \cdot T - \delta T_n(t)), \quad (2.15)$$

where  $\delta T_n(t)$  is the temporal variation of the  $n^{\text{th}}$  pulse from its ideal occurrence at time  $n \cdot T$ . Assuming small temporal variations,

corresponding to small phase shift  $\varphi_n(t) = n \cdot 2\pi f_{\text{rep}} \cdot \delta T_n(t) \ll 1$  rad, the PSD of the Dirac comb takes the form

$$\begin{aligned} S_{P,\text{time}}(f) &= (P_{\text{av}})^2 \cdot \sum_{n=-\infty}^{+\infty} \left[ \delta(f - n \cdot f_{\text{rep}}) + (n \cdot 2\pi f_{\text{rep}})^2 \cdot S_{\delta T}(f - n \cdot f_{\text{rep}}) \right] \\ &= S_{P,\text{ideal}}(f) + (P_{\text{av}})^2 \cdot \sum_{n=-\infty}^{+\infty} (n \cdot 2\pi f_{\text{rep}})^2 \cdot S_{\delta T}(f - n \cdot f_{\text{rep}}), \end{aligned} \quad (2.16)$$

with  $S_{\delta T}$  corresponding to the PSD of the temporal variation (in  $\text{s}^2/\text{Hz}$ ). As schematized in Figure 2.3, these timing fluctuations also add sidebands in the frequency spectrum, however their power scales with the square of the harmonic number  $n$ .

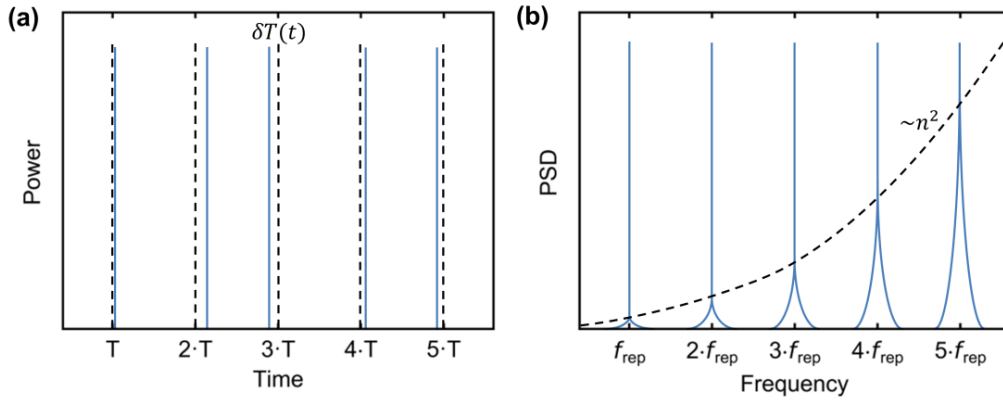


Figure 2.3: Timing phase noise of a pulse train in the time domain (a) and frequency domain (b). The time shift from pulse to pulse corresponds to additional wings in the frequency spectrum whose power scales with the square of the harmonic number  $n$ .

Here again, one typically characterizes the noise around one harmonic  $m$

$$S_{m,\text{time}}(f) = \left( m \cdot 2\pi f_{\text{rep}} \right)^2 \cdot S_{\delta T}(f - m \cdot f_{\text{rep}}). \quad (2.17)$$

A single number can be used to describe the contribution of the timing phase noise in a given frequency range

$$\sigma_{\text{jitter}}|_{[f_{\text{low}}, f_{\text{high}}]} = \frac{\sqrt{2 \cdot \int_{f_{\text{low}}}^{f_{\text{high}}} S_{m,\text{time}}(f) df}}{2\pi m f_{\text{rep}}} = \sqrt{2 \cdot \int_{f_{\text{low}}}^{f_{\text{high}}} S_{\delta T}(f) df}. \quad (2.18)$$

It is called the RMS timing jitter or integrated timing jitter.

### CEO phase noise

Every pulse of the optical pulse train can be described with an intensity envelope, as studied earlier, and an underlying oscillating electric field (the carrier wave). The dispersion and nonlinearities of the resonator cause a phase slippage of the peak of the electric field from the peak of the intensity envelope from pulse to pulse (see Figure 2.4). It is defined as the carrier-envelope phase slip. In the frequency domain, it corresponds to a frequency offset of the comb spectrum from the zero frequency. This frequency offset is defined as the CEO frequency  $f_{\text{CEO}}$ , and every line of the comb spectrum can be written as

$$\nu_N = N \cdot f_{\text{rep}} + f_{\text{CEO}}, \quad (2.19)$$

where  $N$  represents the mode number. The fluctuation of the CEO frequency induces a fluctuation of the entire comb spectrum. Therefore a noise characterization together with a stabilization of the CEO frequency are relevant.

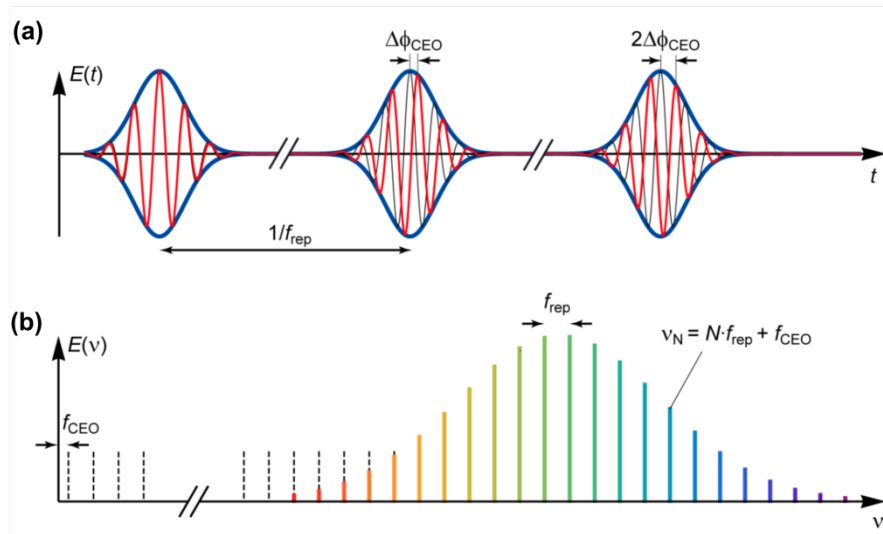


Figure 2.4: (a) time and (b) frequency domain representation of a frequency comb. Figure taken from Schilt and Südmeyer<sup>10</sup>.

Unlike  $f_{\text{rep}}$ , which can be easily measured with a high bandwidth photodiode and a microwave spectrum analyzer, the CEO frequency is not directly accessible as it does not appear in the optical spectrum of the laser. Therefore new techniques have been developed for its detection. The mostly used is the  $f$ -to- $2f$  interferometry<sup>6</sup>, described and implemented in chapter 4. This technique necessitates in particular the generation of a coherent supercontinuum spectrum that covers a frequency octave (i.e. ranging from frequency  $f$  to frequency  $2f$ ). This property is not directly obtained from the laser (apart a few special configurations of Ti:sapphire modelocked lasers<sup>113,114</sup>) and can be pretty challenging to achieve especially for lasers with a high repetition rate in the GHz-regime. To circumvent this constraint, the following sections 2.3 and 2.4 present an alternative technique to detect and characterize the noise of the CEO frequency without the use of an  $f$ -to- $2f$  interferometer.

### **$\beta$ -separation line**

The  $\beta$ -separation line described at the end of section 2.1.1 can be used to characterize the noise of the CEO frequency. The crossing point between

the line and the CEO frequency noise PSD gives a good estimate of the bandwidth needed to achieve a tight lock in a CEO stabilization loop. When the frequency noise is entirely reduced below the  $\beta$ -separation line, the linewidth of the CEO is suppressed, which results in a tight-lock that is characterized by the occurrence of a coherent peak in the RF spectrum of the CEO beat, targeted for most applications of optical frequency combs.

## **2.2 Repetition rate frequency noise characterization and stabilization of an ultrafast SDL**

The laser prototype characterized in this chapter and further used in chapters 3 is a 1.8-GHz SESAM-modelocked VECSEL developed at ETH Zurich. A second prototype based on the same design with similar VECSEL gain chip and SESAM was assembled in our laboratory. The second prototype is used in the results presented in chapter 4. Both lasers were carefully characterized and demonstrate comparable operation and noise behavior. In this section, the detailed characterization of the first prototype is presented.

The laser has a simple V-shaped cavity with the VECSEL gain chip as folding mirror and the SESAM and output coupler (OC) as end mirrors, as presented in Figure 2.5(a).

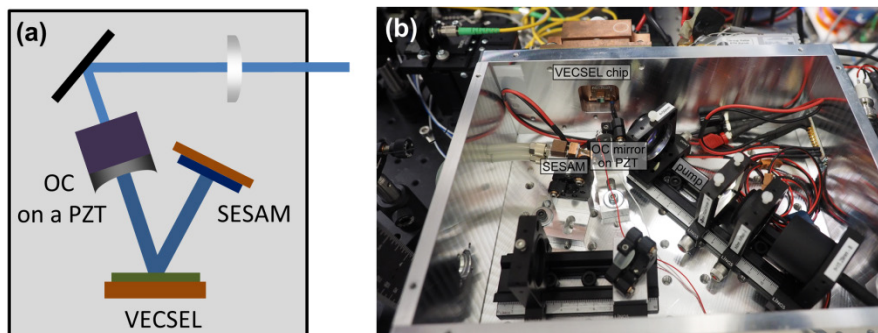


Figure 2.5 (a): Scheme of the SESAM-modelocked VECSEL cavity. (b) Picture of the boxed prototype in its aluminum housing.

The laser properties are summarized in Table 2.1. Pulses with a duration of 300 fs are generated from the prototype at a central emission wavelength of 1030 nm and with an average output power of 90 mW. The laser is boxed in an aluminum housing [Figure 2.5(b)] to minimize the influence of technical noise such as acoustic noise and thermal effects.

<b>VECSEL prototype</b>			
Pump power	17 W	Pulse duration	300 fs
Output power	90 mW	Central emission wavelength	1030 nm
Repetition frequency	1.77 GHz	Spectral bandwidth	4 nm

Table 2.1 Parameters of the ultrafast VECSEL.

The stabilization of the repetition frequency  $f_{\text{rep}}$  is performed using a PZT placed underneath the OC to change the cavity length and therefore adjust  $f_{\text{rep}}$ . The main steps of the stabilization are the detection and amplification of the  $f_{\text{rep}}$  signal, followed by its phase stabilization to a reference signal by controlling the cavity length with the PZT using a phase-locked loop (PLL) circuit.

The noise of the stabilized signal and the stability of the lock depend on several parameters of the PLL such as the range of the PZT, the gain of the locking electronics or the noise of the reference signal. The noise of the

reference signal is characterized by measuring its frequency noise (FN) PSD and typically sets the limiting noise level for the stabilization at low Fourier frequencies. The gain of the locking electronics is usually limited by the PZT and is optimized by a careful adjustment while monitoring the  $f_{\text{rep}}$  FN-PSD. Finally, a careful study of the PZT bandwidth (and therefore of the speed with which the control loop can react) is performed by a measurement of its transfer function. This measurement helps understanding the potential limitations and the reaction of the system before performing the stabilization.

### 2.2.1 Repetition rate transfer function

Two parameters are important in a PLL:

- the linear tuning range
- the amplitude and phase responses (and therefore the bandwidth of the loop)

To investigate the linear range, we performed a static measurement of the tuning response of  $f_{\text{rep}}$  (measured with an RF spectrum analyzer) to a change of the driving voltage of the PZT. This measurement is presented in Figure 2.6(b). Here we implemented a high voltage amplifier (HVA, Menlo HVA150, gain  $\sim 15$ ) to drive the PZT in a range of 0-150 V. We performed this measurement in our ultrafast VECSEL using the 5<sup>th</sup>-harmonic of  $f_{\text{rep}}$  (8.84 GHz), which will later be used for the stabilization, and divided the result by 5 to get the behavior of  $f_{\text{rep}}$ . We see that the PZT provides a response that spans over more than 40 kHz with a linear tuning coefficient of  $\sim 350$  Hz/V. This is widely sufficient for  $f_{\text{rep}}$  stabilization, even at the GHz repetition rate.

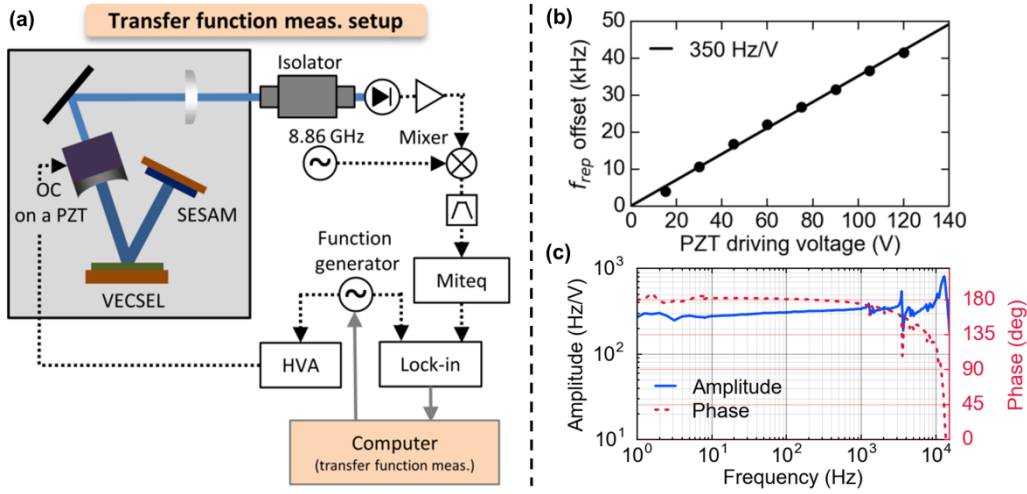


Figure 2.6: (a) Transfer function measurement scheme. (b) Static tuning of  $f_{\text{rep}}$  as a function of the PZT voltage. (c) Amplitude (left axis, blue) and phase (right axis, red) transfer function of  $f_{\text{rep}}$  for PZT modulation.

The amplitude and phase responses are assessed in a dynamic measurement, called transfer function. This measurement gives the amplitude attenuation / amplification and the phase delay as a function of the PZT voltage modulation frequency. The PLL bandwidth is determined by the frequency at which the phase of the transfer function shifts by 90°, which typically corresponds to 3 dB (50%) attenuation in amplitude for a 1<sup>st</sup> order low-pass filter. We use this approximation to estimate the PLL bandwidth, even if the transfer function does not fit a 1<sup>st</sup> order low-pass filter. Figure 2.6(a) presents the measurement setup of the transfer function. The basic principle is to apply a sinusoidal signal from a function generator to the HVA in order to modulate the PZT and use a lock-in amplifier to detect the amplitude and phase response of  $f_{\text{rep}}$ . A frequency discriminator (Miteq FMDM 21.4/4-2) is used before the lock-in amplifier to convert the frequency fluctuations into voltage fluctuations analyzed by the lock-in. Here again we performed the measurements on the 5<sup>th</sup>-harmonic of  $f_{\text{rep}}$ . As the frequency discriminator has an operating range of 18-26 MHz, the multi-GHz signal is first down converted to ~20 MHz using a mixer and a reference oscillator. The transfer function is presented

in Figure 2.6(c). It has a  $90^\circ$  phase shift at frequency slightly above 10 kHz. We also see two resonances of the PZT at  $\sim 1.3$  kHz and 3.5 kHz which may add some peaks in the FN-PSD of the stabilized signal.

### 2.2.2 Repetition rate frequency stabilization

The stabilization of the repetition frequency is performed on its 5<sup>th</sup> harmonic ( $5 \cdot f_{\text{rep}} = 8.84$  GHz) to enhance the phase noise sensitivity compared to the fundamental frequency (see section 2.1.2). The signal was first detected using a high-bandwidth photodiode (New Focus 1014), then amplified and phase-compared in a mixer with a reference synthesizer (Rohde-Schwarz SMF-100A), see Figure 2.7(a). The resulting phase error signal was low-pass filtered and sent to the proportional integral (PI) servo-controller (Menlo PIC210) to generate the correction signal driving the HVA to modulate the OC mounted on the PZT.

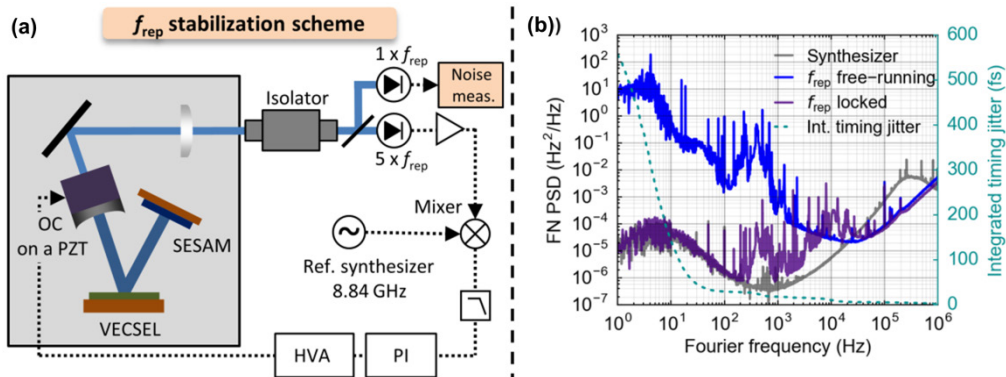


Figure 2.7: (a) Repetition frequency stabilization scheme. (b) FN-PSD of the free-running (blue) and phase-locked (violet) repetition frequency and of the reference synthesizer (grey). Right axis: Integrated timing jitter as a function of the low cut-off frequency (dashed line).

We recorded the noise of the 1<sup>st</sup>-harmonic of the repetition frequency using the signal from a second photodetector (New Focus 1434) and a phase noise analyzer (Rohde-Schwarz FSWP26). The free-running (blue) and stabilized (violet) FN-PSDs of the repetition frequency are presented

in Figure 2.7(b). In addition, the frequency noise of the synthesizer used as a reference signal in the PLL was measured at 8.84 GHz and is plotted in Figure 2.7(b) after down scaling by a factor of  $5^2$  for comparison with the noise of the 1<sup>st</sup> harmonic. We see that the noise of the stabilized  $f_{\text{rep}}$  is reduced to the level of the reference synthesizer for Fourier frequencies up to 200 Hz. We also see the servo bump at  $\sim 10$  kHz, which gives the stabilization bandwidth and is consistent with the results of section 2.2.1. The free-running integrated timing jitter of 1.7 ps is reduced to 30 fs integrated from 100 Hz to 1 MHz, which is remarkably low for a GHz laser.

### 2.3 Theoretical principle for the characterization of the CEO frequency noise without $f$ -to- $2f$ interferometry

This section summarizes the basic principle of the indirect characterization of the CEO frequency noise as described in the work of Brochard *et al.*<sup>115</sup>.

The method is based on an appropriate combination of different signals from the modelocked laser and a narrow linewidth CW laser. A scheme of the detection method is presented in Figure 2.8. On one side a high harmonic

$$f_A = N_1 \cdot f_{\text{rep}} \quad (2.20)$$

of the repetition rate is measured using a fast photodetector (lower branch of Figure 2.8 on PD-1). On the other side, the heterodyne beat between the modelocked laser and the CW laser is measured on a second fast photodetector PD-2. This beat note corresponds to an RF signal

$$f_{\text{beat}} = \nu_N - \nu_{\text{laser}}, \quad (2.21)$$

where  $\nu_N = N \cdot f_{\text{rep}} + f_{\text{CEO}}$  is the frequency of the comb line that beats the CW laser [see equation (2.19)] and  $\nu_{\text{laser}}$  is the frequency of the CW laser. The beat note is then frequency-divided by an integer number  $N_2$

(typically  $N_2 \sim 10^4$ ) carefully chosen such that the product of  $N_1$  and  $N_2$  equals the index  $N$  of the modelocked laser comb line

$$N = N_1 \cdot N_2. \quad (2.22)$$

The resulting signal is

$$f_B = \frac{f_{\text{beat}}}{N_2} = N_1 \cdot f_{\text{rep}} + \frac{f_{\text{CEO}} - \nu_{\text{laser}}}{N_2}, \quad (2.23)$$

Finally the two signals  $f_A$  and  $f_B$  are mixed to produce a signal  $f_{\text{out}}$  that is exempt from the contribution of  $f_{\text{rep}}$

$$f_{\text{out}} = f_B - f_A = \frac{f_{\text{CEO}} - \nu_{\text{laser}}}{N_2}, \quad (2.24)$$

Now assuming that the frequency noise of the CW laser  $\delta\nu_{\text{laser}}$  is sufficiently lower than the frequency noise  $\delta f_{\text{CEO}}$  of the CEO beat under investigation, its contribution can be neglected. Then

$$\delta f_{\text{out}} \cong \frac{\delta f_{\text{CEO}}}{N_2}, \quad (2.25)$$

and the FN-PSD of the output signal depicts the PSD of CEO frequency divided by  $N_2^2$ . Note that this technique enables accessing the CEO frequency noise, but does not give a direct access to the absolute  $f_{\text{CEO}}$  measurement as the absolute CW-laser frequency ( $\nu_{\text{laser}}$ ) is not known exactly.

### 2.3 Theoretical principle for the indirect characterization of $f_{\text{CEO}}$ noise

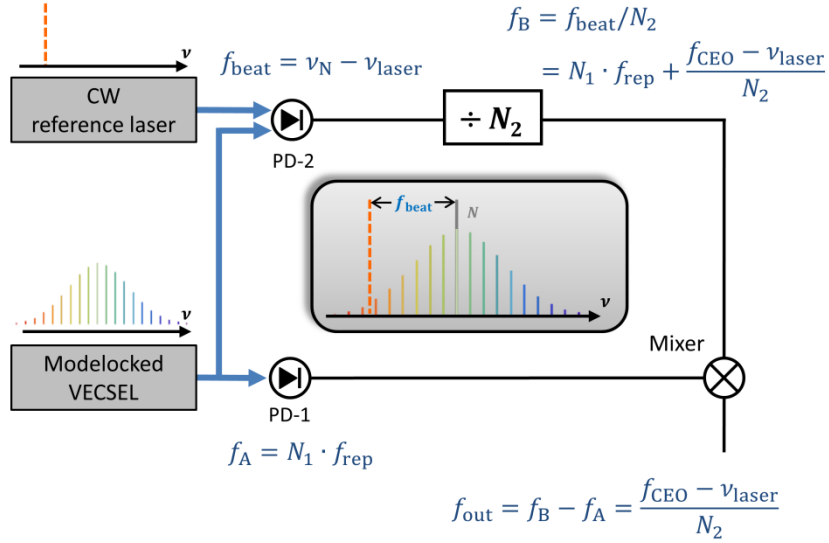


Figure 2.8: Basic principle of the proposed scheme to characterize the CEO beat without directly detecting it. A high harmonic  $N_1$  of the repetition rate (lower branch, signal  $f_A$ ) is mixed with the heterodyne beat with a CW laser, frequency-divided by  $N_2$  (higher branch, signal  $f_B$ ), to produce a signal  $f_{\text{out}}$  that is exempt from the contribution of  $f_{\text{rep}}$  if  $N = N_1 \cdot N_2$ . PD: fast photodiode.

In addition to the difference frequency component ( $f_B - f_A$ ) measured at the output of the mixer, there is also the sum frequency component ( $f_B + f_A$ ) which includes twice the noise of the repetition frequency. Therefore the signal has to be selected carefully to guaranty that the correct beat note is used for the characterization of the CEO frequency.

This method has been validated with a commercial Er:fiber frequency comb<sup>115</sup>. The measured CEO frequency noise showed an excellent agreement with the results obtained with a traditional  $f$ -to- $2f$  interferometer.

The noise characterization of the CEO frequency of the ultrafast VECSEL using the indirect method described here is presented in the following section, which is a reprint of our article published in Optics Letters<sup>116</sup>.

## 2.4 First investigation of the noise and modulation properties of the carrier-envelope offset in a modelocked semiconductor laser

*P. Brochard,<sup>1</sup> N. Jornod,<sup>1</sup> S. Schilt,<sup>1</sup> V. J. Wittwer,<sup>1</sup> S. Hakobyan,<sup>1</sup>  
D. Waldburger,<sup>2</sup> S. M. Link,<sup>2</sup> C. G. E. Alfieri,<sup>2</sup> M. Golling,<sup>2</sup> L. Devenoges,<sup>3</sup>  
J. Morel,<sup>3</sup> U. Keller,<sup>2</sup> and T. Südmeyer<sup>1</sup>*

<sup>1</sup>Laboratoire Temps-Fréquence, Institut de Physique, Université de Neuchâtel, CH-2000 Neuchâtel, Switzerland.

<sup>2</sup>Department of Physics, Institute of Quantum Electronics, ETH Zurich, CH-8093 Zürich, Switzerland.

<sup>3</sup>Federal Institute of Metrology METAS, CH-3003 Bern-Wabern, Switzerland.

We present the first characterization of the noise properties and modulation response of the carrier-envelope offset (CEO) frequency in a semiconductor modelocked laser. The CEO beat of an optically-pumped vertical external-cavity surface-emitting laser (VECSEL) at 1030 nm was characterized without standard  $f$ -to- $2f$  interferometry. Instead, we used an appropriate combination of signals obtained from the modelocked oscillator and an auxiliary continuous-wave laser to extract information about the CEO signal. The estimated linewidth of the free-running CEO beat is approximately 1.5 MHz at 1-s observation time, and the feedback bandwidth to enable a tight CEO phase lock to be achieved in a future stabilization loop is in the order of 300 kHz. We also characterized the amplitude and phase of the pump current to CEO-frequency transfer function, which showed a 3-dB bandwidth of  $\sim 300$  kHz for the CEO frequency modulation. This fulfills the estimated required bandwidth and indicates that the first self-referenced phase-stabilization of a modelocked semiconductor laser should be feasible in the near future.

Optical frequency combs from modelocked solid-state lasers have been a revolution in the field of high precision metrology by directly and coherently linking the optical and microwave parts of the electromagnetic spectrum [1-3]. Such stabilized frequency combs enable the measurement of optical frequencies with an extreme precision [4,5] and constitute a key element of novel optical atomic clocks that have surpassed the best microwave frequency standards in terms of fractional frequency stability [6,7].

Most comb applications today require self-referencing, i.e., the detection and stabilization of the carrier envelope offset (CEO) frequency  $f_{\text{CEO}}$  [1,8]. This has been achieved in various fiber laser systems [9] and solid-state lasers (Ti:Sapphire [2] or diode-pumped solid-state lasers – DPSSLs [10,11]). Electronic feedback modulating the pump power of the femtosecond laser is the most common approach to phase-stabilize  $f_{\text{CEO}}$  to an external reference frequency [3]. Alternative methods have been demonstrated, which make use of an intracavity loss modulator enabling the modulation bandwidth to be extended beyond the gain lifetime limitation, such as a graphene electro-optic modulator [12] or an opto-optical modulation of a semiconductor saturable absorber mirror (SESAM) [13]. Other solutions are based on feedforward corrections applied to the CEO frequency [14] or passive CEO cancellation using a difference frequency generation (DFG) process [15].

Self-referencing modelocked lasers with a higher repetition rate in the GHz range is much more challenging, as the CEO noise typically scales with the repetition rate [16], therefore requiring larger feedback bandwidths. In addition, the standard self-referencing method most often involves  $f$ -to- $2f$  interferometry to detect the CEO frequency [1]. This requires a coherent supercontinuum (SC) spectrum that covers at least one frequency octave, which is fairly challenging to achieve for some novel comb technologies that are presently being developed. The use of higher order nonlinear processes, such as  $2f$ -to- $3f$  [1], slightly reduces the

requirements in terms of spectral width of the SC spectrum, but at the expense of a higher complexity.

Among the emerging comb technologies, modelocked semiconductor lasers are promising for future low-cost high-volume production owing to the benefits of semiconductor manufacturing. Vertical external-cavity surface-emitting lasers (VECSELs) or modelocked integrated external-cavity surface-emitting lasers (MIXSELs) [17] can lead to compact and cost-effective frequency comb systems in the future. However, no such modelocked laser has ever been CEO-frequency-stabilized yet. The main reason is the insufficient peak power and too long pulse duration that have prevented so far the generation of a suitable SC spectrum for CEO detection.

A CEO beat signal from a semiconductor modelocked laser has been detected for the first time by Zaugg *et al.* after external pulse amplification and compression [18], but no further investigation has been reported since then. The 1038-nm VECSEL was first amplified to 5.5 W average power using a fiber amplifier, then the pulses were compressed to 85 fs to generate the necessary octave-spanning SC spectrum in a photonic crystal fiber (PCF). However, the detected CEO signal was not suitable for noise analysis or stabilization as the signal-to-noise ratio (SNR) of  $\sim 15$  dB (in a 100-kHz resolution bandwidth) was insufficient. Extra noise may have been induced in the amplification.

In this Letter, we present the first detailed characterization of the CEO frequency in a modelocked VECSEL, showing promising results for future self-referencing stabilization. For this purpose, we implemented a characterization method of the CEO beat that does not require  $f$ -to- $2f$  interferometry and therefore circumvents the need for a coherent octave-spanning comb spectrum that has not yet been achieved directly from the output of this laser. The information about the CEO noise and modulation response was obtained directly from the output of the oscillator, without any further spectral broadening, pulse compression or amplification. We

recently showed a proof-of-principle demonstration of this method implemented with an Er:fiber frequency comb for which the CEO beat was separately detected using an  $f$ -to- $2f$  interferometer for cross validation [19]. The method proved to be suitable to infer both the frequency noise spectrum of the free-running CEO beat and the transfer function of  $f_{\text{CEO}}$  for a modulation of the laser pump current. Here we report on the implementation of this method for the characterization of the CEO frequency of a modelocked VECSEL.

The investigated ultrafast laser oscillator was a prototype developed at ETH Zurich. The laser cavity had a semiconductor gain chip as folding mirror, and a SESAM and an output coupler (1% transmission) as end mirrors. It generated sub-300-fs pulses at around 1030 nm [20]. The VECSEL was pumped with up to 17 W of optical power from a commercially-available fiber-coupled 808-nm multimode pump diode. The average output power was 90 mW with a spectral width of  $\sim 4$  nm. The pump diode was driven in-parallel by a low-cost constant current source and a home-built voltage-current transducer providing a fast modulation channel for the pump power. A dedicated low-pass filter was implemented between the two current sources to avoid undesirable cross-talks. A 3-dB modulation bandwidth of the pump power of around 1 MHz was therewith achievable with this home-made transducer. Fast modulation capabilities of the pump power are important for future comb self-referencing with direct control of the CEO frequency via pump current modulation. The VECSEL repetition rate  $f_{\text{rep}} \approx 1.77$  GHz was phase-stabilized to a radio-frequency (RF) signal referenced to an H-maser for stable long-term operation at the required level of accuracy. This stabilization was implemented by a phase-locked loop operating at  $5 f_{\text{rep}}$  ( $\sim 8.85$  GHz), with a feedback signal applied to a piezoelectric transducer (PZT) controlling the position of the output coupler within the VECSEL cavity.

The principle of the method applied to characterize the CEO beat without directly detecting it was recently presented in Ref. [19]. It requires an auxiliary continuous wave (cw) laser. Whereas a planar waveguide external-cavity laser with a very low frequency noise was used in our proof-of-principle experiment at 1.55  $\mu\text{m}$ , this type of laser is not available at the 1030-nm emission wavelength of our VECSEL. Therefore, a distributed feedback (DFB) laser (Eagleyard) with a specified linewidth  $<2$  MHz was used in the work reported here. Its frequency noise power spectral density (PSD) has first been measured to assess its suitability for this application. This was realized by heterodyning the laser with the SC spectrum generated in a highly nonlinear fiber from a fully-stabilized Er: fiber frequency comb (Menlo FC 1500-250). The SC spectrum was spectrally filtered using a fibered tunable bandpass filter with a bandwidth of  $\sim 1$  nm and amplified in a semiconductor optical amplifier (Innolume) before being combined with the auxiliary cw laser in a 90/10 fiber coupler. The resulting beat signal was bandpass filtered and its frequency noise was measured using a frequency discriminator [21] and a fast Fourier transform spectrum analyzer. The noise of the auxiliary DFB laser was the dominating contribution in this measurement, leading to the frequency noise spectrum displayed in Figure 2.10.

## 2.4 First investigation of the noise and modulation properties of $f_{\text{CEO}}$

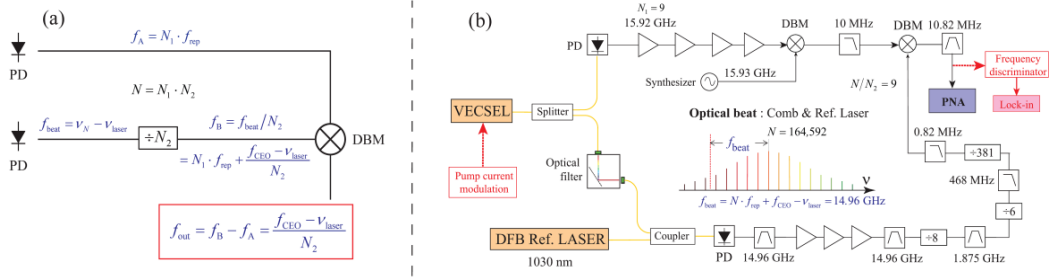


Figure 2.9: (a) Basic principle of the proposed scheme to characterize the CEO beat without directly detecting it [19]. A high harmonic  $N_1$  of the repetition rate (upper branch, signal  $f_A$ ) is mixed with the heterodyne beat with a cw laser, frequency-divided by  $N_2$  (lower branch, signal  $f_B$ ), to produce a signal  $f_{\text{out}}$  that is exempt from the contribution of  $f_{\text{rep}}$ . PD: fast photodiode; DBM: double-balanced mixer. (b) Detailed experimental scheme realized for the implementation of the method with a modelocked VECSEL with  $f_{\text{rep}} \approx 1.77$  GHz using an auxiliary DFB laser at 1030 nm. PNA: phase noise analyzer. All radio-frequency components except the narrow band-pass filters at  $\sim 15$  GHz are standard off-the-shelf components. The frequency discriminator and lock-in amplifier are used for the transfer function.

The experimental setup for the characterization of  $f_{\text{CEO}}$  was implemented in a similar way as in our previous proof-of-principle demonstration. However, different RF components (filters, frequency dividers, amplifiers) were used to account for the different repetition rate and mode number  $N$  involved here. Basically, two RF signals were detected, corresponding to a harmonic  $N_1 = 9$  of the repetition rate (at 15.92 GHz) and to the beat signal  $f_{\text{beat}}$  between one mode of the VECSEL (with a nominal mode number  $N = N_1 \cdot N_2$ ) and the auxiliary laser, which was detected at a frequency of 14.96 GHz. In order to remove the contribution of the VECSEL repetition rate, these signals were processed and combined according to the general principle reported in Ref. [19] and to the detailed scheme displayed in Figure 2.9. Finally, only a frequency-divided contribution of the CEO frequency fluctuations  $\delta f_{\text{CEO}}$  (division by a factor  $N_2 = 18,288$  here) occurred in the noise of the output signal  $\delta f_{\text{out}} = \delta f_{\text{CEO}}/N_2$ . This signal also contained the frequency noise of the cw laser (divided by the same factor  $N_2$ ), but it had a negligible impact as it

was significantly lower than the noise of the free-running CEO beat (as shown in Figure 2.10). Therefore, the CEO noise was retrieved by up-scaling by a factor  $N_2^2$  the phase noise of the output signal measured with

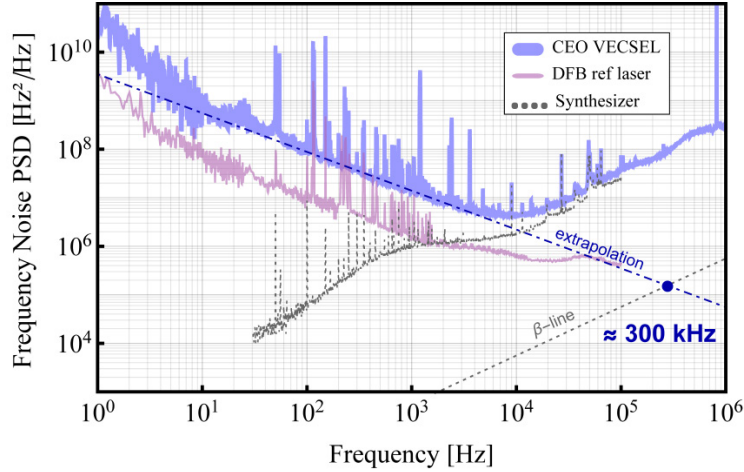


Figure 2.10: Frequency noise PSD of the free-running CEO beat of the VECSEL assessed with the proposed method (thick light blue line). The thin light purple line represents the frequency noise PSD of the free-running cw laser used in this experiment. The CEO noise at frequencies higher than  $\sim 10$  kHz is limited by the noise of a synthesizer used in the experiment (dashed grey line). Therefore an estimation of the feedback bandwidth required for a future phase stabilization of  $f_{\text{CEO}}$  was assessed by extrapolating the  $1/f$  noise (dashed blue line) up to its crossing point with the  $\beta$ -separation line [22].

a phase noise analyzer (FSWP from Rohde & Schwarz). The assessed CEO frequency noise displayed in Figure 2.10 is not affected by the noise of the auxiliary laser (apart from some isolated peaks) and was thus correctly retrieved. In order to verify the correctness of the CEO noise measurement and to check if the considered combination of signals resulted in the expected compensation of the repetition rate noise, we also measured the sum-frequency component signal at the mixer output as discussed in Ref. [19]. This signal contains two times the noise of the repetition rate and thus shows the same noise features as the repetition rate as displayed in

Figure 2.11, which enabled identifying the correct difference-frequency signal.

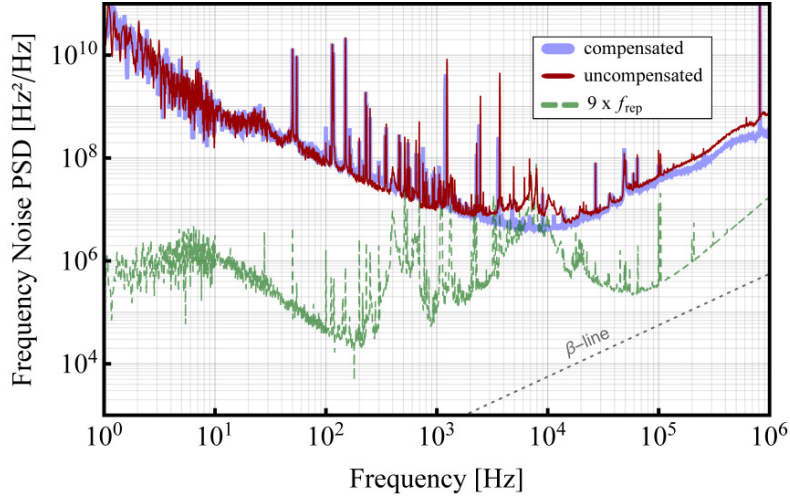


Figure 2.11: Frequency noise PSD corresponding to the up-scaled noise obtained for the two signals at the mixer output (thick light blue line: compensated signal corresponding to the frequency-difference component; thin red line: uncompensated signal corresponding to the sum-frequency component) and comparison with the 9<sup>th</sup> harmonic signal of the repetition rate (thin dashed green line).

At frequencies higher than  $\sim 10$  kHz, the measured CEO noise was limited by the noise floor of the experimental setup, which resulted from an RF synthesizer used to frequency down-convert the signal of the harmonics of  $f_{\text{rep}}$ , as previously discussed [19]. Therefore, we extrapolated the  $1/f$  noise of the CEO signal to higher frequencies (blue dashed line in Figure 2.10) to estimate the feedback bandwidth that would be required to achieve a tight CEO lock in a future self-referencing setup. From the crossing point of the extrapolated noise spectrum with the  $\beta$ -separation line [22], we assessed a full width at half maximum of the CEO beat of  $\sim 1.5$  MHz (1-s observation time) and a corresponding required feedback bandwidth of  $\sim 300$  kHz.

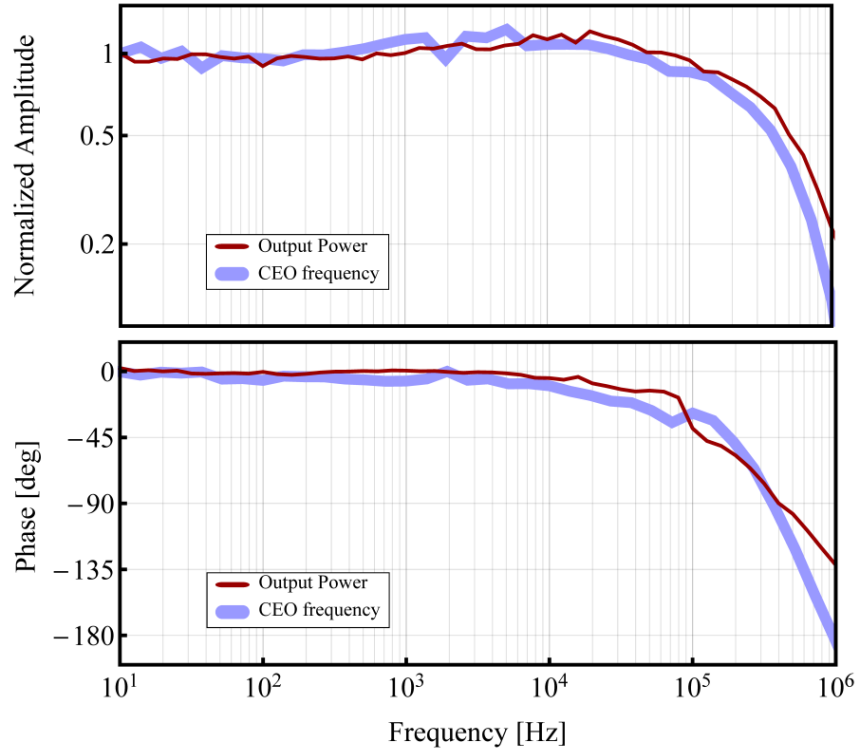


Figure 2.12: Normalized amplitude (top) and phase (bottom) of the measured transfer functions of the VECSEL CEO frequency (thick blue line) and output power (thin red line) obtained for a direct modulation of the pump current. The phase of  $f_{\text{CEO}}$  has been offset by  $180^\circ$  to facilitate the comparison with the phase of the output power transfer function.

To assess if such bandwidth would be achievable using a direct modulation of the pump power via the pump current, we measured the modulation response of  $f_{\text{CEO}}$ . We used the same general setup as before, but demodulated the output signal using a frequency discriminator [21] and a lock-in amplifier referenced to the pump diode modulation applied using our fast modulation electronics. Figure 2.12 shows the measured amplitude and phase of the pump current to  $f_{\text{CEO}}$  transfer function. For comparison, we also measured the transfer function of the VECSEL output power for the same pump current modulation, as it generally has a similar behavior [23], which is indeed the case here. The amplitude of the transfer functions is constant up to at least 100 kHz, resulting in a 3-dB bandwidth

of  $\sim 300$  kHz for  $f_{\text{CEO}}$  modulation. At this frequency, the corresponding phase shift is approximately  $-90^\circ$ . The CEO modulation capability of this VECSEL is significantly faster than usually encountered in DPSSLs or fiber lasers, resulting from the much shorter upper state lifetime in the semiconductor gain. The VECSEL CEO transfer function reported here is not limited by the carrier lifetime, which is much shorter, but by the cavity dynamics [23]. The fast modulation capability of the VECSEL is promising for a future self-referencing stabilization loop.

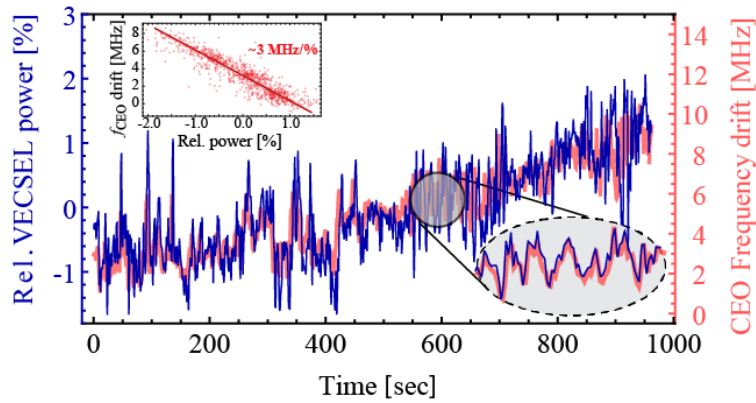


Figure 2.13: CEO frequency drift (thick light red trace) measured by heterodyning the VECSEL emission with the DFB auxiliary laser frequency-locked to an Er:fiber comb fully-stabilized to an H-maser and comparison with the VECSEL output power (thin dark blue line). The inset in the right-bottom corner displays a zoom of the traces over 70 seconds and the top-left inset shows the high correlation between the drift of  $f_{\text{CEO}}$  and the relative variations of the VECSEL output power with a slope of  $\sim 3$  MHz/%.

Finally, we also measured the frequency drift of  $f_{\text{CEO}}$  by recording the beat signal between an optical frequency reference  $\nu_{\text{laser}}$  and one optical mode of the VECSEL (with  $f_{\text{rep}}$  stabilized to an RF synthesizer that was referenced to an H-maser). The optical reference was made of the cw DFB laser stabilized to a line of the SC spectrum of a commercial fully-stabilized Er:fiber frequency comb referenced to the H-maser. In this scheme, the slow frequency fluctuations of the beat signal only reflect the variations of the VECSEL CEO frequency, as all other frequencies ( $f_{\text{rep}}$ ,

$\nu_{\text{laser}}$ ) were stabilized. A slow drift of  $\sim 8$  MHz was observed in 15 min. Furthermore, we measured at the same time the relative variations of the VECSEL output power. A strong correlation was observed between the variations of  $f_{\text{CEO}}$  and the VECSEL output power as shown in Figure 2.13. The intensity noise of the pump diode was likely responsible for this effect. Therefore, a feedback loop acting on the pump diode current is expected to be highly efficient for  $f_{\text{CEO}}$  noise reduction with a large bandwidth, enabling a tight CEO lock to be reached in future self-referencing experiments.

In conclusion, we reported the first thorough analysis of the noise and modulation properties of the CEO beat in a modelocked VECSEL. This was realized using a novel approach that we recently proposed to characterize the CEO beat without directly detecting it using standard  $f$ -to- $2f$  interferometry. Our results show that a modulation of  $f_{\text{CEO}}$  can be achieved by direct pump current modulation with a 3-dB bandwidth of around 300 kHz, which is comparable to the feedback bandwidth needed to achieve a tight CEO lock in a future self-referencing scheme estimated from our noise measurements. These results pave the way for the first self-referencing of a modelocked semiconductor laser that is our next target.

**Funding.** Nano-Tera.ch MIXSEL II (20NA21\_145932); EU-FP7 ITN FACT (PITN-GA-2013-607493).

## 2.4.1 References

- [1] H. R. Telle, G. Steinmeyer, A. E. Dunlop, J. Stenger, D. H. Sutter, and U. Keller, "Carrier-envelope offset phase control: A novel concept for absolute optical frequency measurement and ultrashort pulse generation," *Appl. Phys. B* **69**(4), 327–332 (1999).
- [2] D. J. Jones, S. A. Diddams, J. K. Ranka, A. Stentz, R. S. Windeler, J. L. Hall, and S. T. Cundiff, "Carrier-Envelope Phase Control of

- Femtosecond Mode-Locked Lasers and Direct Optical Frequency Synthesis," *Science* **288**(5466), 635–639 (2000).
- [3] A. Apolonski, A. Poppe, G. Tempea, C. Spielmann, T. Udem, R. Holzwarth, T. W. Hänsch, and F. Krausz, "Controlling the Phase Evolution of Few-Cycle Light Pulses," *Phys. Rev. Lett.* **85**(4), 740–743 (2000).
- [4] T. W. Hänsch, "Nobel Lecture: Passion for precision," *Rev. Mod. Phys.* **78**(4), 1297–1309 (2006).
- [5] J. Ye, H. Schnatz, and L. W. Hollberg, "Optical frequency combs: from frequency metrology to optical phase control," *IEEE J. Sel. Top. Quantum Electron.* **9**(4), 1041–1058 (2003).
- [6] S. A. Diddams, L. Hollberg, and V. Mbele, "Molecular fingerprinting with the resolved modes of a femtosecond laser frequency comb," *Nature* **445**(7128), 627–630 (2007).
- [7] S. Schiller, "Spectrometry with frequency combs," *Opt. Lett.* **27**(9), 766–768 (2002).
- [8] U. Keller, "Ultrafast solid-state laser oscillators: a success story for the last 20 years with no end in sight," *Appl. Phys. B* **100**(1), 15–28 (2010).
- [9] B. R. Washburn, S. A. Diddams, N. R. Newbury, J. W. Nicholson, M. F. Yan, and C. G. Jørgensen, "Phase-locked, erbium-fiber-laser-based frequency comb in the near infrared," *Opt. Lett.* **29**(3), 250–252 (2004).
- [10] S. Schilt, N. Bucalovic, V. Dolgovskiy, C. Schori, M. C. Stumpf, G. Di Domenico, S. Pekarek, A. E. H. Oehler, T. Südmeyer, U. Keller, and P. Thomann, "Fully stabilized optical frequency comb with sub-radian CEO phase noise from a SESAM-modelocked 1.5- $\mu\text{m}$  solid-state laser," *Opt. Express* **19**(24), 24171–24181 (2011).
- [11] A. Klenner, S. Schilt, T. Südmeyer, and U. Keller, "Gigahertz frequency comb from a diode-pumped solid-state laser," *Opt. Express* **22**(25), 31008 (2014).

- [12] C.-C. Lee, C. Mohr, J. Bethge, S. Suzuki, M. E. Fermann, I. Hartl, and T. R. Schibli, "Frequency comb stabilization with bandwidth beyond the limit of gain lifetime by an intracavity graphene electro-optical modulator," *Opt. Lett.* **37**(15), 3084–3086 (2012).
- [13] M. Hoffmann, S. Schilt, and T. Südmeyer, "CEO stabilization of a femtosecond laser using a SESAM as fast opto-optical modulator," *Opt. Express* **21**(24), 30054 (2013).
- [14] S. Koke, C. Grebing, H. Frei, A. Anderson, A. Assion, and G. Steinmeyer, "Direct frequency comb synthesis with arbitrary offset and shot-noise-limited phase noise," *Nat. Photonics* **4**(7), 462–465 (2010).
- [15] G. Krauss, D. Fehrenbacher, D. Brida, C. Riek, A. Sell, R. Huber, and A. Leitenstorfer, "All-passive phase locking of a compact Er: fiber laser system," *Opt. Lett.* **36**(4), 540–542 (2011).
- [16] B. R. Washburn, W. C. Swann, and N. R. Newbury, "Response dynamics of the frequency comb output from a femtosecond fiber laser," *Opt. Express* **13**(26), 10622–10633 (2005).
- [17] B. W. Tilma, M. Mangold, C. A. Zaugg, S. M. Link, D. Waldburger, A. Klenner, A. S. Mayer, E. Gini, M. Golling, and U. Keller, "Recent advances in ultrafast semiconductor disk lasers," *Light Sci. Appl.* **4**(7), e310 (2015).
- [18] C. A. Zaugg, A. Klenner, M. Mangold, A. S. Mayer, S. M. Link, F. Emaury, M. Golling, E. Gini, C. J. Saraceno, B. W. Tilma, and U. Keller, "Gigahertz self-referenceable frequency comb from a semiconductor disk laser," *Opt. Express* **22**(13), 16445–16455 (2014).
- [19] P. Brochard, S. Schilt, V. J. Wittwer, and T. Südmeyer, "Characterizing the carrier-envelope offset in an optical frequency comb without traditional  $f$ -to- $2f$  interferometry," *Opt. Lett.* **40**(23), 5522–5525 (2015).

- [20] D. Waldburger, S. M. Link, M. Mangold, C. G. E. Alfieri, E. Gini, M. Golling, B. W. Tilma, and U. Keller, "High-power 100 fs semiconductor disk lasers," *Optica* **3**(8), 844–852 (2016).
- [21] S. Schilt, N. Bucalovic, L. Tombez, V. Dolgovskiy, C. Schori, G. Di Domenico, M. Zaffalon, and P. Thomann, "Frequency discriminators for the characterization of narrow-spectrum heterodyne beat signals: Application to the measurement of a sub-hertz carrier-envelope-offset beat in an optical frequency comb," *Rev. Sci. Instrum.* **82**(12), 123116 (2011).
- [22] G. Di Domenico, S. Schilt, and P. Thomann, "Simple approach to the relation between laser frequency noise and laser line shape," *Appl. Opt.* **49**(25), 4801–4807 (2010).
- [23] F. Emaury, A. Diebold, A. Klenner, C. J. Saraceno, S. Schilt, T. Südmeyer, and U. Keller, "Frequency comb offset dynamics of SESAM modelocked thin disk lasers," *Opt. Express* **23**(17), 21836 (2015).



# Chapter 3

## Amplification of an ultrafast SDL

The previous chapter showed that the CEO frequency stabilization of the ultrafast SDL via modulation of the laser pump current appears to be achievable. The next step towards the self-referencing of the SDL is to implement a standard  $f$ -to- $2f$  interferometer to directly measure the CEO frequency. As described in the introduction of this thesis, the detection requires a coherent octave-spanning spectrum which is usually generated in a nonlinear fiber such as a PCF. This generation has strong requirements from the laser, namely a peak power of several kW to generate the octave and short pulse durations  $<200$  fs to guarantee the coherence<sup>117</sup>. However the ultrafast SDL described in chapter 2 demonstrates only 150 W of peak power. The first challenge is to obtain sufficient output power from the laser. This is achieved with the implementation of an external amplifier.

In this chapter, the amplification of the ultrafast SDL based on the crystalline waveguide technology developed at the University of Hamburg is presented. The efficient amplification enables generating 2.9 W of output power from only 8.3 mm of crystal length. The following results are a reprint of our publication in Optics Express<sup>118</sup>.

### 3.1 High-power amplification of a femtosecond vertical external-cavity surface-emitting laser in an Yb:YAG waveguide

*Nayara Jornod,<sup>1,\*</sup> Valentin J. Wittwer,<sup>1</sup> Christian Kränkel,<sup>2,3</sup>  
Dominik Waldburger,<sup>4</sup> Ursula Keller,<sup>4</sup> Thomas Südmeyer,<sup>1</sup> and Thomas  
Calmano<sup>2,3</sup>*

<sup>1</sup>Laboratoire Temps-Fréquence, Université de Neuchâtel, CH-2000 Neuchâtel, Switzerland

<sup>2</sup>Institut für Laser-Physik, Universität Hamburg, Luruper Chaussee 149, 22761 Hamburg, Germany

<sup>3</sup>The Hamburg Center for Ultrafast Imaging, Universität Hamburg, Luruper Chaussee 149, 22761 Hamburg, Germany

<sup>4</sup>Department of Physics, Institute for Quantum Electronics, ETH Zürich, 8093 Zürich, Switzerland

**We present the amplification of a mode-locked vertical external-cavity surface-emitting laser (VECSEL) using an Yb:YAG crystalline waveguide as gain medium. The VECSEL seed laser operates at a center wavelength of 1030 nm and generates 300-fs pulses at a repetition rate of 1.77 GHz. An average seed power of 60 mW was launched onto a 8.3 mm long fs-laser written Yb:YAG waveguide pumped by 7.7 W from a 969-nm continuous-wave VECSEL. The amplifier achieves an average output power of up to 2.9 W, corresponding to an amplification factor of 17 dB. Due to gain narrowing, the pulse duration increases to 629 fs. Our results show that crystalline waveguides are a promising technique for the realization of compact multi-watt ultrafast amplifier systems.**

### 3.1.1 Introduction

Ultrafast lasers have undergone rapid and important progress in the last decades, leading to higher output powers, shorter pulse durations and increased peak powers [1–3]. The improved performance of fiber and solid-state ultrafast lasers has revolutionized many fields in fundamental science as well as industrial applications. Ultrashort laser pulses are nowadays routinely implemented in numerous applications such as multiphoton microscopy in medicine and biology, material processing and precision metrology. Most commercial ultrafast systems rely on semiconductor saturable absorber mirrors (SESAMs) [4] for pulse formation. The simplicity and robustness of SESAM-mode locking was important for the commercial success of ultrafast sources in real world applications. Progressing to semiconductor gain materials has the potential to provide even simpler, more compact and less expensive solutions [5–7].

The most suitable semiconductor laser technology for the generation of ultrashort pulses with excellent beam quality and high power levels is based on semiconductor disk lasers (SDLs). They are also known as vertical external-cavity surface-emitting lasers (VECSELs) or optically pumped semiconductor lasers (OPSLs) [8]. The first demonstrated SESAM mode-locked VECSEL [9] was limited in output power to a few milliwatts and to 22-ps pulse duration. Since then, both output power and pulse duration have made huge progress and nowadays the average output power has surpassed 5 W in pulsed operation at sub-picosecond pulse duration [10]. However, the up-scaling of the pulse energy and peak power levels of VECSELs still remains a challenge. Today, mode-locked VECSELs in the fs-regime are limited to 5.1 W of average output power [10] or to 4.35 kW of peak power [11]. Until now, the combination of sub-100 fs pulses and watt-level average output power directly generated by a VECSEL is not achieved.

An alternative to direct power scaling of the mode-locked VECSEL is external amplification of the ultrashort pulses. With fiber amplifiers average power levels above 200 W were generated [12]. The amplified signal was employed for the generation of supercontinuum [13,14] as well as for the first carrier-envelope offset (CEO) frequency detection of a VECSEL [15]. However, the long fiber results in a relatively large footprint of the system. In order to preserve the simplicity of SDLs, an external amplification system should remain compact and easy to integrate.

Crystalline waveguide amplifiers are an attractive technology for this task. Similar to fiber amplifiers they offer high light confinement and a very good overlap between pump and laser mode. Due to an excellent thermal conductivity and high emission and absorption cross sections, multi-watt power levels have been obtained from waveguide lasers that are only few mm-long [16].

In this paper we present the first amplification of a femtosecond VECSEL using a crystalline waveguide. As gain material, we selected Ytterbium-doped  $Y_3Al_5O_{12}$  (Yb:YAG), which is one of the best developed crystalline active materials for channel waveguides in terms of lasing properties, i.e. slope efficiencies and output powers [16–18]. The fabrication of low-loss YAG waveguides has been performed with different techniques such as ion implantation [19], proton beam writing [20] or femtosecond laser writing [21], which enables the direct inscription of refractive index changes in a wide range of dielectric materials. Since the first study of the influence of fs-laser radiation on dielectric material by Davis et al. in 1996 [22], fs-laser writing has shown to be a versatile and efficient method for the fabrication of various active and passive waveguiding optical devices in different materials [21]. For many laser crystals the inscription of two parallel tracks with distances in the order of 20  $\mu\text{m}$  is the method of choice for single mode waveguides with small mode field diameter [23,24]. In this case the refractive index change is induced by stress resulting from the tracks and the waveguiding region

is located in the center between the tracks. Recently, a novel writing scheme has been developed that adds a sinusoidal oscillation to the longitudinal translation during the inscription [25]. With this method the waveguide losses could be decreased and the stress induced by the tracks was increased. This results in a higher refractive index change and thus provides a stronger confinement of the guided modes. Typically, the gain provided by these waveguides is high enough to compensate for very high output-coupling losses and allows for laser oscillation only from the Fresnel-reflection of the waveguides end-facets. All these characteristics led to the demonstration of efficient waveguide lasers with high output powers and low laser thresholds [16,24]. Here, we reveal that such fs-written Yb:YAG waveguides are also very well suited as external amplifiers for ultrashort pulses, demonstrating a gain bandwidth large enough to support femtosecond pulse durations. We show that a femtosecond VECSEL seed source with sub-100 mW average seed power can be amplified to multi-watt output power in a compact Yb:YAG waveguide with only 8.3 mm length. Both femtosecond VECSEL and crystalline waveguide amplifier technologies can be integrated and their combination has a large potential for providing robust and compact multi-watt ultrafast gigahertz repetition rate sources for science and industry.

### 3.1.2 Experimental setup

#### 3.1.2.1 SESAM mode-locked VECSEL oscillator

Our femtosecond seed oscillator is a SESAM mode-locked VECSEL prototype developed at ETH Zurich. The cavity is located in a closed housing for high stability and low noise operation. The design of the ultrafast VECSEL chip is similar to the one described in [26]. The cavity is V-shaped with the VECSEL-chip as folding mirror and the SESAM and output coupler (OC) (radius of curvature of 100 mm and transmission of 1.0% at the laser wavelength) as end mirrors. The VECSEL is pumped under an angle of 45° with a commercially available 808-nm multimode

fiber coupled pump diode typically operated with 19 W of output power. Both the SESAM and the VECSEL are temperature controlled for more stable operation and for optimization of the pulse duration, operation wavelength, and output power.

The operation wavelength was adapted by tuning the temperature of the SESAM and VECSEL chips to be as close as possible to 1030 nm, the peak gain wavelength of Yb:YAG. In stable operation, the central emission wavelength of the seed laser was 1032.6 nm [Figure 3.1(a)] with a pulse duration of 300 fs [Figure 3.1(b)]. The radiofrequency (RF) spectrum [Figure 3.1(c)] reveals stable mode locking with a repetition rate of 1.77 GHz. The average output power is 90 mW with a spectral bandwidth of 4.1 nm full width at half maximum (FWHM) and an  $M^2$  factor of 1.05.

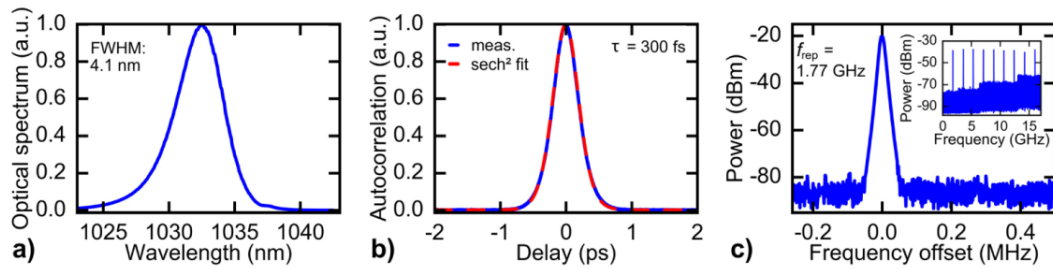


Figure 3.1: Pulse characterization of the seed laser. a) Optical spectrum centered at 1032.6 nm with a FWHM of 4.1 nm. b) Autocorrelation trace (blue) and fit to the autocorrelation of sech<sup>2</sup> pulses (dashed red) corresponding to a pulse duration of 300 fs. c) Microwave spectrum centered at 1.77 GHz measured with a resolution band width (RBW) of 10 kHz. Inset: Wide span RF spectrum of the higher harmonics of the repetition rate measured with a RBW of 100 kHz.

### 3.1.2.2 Yb:YAG waveguide amplifier

The VECSEL seed beam is amplified in an 8.34 mm-long waveguide, which was fabricated by femtosecond laser inscription in a 7% Yb-doped YAG crystal. The waveguiding region is centered between two parallel tracks, separated by 29  $\mu\text{m}$ . The tracks are inscribed by a linear translation with a velocity of 25  $\mu\text{m}/\text{s}$  of the sample perpendicular to the incident fs-

### 3.1 High power amplification of a fs VECSEL in an Yb:YAG waveguide

laser beam. To improve the confinement of the laser mode the translation is superimposed with a sine oscillation with an amplitude of  $3.5\ \mu\text{m}$  and an oscillation frequency of 70 Hz. In contrast to previous waveguides fabricated in Hamburg [16,24,27] a pinhole with  $600\ \mu\text{m}$  diameter was inserted in the beam path of the fs-laser to improve its beam quality by mode cleaning. Due to the large distance between the pinhole and the aspheric focusing lens ( $f = 3.1\ \text{mm}$ ,  $\text{NA} = 0.68$ ) employed for the laser inscription, only the 0<sup>th</sup> order of the resulting diffraction pattern is transmitted through the aperture of this lens. The position of the pinhole was adjusted in such a way that the aperture of the lens was completely filled. After waveguide inscription, the output facet was wedged by approximately  $24^\circ$  to avoid parasitic laser oscillation due to the feedback from the Fresnel-reflections. Afterwards both end-facets were polished.

The amplification setup is shown in Figure 3.2. The waveguide was longitudinally pumped by a continuous-wave (CW) VECSEL providing up to  $\approx 9\ \text{W}$  of output power at a central wavelength of 969 nm. A diode laser emitting 30 W at 814 nm was used to optically pump the CW gain chip. Seed and pump beam are combined with a dichroic mirror and are co-propagating through the waveguide. A lens with a focal length of 30 mm was used for coupling of the pump and the seed beam into the waveguide. The waveguide mode field diameter for the pump and seed wavelength is approximately  $18\ \mu\text{m}$ . After amplification, a dichroic mirror is used as a filter to separate the residual pump and amplified laser light and the nearly collimated beam is split with wedged glass plates. The near field of the waveguide mode is imaged on the chip of a CCD camera (WinCamD-UCD15) with a microscope objective to analyze the mode profile. Simultaneously, we recorded pulse characteristics on an autocorrelator (Femtochrome FR-103), spectral characteristics with an optical spectrum analyzer (Yokogawa AQ6370C), and used an ultrafast photodiode (New Focus Model 1014) and a radiofrequency analyzer (HP8562A) for detecting the repetition rate. The seed and pump power

were measured before the focusing lens and are then corrected by the transmission of the lens (97.5%) and the Fresnel reflection losses on the crystal-air interface (8.4%) in the following. The resulting VECSEL seed power amounted to 60 mW.

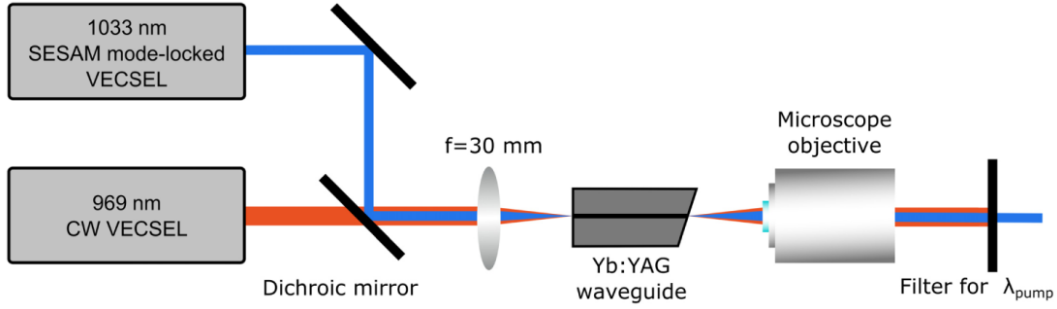


Figure 3.2: Schematic setup for amplification of the mode-locked VECSEL seed beam in the wedged Yb:YAG waveguide.

As a first step, we evaluated the waveguide amplification in the CW-regime. Our seed source was a fiber coupled distributed feedback laser (Eagleyard Photonics EYP-DFB-1030-00500-1500-BFY02-0010). The laser provided a seed power of 42 mW at a wavelength of 1029.6 nm. In this configuration, the maximum amplified output power reached 4.14 W for a pump power of 7.64 W. This corresponds to an amplification factor of 99, i.e. 20 dB.

### 3.1.3 Results and discussion

The characteristics of the amplification of the mode-locked VECSEL are presented in Figure 3.3. A maximum amplified output power of 2.89 W was achieved with a pump power of 7.68 W and a seed power of 60 mW. The corresponding amplification factor is 48 (17 dB), which is two times lower than for the CW seed source. The coupling efficiency  $\eta_c$  of the VECSEL was roughly estimated to 60% by measuring the transmission of the unpumped amplifier for the seed and considering the scattering losses of  $\sim 0.5$  dB/cm, the Fresnel reflection at both end facets as well as the

### 3.1 High power amplification of a fs VECSEL in an Yb:YAG waveguide

small-signal absorption at 1032.6 nm. This estimation neglects bleaching effects and thus overestimates  $\eta_c$ , which could be as low as 40% assuming total bleaching. However, as the coupling efficiency for the CW seed should be in the same order, the lower amplification for the fs-seed beam is not only attributed to a different  $\eta_c$ . In addition the CW seed laser exhibits a narrow spectrum close to the gain maximum of Yb:YAG at 1030 nm [28]. In contrast, the fs-VECSEL seed beam is centered at 1032.6 nm and broader than the gain of our Yb:YAG waveguide [see Figure 3.3(b)]. Consequently, only a part of the 300 fs seed spectrum is successfully amplified and the central wavelength is shifted to 1030.4 nm. This shift is accompanied by a narrowing of the optical bandwidth from the initial 4.1 nm of the fs-seed to 2.1 nm (FWHM) at the output, still supporting 520 fs pulses. The measured pulse duration of 629 fs thus indicates a low effect of self-phase modulation or dispersion during the amplification and the resulting time-bandwidth product of 0.381 is only slightly above the value of 0.315 for ideal  $\text{sech}^2$ -pulses [see Figure 3.3(c), (d)].

A slope efficiency of 50% was achieved for pump powers below 3 W [see Figure 3.3(a)]. The right axis presents the extraction efficiency, calculated as the ratio of amplified output power minus seed power to pump power. The maximum extraction efficiency is 46% at 1.3 W of amplified power and decreases to 37% at maximum output power. This decrease in efficiency results from an increase in the unabsorbed pump that reaches 1.7 W at the maximum amplification and indicates gain saturation. An improved performance can be expected by operating the amplifier in a counterpropagating scheme, improving the spatial overlap of high excitation densities and high signal intensities. The mode profile remains nearly circular even at maximum amplified output power [inset of Figure 3.3(a)] as expected for fs-written waveguides [24].

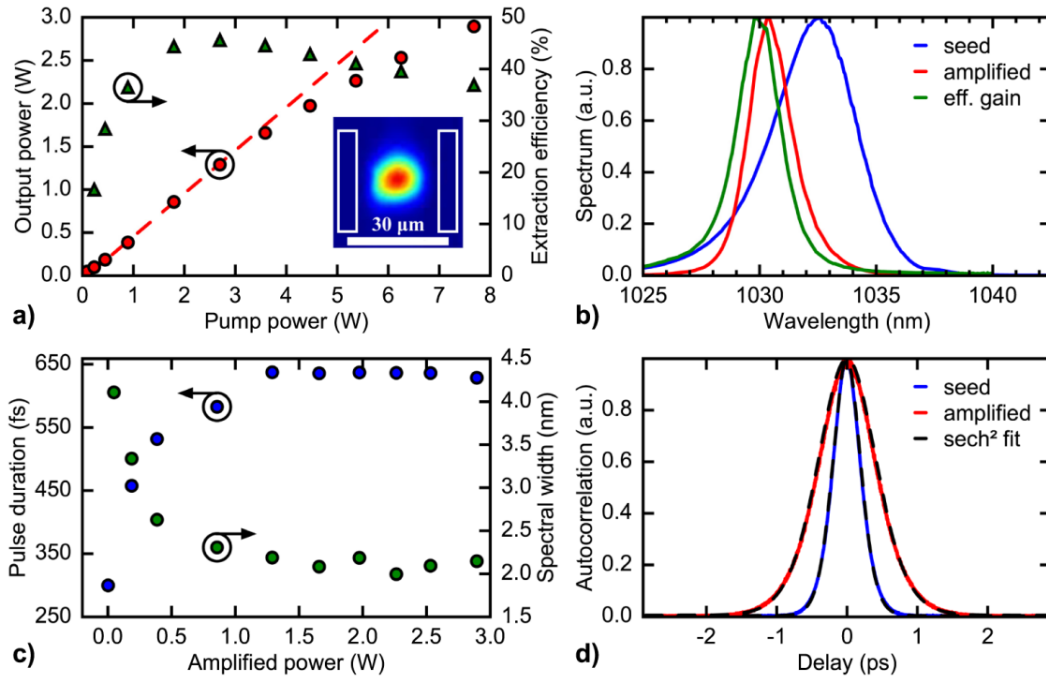


Figure 3.3: Characterization of the amplified signal. a) Amplified signal power as a function of the pump power in red, slope efficiency for pump powers below 3 W (dashed red) and extraction efficiency in green. Inset: beam profile of the amplified seed with a pump power of 7.7 W. The two rectangles represent the inscribed tracks of the waveguide. b) Normalized optical spectrum of the seed in blue with a central wavelength of 1032.6 nm and FWHM of 4.1 nm, of the amplified signal in red with a central wavelength of 1030.4 nm and FWHM of 2.1 nm and the normalized effective gain spectrum of our waveguide amplifier in green (computed from the ratio between amplified and seed spectrum). c) Pulse duration in blue and spectral bandwidth in green as a function of the amplified output power. d) Autocorrelation trace before amplification in blue and with maximum amplified power in red and fit to the autocorrelation of sech<sup>2</sup> pulses corresponding to an amplified signal pulse duration of 629 fs.

In this proof-of-principle demonstration, the achieved amplification factor and efficiency for the fs-seed do not yet reach the values of typical Yb<sup>3+</sup>-doped fiber amplifiers. As an example, the amplification of a VECSEL provides 72% of efficiency and 21 dB of amplification in a 12 m-long fiber [12], corresponding to 0.175 dB/cm. However, our waveguide amplifier is only 8.34 mm long with a corresponding gain per

length of 20 dB/cm and has the potential of a very compact setup and much higher efficiency at better spectral match of seed and amplifier as well as optimized coupling efficiency.

When compared to previous experiments with a low-doped transversally single-sided pumped Yb:YAG planar waveguide amplifier, where 5 passes through a 13 mm long amplifier were necessary to obtain 12 dB of gain [29], the higher doping concentration and the better laser mode confinement in our fs-written waveguide permit an improved efficiency and amplification factor.

### 3.1.4 Conclusion

We have demonstrated the amplification of femtosecond pulses from a semiconductor disk laser in a crystalline waveguide. The forward-pumping amplifier configuration provided 2.89 W average output power pulses with a duration of 629 fs and a repetition rate of 1.77 GHz. This encouraging result promises an elegant way of combining the advantages of ultrafast semiconductor lasers and crystalline waveguides with respect to simplicity and integration. In this experiment, the pump power is not fully absorbed in the waveguide. As a next step, an optimization of the waveguide length, pump scheme and coupling efficiency should lead to higher amplified power. The efficiency and pulse duration are also limited by the offset between the VECSEL emission peak wavelength at 1033 nm and the waveguide gain maximum at 1030 nm. This can be improved by using a femtosecond VECSEL with a better matching center wavelength. Even shorter pulses should be supported by using gain materials with broader emission bandwidth. Particularly promising is Yb:CALGO [27], which exhibits a significantly broader spectral gain bandwidth than Yb:YAG allowing the amplification of the full VECSEL seed spectrum. Finally, an even more compact system could be realized with a mode-locked integrated external-cavity surface emitting laser (MIXSEL) [30] as

seed source, which integrates the semiconductor saturable absorber and the gain chip.

### **Funding**

Deutsche Forschungsgemeinschaft (DFG) (EXC 1074, CA 1380/1-1); Swiss National Science Foundation (SNSF) (146738); Nano-Tera.ch MIXSEL II (20NA21\_145932).

### **3.1.5 References and links**

- [1] U. Keller, "Ultrafast solid-state laser oscillators: a success story for the last 20 years with no end in sight," *Appl. Phys. B* **100**(1), 15–28 (2010).
- [2] C. Jauregui, J. Limpert, and A. Tünnermann, "High-power fibre lasers," *Nat. Photonics* **7**(11), 861–867 (2013).
- [3] M. E. Fermann and I. Hartl, "Ultrafast Fiber Laser Technology," *IEEE J. Sel. Top. Quantum Electron.* **15**(1), 191–206 (2009).
- [4] U. Keller, K. J. Weingarten, F. X. Kärtner, D. Kopf, B. Braun, I. D. Jung, R. Fluck, C. Hönninger, N. Matuschek, and J. Aus der Au, "Semiconductor Saturable Absorber Mirrors (SESAM's) for Femtosecond to Nanosecond Pulse Generation in Solid-State Lasers," *IEEE J. Sel. Top. Quantum Electron.* **2**(3), 435–453 (1996).
- [5] B. W. Tilma, M. Mangold, C. A. Zaugg, S. M. Link, D. Waldburger, A. Klenner, A. S. Mayer, E. Gini, M. Golling, and U. Keller, "Recent advances in ultrafast semiconductor disk lasers," *Light Sci. Appl.* **4**(7), e310 (2015).
- [6] M. A. Gaafar, A. Rahimi-Iman, K. A. Fedorova, W. Stolz, E. U. Rafailov, and M. Koch, "Mode-locked semiconductor disk lasers," *Adv. Opt. Photonics* **8**(3), 370–400 (2016).
- [7] A. Rahimi-Iman, "Recent advances in VECSELs," *J. Opt.* **18**(9), 093003 (2016).

- [8] M. Kuznetsov, F. Hakimi, R. Sprague, and A. Mooradian, "High-Power (>0.5-W CW) Diode-Pumped Vertical-External-Cavity Surface-Emitting Semiconductor Lasers with Circular TEM<sub>00</sub> Beams," *IEEE Photonics Technol. Lett.* **9**(8), 1063–1065 (1997).
- [9] S. Hoogland, S. Dhanjal, A. C. Tropper, J. S. Roberts, R. Häring, R. Paschotta, F. Morier-Genoud, and U. Keller, "Passively Mode-Locked Diode-Pumped Surface-Emitting Semiconductor Laser," *IEEE Photonics Technol. Lett.* **12**(9), 1135–1137 (2000).
- [10] M. Scheller, T.-L. Wang, B. Kunert, W. Stolz, S. W. Koch, and J. V. Moloney, "Passively modelocked VECSEL emitting 682 fs pulses with 5.1 W of average output power," *Electron. Lett.* **48**(10), 588–589 (2012).
- [11] K. G. Wilcox, A. C. Tropper, H. E. Beere, D. A. Ritchie, B. Kunert, B. Heinen, and W. Stolz, "4.35 kW peak power femtosecond pulse mode-locked VECSEL for supercontinuum generation," *Opt. Express* **21**(2), 1599–1605 (2013).
- [12] P. Dupriez, C. Finot, A. Malinowski, J. K. Sahu, J. Nilsson, D. J. Richardson, K. G. Wilcox, H. D. Foreman, and A. C. Tropper, "High-power, high repetition rate picosecond and femtosecond sources based on Yb-doped fiber amplification of VECSELs," *Opt. Express* **14**(21), 9611–9616 (2006).
- [13] C. R. Head, H.-Y. Chan, J. S. Feehan, D. P. Shepherd, S. Alam, A. C. Tropper, J. H. V. Price, and K. G. Wilcox, "Supercontinuum generation with GHz repetition rate femtosecond-pulse fiber-amplified VECSELs," *IEEE Photonics Technol. Lett.* **25**(5), 464–467 (2013).
- [14] A. Chamorovskiy, J. Kerttula, J. Rautiainen, and O. G. Okhotnikov, "Supercontinuum generation with amplified 1.57  $\mu\text{m}$  picosecond semiconductor disk laser," *Electron. Lett.* **48**(16), 1010–1012 (2012).

- [15] C. A. Zaugg, A. Klenner, M. Mangold, A. S. Mayer, S. M. Link, F. Emaury, M. Golling, E. Gini, C. J. Saraceno, B. W. Tilma, and U. Keller, "Gigahertz self-referenceable frequency comb from a semiconductor disk laser," *Opt. Express* **22**(13), 16445–16455 (2014).
- [16] T. Calmano, J. Siebenmorgen, A.-G. Paschke, C. Fiebig, K. Paschke, G. Erbert, K. Petermann, and G. Huber, "Diode pumped high power operation of a femtosecond laser inscribed Yb:YAG waveguide laser [Invited]," *Opt. Mater. Express* **1**(3), 428–433 (2011).
- [17] J. Siebenmorgen, T. Calmano, K. Petermann, and G. Huber, "Highly efficient Yb:YAG channel waveguide laser written with a femtosecond-laser," *Opt. Express* **18**(15), 16035–16041 (2010).
- [18] S. Hakobyan, V. J. Wittwer, K. Hasse, C. Kränkel, T. Südmeyer, and T. Calmano, "Highly efficient Q-switched Yb:YAG channel waveguide laser with 5.6 W of average output power," *Opt. Lett.* **41**(20), 4715–4718 (2016).
- [19] F. Chen, "Micro- and submicrometric waveguiding structures in optical crystals produced by ion beams for photonic applications," *Laser Photonics Rev.* **6**(5), 622–640 (2012).
- [20] A. A. Bettiol, S. Venugopal Rao, T. C. Sum, J. A. van Kan, and F. Watt, "Fabrication of optical waveguides using proton beam writing," *J. Cryst. Growth* **288**(1), 209–212 (2006).
- [21] R. R. Gattass and E. Mazur, "Femtosecond laser micromachining in transparent materials," *Nat. Photonics* **2**(4), 219–225 (2008).
- [22] K. M. Davis, K. Miura, N. Sugimoto, and K. Hirao, "Writing waveguides in glass with a femtosecond laser," *Opt. Lett.* **21**(21), 1729–1731 (1996).
- [23] F. Chen and J. R. Vázquez de Aldana, "Optical waveguides in crystalline dielectric materials produced by femtosecond-laser micromachining," *Laser Photonics Rev.* **8**(2), 251–275 (2014).

- [24] T. Calmano and S. Müller, "Crystalline waveguide lasers in the visible and near-infrared spectral range," *IEEE J. Sel. Top. Quantum Electron.* **21**(1), 401–413 (2015).
- [25] T. Calmano, A.-G. Paschke, S. Müller, C. Kränkel, and G. Huber, "Curved Yb:YAG waveguide lasers, fabricated by femtosecond laser inscription," *Opt. Express* **21**(21), 25501–25508 (2013).
- [26] D. Waldburger, S. M. Link, M. Mangold, C. G. E. Alfieri, E. Gini, M. Golling, B. W. Tilma, and U. Keller, "High-power 100 fs semiconductor disk lasers," *Optica* **3**(8), 844–852 (2016).
- [27] K. Hasse, T. Calmano, B. Deppe, C. Liebald, and C. Kränkel, "Efficient  $\text{Yb}^{3+}:\text{CaGdAlO}_4$  bulk and femtosecond-laser-written waveguide lasers," *Opt. Lett.* **40**(15), 3552–3555 (2015).
- [28] J. Koerner, C. Vorholt, H. Liebetrau, M. Kahle, D. Kloepfel, R. Seifert, J. Hein, and M. C. Kaluza, "Measurement of temperature-dependent absorption and emission spectra of Yb:YAG, Yb:LuAG, and Yb:CaF<sub>2</sub> between 20 °C and 200 °C and predictions on their influence on laser performance," *J. Opt. Soc. Am. B* **29**(9), 2493–2502 (2012).
- [29] C. G. Leburn, C. Y. Ramírez-Corral, I. J. Thomson, D. R. Hall, H. J. Baker, and D. T. Reid, "Femtosecond pulses at 50-W average power from an Yb:YAG planar waveguide amplifier seeded by an Yb:KYW oscillator," *Opt. Express* **20**(16), 17367–17373 (2012).
- [30] D. J. H. C. Maas, A.-R. Bellancourt, B. Rudin, M. Golling, H. J. Unold, T. Südmeyer, and U. Keller, "Vertical integration of ultrafast semiconductor lasers," *Appl. Phys. B* **88**(4), 493–497 (2007).



## Chapter 4

# CEO frequency stabilization of an ultrafast SDL

In the previous chapter, an efficient amplification of an ultrafast SDL was demonstrated in a compact crystalline waveguide. During the process, the pulse duration was broadened to 630 fs and the spectral bandwidth was reduced to 2.1 nm. The resulting peak power is more than 2 kW, which is promising for the generation of the octave spectrum in a nonlinear PCF.

For the detection of the CEO frequency, the spectrum needs also to keep its temporal coherence during the SC generation. Figure 4.1 presents the simulations of the SC spectrum (left graphs) and the degree of coherence (right graphs) in a PCF of 1-m length using a split-step Fourier-transform algorithm, where the pulse propagation in the fiber is described by solving the generalized nonlinear Schrödinger equation. For more details refer to the book by Dudley and Taylor<sup>119</sup>. By launching the laser output directly in the nonlinear fiber, without previous amplification, the simulations show that there is not enough peak power to broaden the spectrum [Figure 4.1(a)]. The amplified pulses on their side would enable the generation of an octave spectrum, however the coherence is

completely lost due to the long pulse duration [Figure 4.1(b)] and therefore no information on the CEO can be retrieved from this spectrum.

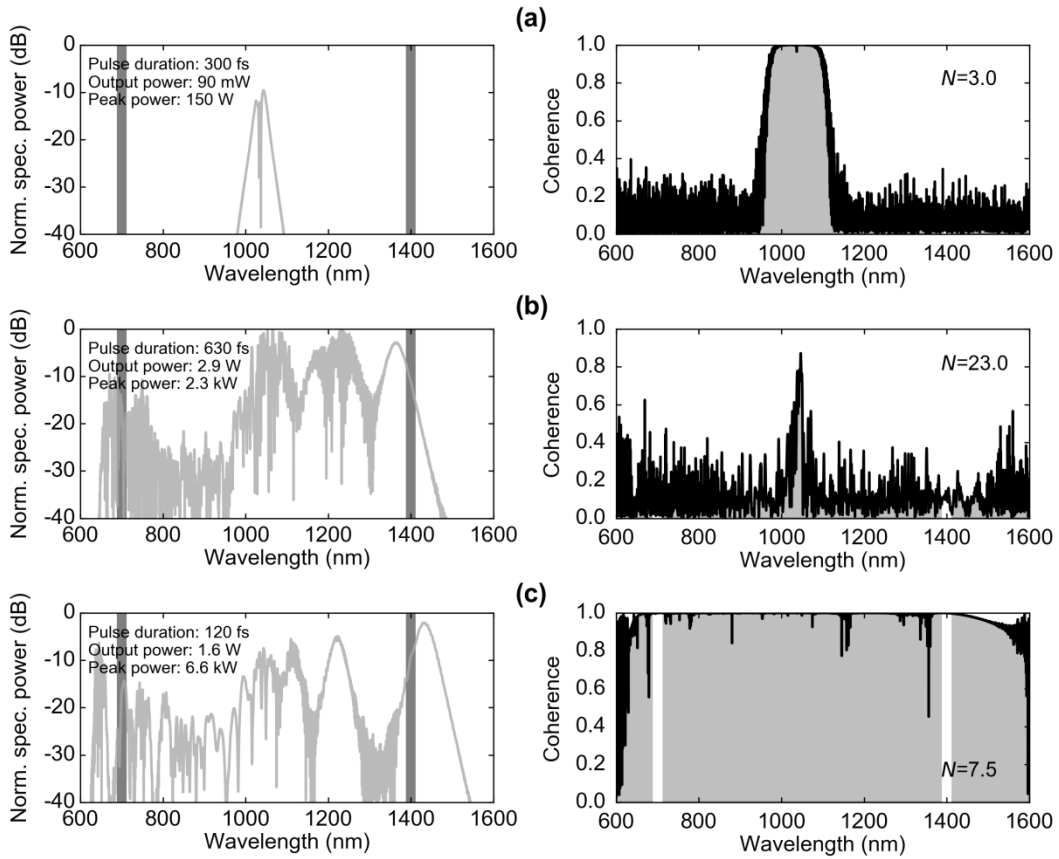


Figure 4.1: Simulated optical spectra (left) and temporal coherence (right) as a function of the wavelength for pulses of (a) the laser output without amplification with 100 mW of output power, 300-fs pulse duration and 150 W of peak power; (b) the amplified pulses of chapter 3 with 2.9 W of output power, 630-fs pulse duration and 2.3 kW of peak power and (c) the amplified and compressed pulses demonstrated in chapter 4 with 1.6 W of output power, 120-fs pulse duration and 6.6 kW of peak power. The vertical lines correspond to the two wavelength used for the detection of the CEO frequency in the  $f$ -to- $2f$  detection scheme.

---

A useful parameter that can be used to estimate the coherence of a SC is the soliton order  $N$  introduced by Dudley *et al.*<sup>117,120</sup>, defined as

$$N = \sqrt{0.283 \tau \frac{P_{\text{av}}}{f_{\text{rep}}} \frac{\gamma}{|\beta_2|}}. \quad (4.1)$$

Here  $\gamma$  is the fiber nonlinear coefficient and  $\beta_2$  its second order dispersion. The soliton order should remain below 10 in order to keep the temporal coherence. For higher values of  $N$ , Raman and dispersive perturbations induce pulse breakup and prevent a coherent SC generation. The soliton order depends on fiber parameters, on the beam power and on the pulse duration. Shortening the pulse duration enables reducing  $N = 23$  for 630-fs pulses to  $N = 7.5$  for short pulses with 120 fs duration. The short pulses enable the generation of a coherent octave-spanning spectrum, as depicted in Figure 4.1(c).

In order to reduce the pulse duration, the pulses need additional spectral broadening and temporal compression stages. Even though this is feasible, it makes the setup pretty complex and lowers the available power.

In this chapter, an alternative technique for the laser amplification is implemented, where the amplifier directly includes a spectral broadening stage. The amplified pulses are then temporally compressed and enable the coherent octave-spanning spectrum generation used for the direct CEO frequency detection in an  $f$ -to- $2f$  interferometer. The ultrafast SDL amplification and temporal compression, the CEO frequency detection and its stabilization are presented in the following Optica publication<sup>121</sup>.

## 4.1 Carrier-envelope offset frequency stabilization of a gigahertz semiconductor disk laser

*N. Jornod,<sup>1,\*</sup> K. Gürel,<sup>1</sup> V. J. Wittwer,<sup>1</sup> P. Brochard,<sup>1</sup> S. Hakobyan,<sup>1</sup>  
S. Schilt,<sup>1</sup> D. Waldburger,<sup>2</sup> U. Keller,<sup>2</sup> and T. Südmeyer<sup>1</sup>*

<sup>1</sup>Laboratoire Temps-Fréquence, Université de Neuchâtel, Av. de Bellevaux 51, CH-2000 Neuchâtel, Switzerland

<sup>2</sup>Department of Physics, Institute for Quantum Electronics, ETH Zürich, CH-8093 Zürich, Switzerland

Optical frequency combs based on ultrafast lasers have enabled numerous scientific breakthroughs. However, their use for commercial applications is limited by the complexity and cost of femtosecond laser technology. Ultrafast semiconductor lasers might change this issue as they can be mass produced in a cost-efficient way while providing large spectral coverage from a single technology. However, it has not been proven to date if ultrafast semiconductor lasers are suitable for stabilization of their carrier-envelope offset (CEO) frequency. Here we present what we believe to be the first CEO frequency stabilization of an ultrafast semiconductor disk laser (SDL). The optically pumped SDL is passively modelocked by a semiconductor saturable absorber mirror. It operates at a repetition rate of 1.8 GHz and a center wavelength of 1034 nm. The 273 fs pulses of the oscillator are amplified to an average power level of 6 W and temporally compressed down to 120 fs. A coherent octave-spanning supercontinuum spectrum is generated in a photonic crystal fiber. The CEO frequency is detected in a standard  $f$ -to- $2f$  interferometer and phase locked to an external reference by feedback applied to the current of the SDL pump diode. This proof-of-principle demonstrates that ultrafast SDLs are suitable for CEO stabilization and constitutes a key step for further developments of this comb technology expected in the coming years.

### 4.1.1 Introduction

Self-referenced optical frequency combs [1–3] have been revolutionizing numerous areas in metrology and spectroscopy. Today, most comb systems rely on ultrafast Ti:sapphire [4] or fiber lasers [5]. Recently, ultrafast diode-pumped solid-state lasers have also been extensively studied [6], and even diode-pumped Ti:sapphire systems have been presented [7]. However, these technologies are usually complex, bulky, and typically restricted to a narrow wavelength emission band enforced by the gain material. In contrast, semiconductor laser technology offers a simple laser system with the potential of a compact and cheaper solution owing to mass production on the wafer scale. Another key advantage of this technology is the wavelength flexibility inherent to the bandgap engineering, which enables emission at central wavelengths ranging from the ultraviolet to the mid-infrared [8,9]. Moreover, they can easily operate in the gigahertz (GHz) repetition rate regime, which leads to an increased optical power per comb mode and to easier access to individual comb lines. Such performance is attractive for application areas such as the calibration of astronomical spectrographs [10,11], the generation of ultra-low-noise microwave signals [12,13], or molecular spectroscopy [14,15]. Among all ultrafast semiconductor lasers, the semiconductor disk laser (SDL) technology, also called optically-pumped vertical external-cavity surface-emitting lasers (VECSELs) [16] has so far achieved the highest average output powers and shortest pulse durations [17,18]. With a semiconductor saturable absorber mirror (SESAM) [19], they provide a simple and compact modelocked laser with the potential for multi-GHz operation [20,21]. For further integration, the SESAM can be combined in the same semiconductor structure as the gain medium, which is referred to as the modelocked integrated external-cavity surface emitting laser (MIXSEL) [22]. VECSELs have been identified as a promising candidate for fully-stabilized frequency combs, as they demonstrate low timing jitter and amplitude noise when stabilized in repetition frequency [23].

However, no stabilization of the carrier-envelope offset (CEO) frequency of a VECSEL has been demonstrated so far. The first detection of the CEO beat from a VECSEL was reported in 2014 [24], and required external amplification and compression of the emitted pulses. The insufficient signal-to-noise ratio (SNR) of the CEO beat hindered detailed noise characterization or frequency stabilization of this system. In 2016, we used an indirect method based on an appropriate combination of different signals from a VECSEL and a continuous-wave laser to characterize both the frequency noise and the modulation bandwidth of the CEO beat for direct pump current modulation [25], without detecting the CEO beat by a standard nonlinear interferometry method [1]. Here we present the first self-referenced stabilization of the CEO frequency of a modelocked semiconductor disk laser with a repetition frequency ( $f_{\text{rep}}$ ) of 1.8 GHz. CEO frequency detection was realized using the standard  $f$ -to- $2f$  interferometry technique after amplification and compression of the laser pulses, resulting in a CEO beat note with an SNR of around 30 dB [in a resolution bandwidth (RBW) of 300 kHz]. The stabilization was achieved by direct pump current modulation, resulting in a residual integrated phase noise of 4.5 rad [1 Hz - 10 MHz] limited by the amplitude noise of the pump diode. The small footprint of the VECSEL and fiber amplifier enables simple and compact systems that are highly attractive for frequency comb applications. Moreover, the fiber amplifier could be replaced by a few-millimeters-long waveguide amplifier to further simplify and integrate the system [26]. In the near future, we expect that VECSEL-based combs will be able to operate without additional amplifiers, combining the higher peak powers [18,27] with the direct octave-spanning supercontinuum generation (SCG) in silicon nitride waveguides [28].

## 4.1.2 Experiment and results

### 4.1.2.1 SESAM modelocked VECSEL

The ultrafast semiconductor disk laser is a VECSEL prototype designed at ETH Zürich. The VECSEL and SESAM structures are described in Ref. [18]. The simple laser cavity consists of only three elements mounted in a V-shaped configuration: the VECSEL gain chip, a SESAM for modelocking operation, and an output coupler with a radius of curvature of 100 mm and a transmission of 1.0%. The cavity length is shorter than 10 cm with a corresponding repetition frequency of 1.8 GHz. The setup is enclosed in an aluminum housing to reduce the influence of external perturbations such as air flows, leading to a higher stability and lower noise operation of the VECSEL. The temperatures of the SESAM and of the VECSEL chip are regulated to 21°C and 19°C, respectively, by means of thermo-electrical coolers, for more stable operation. The VECSEL gain chip is optically pumped with a typical power of 9 W by a multimode (NA = 0.22, core diameter = 100  $\mu\text{m}$ ,  $M^2 = 43$ ) fiber-coupled 808 nm laser diode (LIMO35-F100-DL808-EX2009) that is wavelength stabilized by a volume Bragg grating (VBG). The pump laser is driven in parallel by a high DC current source (Delta Elektronika SM 7.5-80) and a home-built voltage-to-current converter, providing a high bandwidth modulation channel of the pump power for CEO frequency stabilization. We previously measured a modulation bandwidth in the range of 300 kHz (cutoff at -3 dB amplitude or -90° phase shift) for the CEO frequency modulated by the pump power in a similar laser using an indirect method [25]. In addition, a low-pass electrical filter is implemented between the DC current source and the pump diode to filter out the driver noise and to furthermore avoid any cross-talk between the two current drivers.

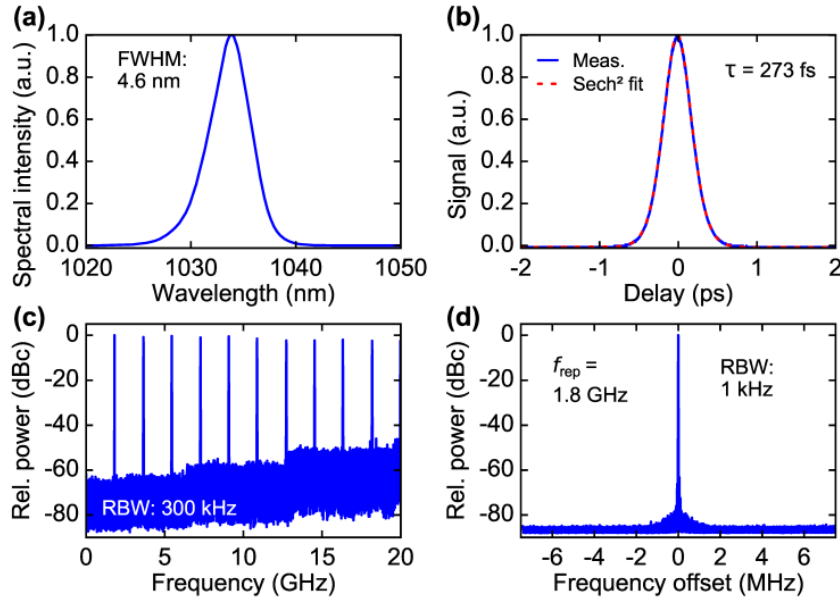


Figure 4.2: Characterization of the modelocked VECSEL. (a) Normalized optical spectrum centered at 1033.9 nm with a FWHM of 4.6 nm. (b) Measured autocorrelation trace (blue curve) with corresponding sech<sup>2</sup> fit (dashed red). (c) Microwave spectrum at a RBW of 300 kHz. (d) Microwave spectrum centered at the repetition frequency of 1.8 GHz with a RBW of 1 kHz.

The laser emits 273 fs pulses at a center wavelength of 1033.9 nm with a spectral full width at half maximum (FWHM) of 4.6 nm, close to the transform limit (see Figure 4.2). The average output power is 60 mW, corresponding to a peak power in the range of 100 W. Since this peak power is insufficient for the generation of a coherent supercontinuum (SC) spectrum in a nonlinear fiber, a Yb-fiber amplification stage has been implemented before the self-referencing CEO frequency detection scheme.

An overview of the complete setup is depicted in Figure 4.3. An optical isolator is placed at the output of the laser to avoid any back-reflection from disturbing the laser operation.

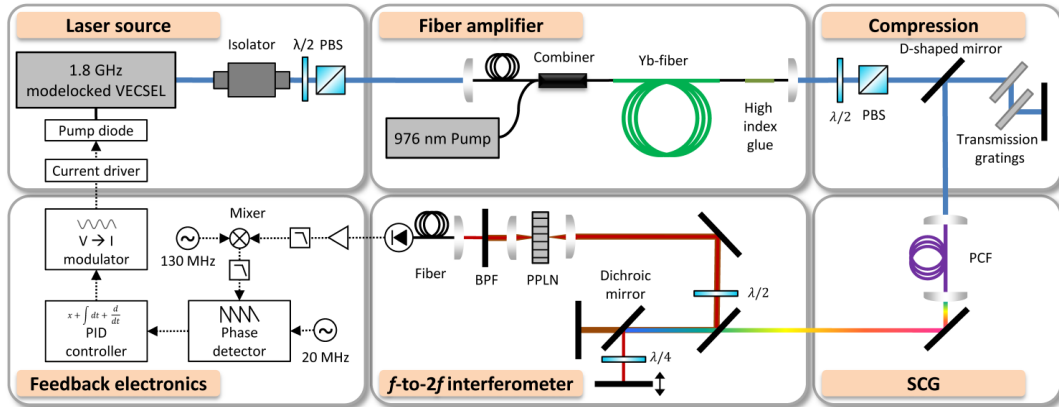


Figure 4.3: Diagram of the complete experimental setup made of the ultrafast laser source with its pump diode and current driver, the fiber amplifier, the compression and supercontinuum generation (SCG) stages, the  $f$ -to- $2f$  interferometer, and the stabilization electronics. PBS, polarizing beamsplitter; PPLN, periodically poled lithium niobate crystal; BPF, bandpass optical filter; PID, proportional-integral-derivative controller.

#### 4.1.2.2 Yb-Fiber amplifier

The amplification stage is made of a 3.5-m-long Yb-doped polarization-maintaining (PM) double-clad fiber with a core diameter of  $6\ \mu\text{m}$  (Coractive DF-YB-6/128S-PM). The fiber is pumped in the forward direction by a commercial VBG-stabilized laser diode (Dilas I5F1P15-976.1-25C-HS1.4) emitting at 976 nm (see setup in Figure 4.3). A multimode pump combiner (MPC) is spliced to combine the 976 nm pump and the 1034 nm polarized signal. An additional length of  $\sim 40$  cm of passive PM fiber is spliced at the end of the gain fiber where the unabsorbed pump light is removed from the fiber cladding using high refractive index acrylate coating to prevent thermal issues at the fiber tip and the use of an additional optical filter at the output.

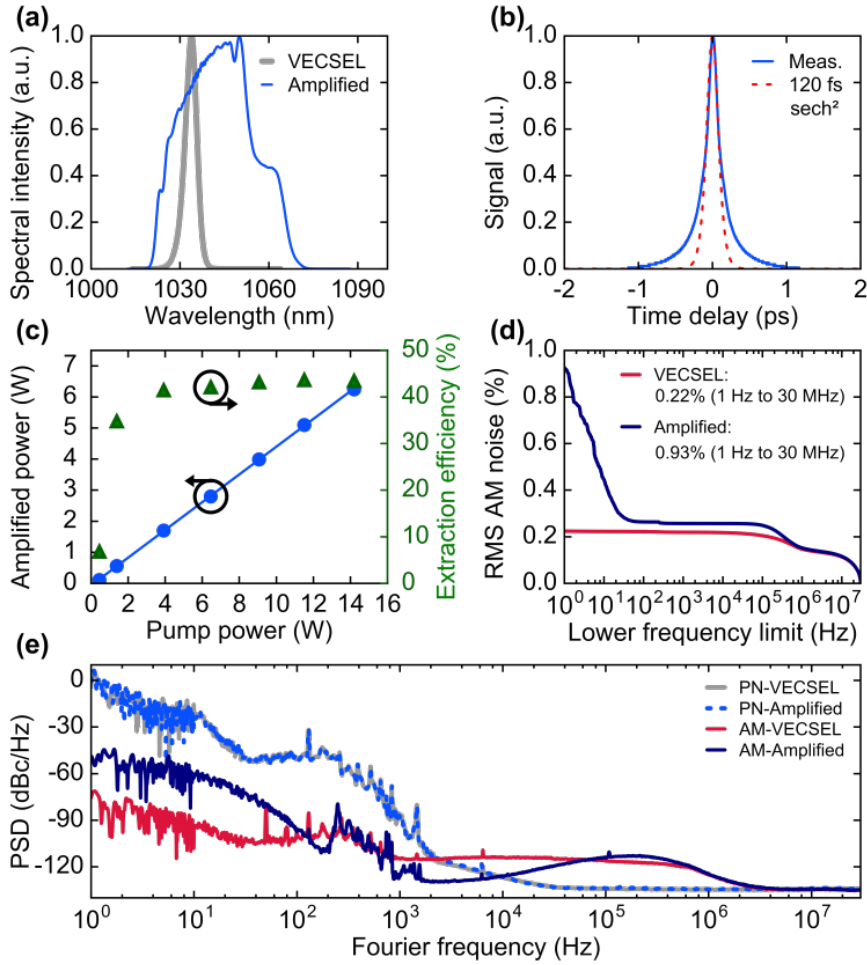


Figure 4.4: Characterization of the fiber amplifier. (a) Normalized optical spectrum of the signal after amplification. (b) Autocorrelation trace of the compressed pulses (blue) and comparison with a 120 fs sech<sup>2</sup> pulse. (c) Amplified signal power as a function of the pump power (blue, left axis) and corresponding extraction efficiency (green, right axis). (d) RMS AM noise as a function of the lower frequency integration limit. (e) Phase noise (PN) power spectral density (PSD) of the repetition frequency before (grey) and after (dashed light blue) the amplification, and AM noise of the repetition frequency before (red) and after (dark blue) the amplification.

The VECSEL seed signal is first sent through polarization selective elements and coupled into a PM fiber with an efficiency of 88%, resulting in a coupled optical power of 46 mW.

The characteristics of the amplifier are shown in Figure 4.4. The pump diode delivers output power up to 25 W, from which only 14 W was used for typical operation of the amplifier, generating an amplified signal power of more than 6 W. The corresponding amplification factor is of the order of  $\sim 130$  (21 dB) and the extraction efficiency, computed as the ratio between the amplified output power minus the seed power and the pump power, is 44%.

The small core diameter of the gain fiber (6  $\mu\text{m}$ ) and the additional passive PM fiber segment enable spectral broadening directly in the amplifier. The 4.6 nm bandwidth (FWHM) of the laser optical spectrum is broadened to more than 25 nm in the amplifier [Figure 4.4(a)]. During amplification, the temporal pulse duration is also broadened to more than 2 ps.

The amplified pulses are then temporally compressed in two transmission gratings in a double-pass configuration (Figure 4.3). At the output, the pulse duration is reduced to sub-120-fs with an average power at the 3 W level. The autocorrelation trace of the compressed pulses [Figure 4.4(b)] shows small distortions from a  $\text{sech}^2$  pulse shape. We believe that a nonlinear chirp is induced during the amplification process, which prevents the compression from achieving the transform-limited pulse duration supported by the optical bandwidth.

The phase noise of the repetition frequency of the optical pulses measured before and after amplification shows a negligible contribution of the amplifier [Figure 4.4(e)]; only significant additional amplitude modulation (AM) noise at frequencies below 100 Hz is observed, increasing the root mean square (RMS) AM noise from 0.2% to 0.9% (1 Hz-30 MHz) [Figure 4.4(d)].

#### 4.1.2.3 CEO beat detection

After compression, an average power of 1.65 W is finally coupled into an angle-polished, collapsed 1-m-long photonic crystal fiber (PCF, NKT

Photonics NL-3.2-945), corresponding to a coupling efficiency of  $\sim 80\%$ , to generate a coherent octave-spanning SC spectrum [see Figure 4.5(a)].

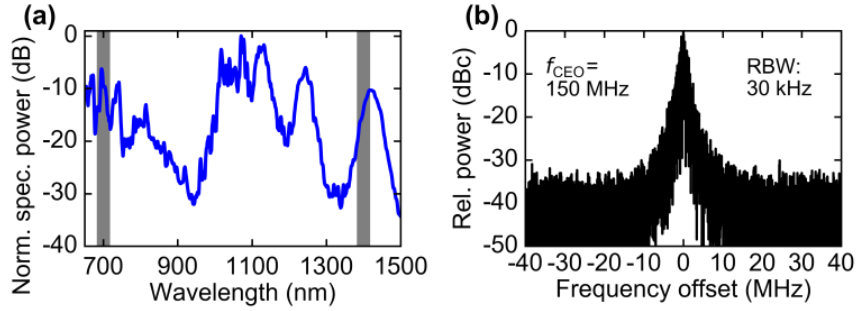


Figure 4.5: (a) Measured octave-spanning SC spectrum generated in the PCF. The grey spectral bands centered at 700 nm and 1400 nm are used for CEO beat detection in the  $f$ -to- $2f$  interferometer. (b) Detected free-running CEO beat at 150 MHz with a RBW of 30 kHz.

The SC light is sent to a quasi-common path  $f$ -to- $2f$  interferometer schematized in the bottom part of Figure 4.3. The 700 nm and 1400 nm components of the spectrum are separated by a dichroic mirror. An adjustable delay line in the low wavelength path enables its temporal tuning. The two spectral components are then recombined using the same mirror and co-propagate through a magnesium-oxide-doped periodically poled lithium niobate (MgO:PPLN) crystal where the 1400 nm light is frequency-doubled (poling period 14  $\mu\text{m}$ , crystal temperature 70°C). A half-wave plate is placed in the common path before the crystal for optimization of the second harmonic generation (SHG) process, and a quarter-wave plate is used in the 700 nm adjustable delay line to align the polarization of the two beams.

The resulting 700 nm light from the two beams is optically bandpass filtered at the output of the crystal and is coupled into a single-mode fiber to ensure an optimum spatial overlap. Their beat signal is detected using a variable-gain avalanche photodetector (Thorlabs APD430A/M) with a

bandwidth of 400 MHz for stabilization and a fast photodetector (New Focus 1014, 45 GHz bandwidth) for static tuning curve measurements. The detected CEO beat has an SNR of  $\sim 30$  dB in a 300 kHz RBW. Figure 4.5(b) shows the typical free-running CEO beat measured at  $\sim 150$  MHz and used later for stabilization. The photodiode output signal is bandpass filtered and amplified. We observed a strong dependence of the CEO frequency  $f_{\text{CEO}}$  to the operation mode of the VECSEL. Changes in the laser parameters (such as fine cavity alignment, pump power, gain, or SESAM temperature) were used to efficiently tune the CEO beat note to a desired frequency in the detector bandwidth. A characterization of the tuning curve of  $f_{\text{CEO}}$  as a function of the current of the VECSEL pump diode is shown in Figure 4.6(a) for CEO frequencies in the range of 500 MHz. The tuning coefficient is  $\sim 0.3$  MHz/mA.

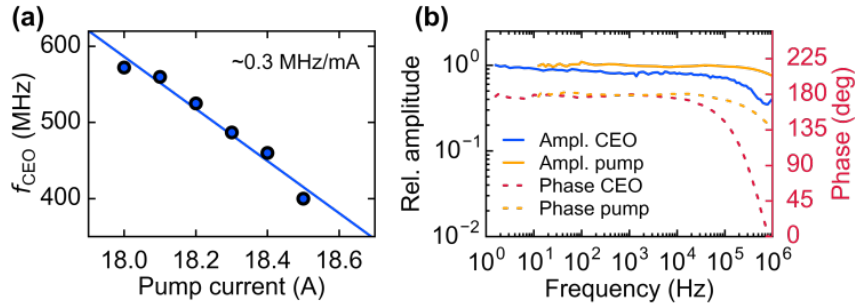


Figure 4.6: (a) Static tuning curve of the CEO frequency with the pump current. (b) Left axis: relative amplitude of the transfer functions of the pump optical power (orange) and of  $f_{\text{CEO}}$  (blue) for a modulation of the pump current. Right axis: phase of the transfer functions of the pump optical power (dashed orange) and of  $f_{\text{CEO}}$  (red) for a modulation of the pump current.

The dynamic response of  $f_{\text{CEO}}$  to a modulation of the pump current was measured in amplitude and phase using a frequency discriminator [29] and a lock-in amplifier (Zurich Instrument HF2LI). The measured transfer function has a -3 dB cutoff frequency of  $\sim 300$  kHz with a corresponding phase shift of approximately  $-90^\circ$  [see Figure 4.6(b)]. This result is in good agreement with our previous measurement performed

indirectly in a similar laser without detecting the CEO beat by  $f$ -to- $2f$  interferometry [25]. In addition, we also measured the transfer function of the optical power of the pump diode [see orange curves in Figure 4.6(b)]. The observed modulation bandwidth is larger than 1 MHz, which is broader than the measured response of  $f_{\text{CEO}}$ . Therefore, the modulation bandwidth of  $f_{\text{CEO}}$  is neither limited by the pump driving electronics, nor by the modulation response of the pump diode itself, but more likely by the cavity dynamics in our laser (the short upper-state lifetime in the semiconductor gain is not expected to be a limitation).

We measured the frequency noise power spectral density (FN-PSD) of the free-running CEO beat using a phase noise analyzer (Rohde-Schwarz FSWP26). The result is presented in Figure 4.7 (blue curve). The corresponding free-running CEO linewidth calculated using the approximation of the  $\beta$ -separation line [30] is 1.3 MHz (at 1 s integration time). A feedback bandwidth in the range of 600 kHz is estimated to be necessary to achieve a tight CEO lock from the crossing point of the CEO FN-PSD with the  $\beta$ -separation line. This is 2 times larger than our previous estimation made for a similar VECSEL without directly detecting the CEO beat [25]. The reason is the higher frequency noise observed here at Fourier frequencies above  $\sim 1$  kHz compared to the  $1/f$  noise behavior extrapolated in our previous study, where the noise measurement was limited by the experimental noise floor at high Fourier frequencies. To understand the origin of this high frequency noise plateau observed at Fourier frequencies between 1 kHz and  $\sim 300$  kHz, we investigated the contribution of the pump noise. We measured the relative intensity noise (RIN) of the pump diode and calculated its contribution to the CEO FN-PSD using the previously recorded frequency response of  $f_{\text{CEO}}$  for pump current modulation (Figure 4.6). The resulting pump-induced frequency noise, depicted in orange in Figure 4.7, overlaps fairly well with the measured free-running CEO FN-PSD at Fourier frequencies above 1 kHz,

demonstrating that the high  $f_{\text{CEO}}$  noise originates from the AM noise of the pump diode.

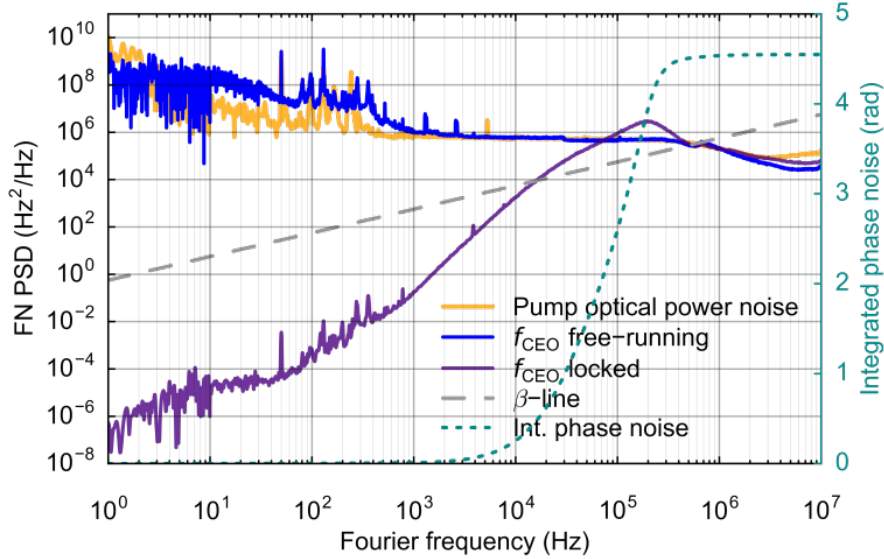


Figure 4.7: Left axis: measured frequency noise PSD of the free-running (blue) and stabilized (violet) CEO signal, and pump-induced frequency noise (orange) calculated from the measured pump RIN multiplied by the pump-power-to- $f_{\text{CEO}}$  transfer function. Right axis: integrated phase noise of the stabilized CEO signal as a function of the upper cut-off frequency.

#### 4.1.2.4 CEO stabilization

The amplified CEO beat note was first frequency down-converted to  $\sim 20$  MHz for comparison to a reference signal from a function generator in a digital phase detector (Menlo Systems DXD200; see bottom part of Figure 4.3). The phase error signal was sent to an analog proportional-integral-derivative (PID) servo-controller (Vescent Photonics D2-125) and the feedback signal was directly applied to our home-built voltage-to-current converter to modulate the VECSEL pump power. The FN-PSD of the stabilized CEO beat displayed in violet in Figure 4.7 shows a clear noise reduction compared to the free-running CEO beat signal at Fourier frequencies up to  $\sim 100$  kHz. The FN-PSD is reduced below the

$\beta$ -separation line at all frequencies below  $\sim 20$  kHz, but it remains above the line in the range of 20-500 kHz, especially at the servo bump ( $\sim 200$  kHz). As a consequence, a tight CEO lock is not achieved in the present situation, and the integrated phase noise is 4.5 rad [1 Hz - 10 MHz]. As shown in Section 4.1.2.3, the AM noise of the pump diode is responsible for the free-running  $f_{\text{CEO}}$  noise at frequencies above 1 kHz, increasing the necessary feedback bandwidth and preventing the achievement of a tight lock.

The achieved integrated phase noise does not compete with the performance reached today by established femtosecond frequency combs, such as 14 mrad integrated phase noise demonstrated by a monolithic Er:Yb:glass laser ( $f_{\text{rep}} = 1$  GHz) [31], 29 mrad from a Ti:sapphire laser ( $f_{\text{rep}} = 75$  MHz) [32] or 68 mrad (out-of-loop) from an Er:fiber laser ( $f_{\text{rep}} = 250$  MHz) with the use of a high bandwidth intra-cavity actuator [33]. However, this is a similar situation than for the first proof-of-principle demonstrations of other comb technologies, such as the first Er:fiber comb that operated at 50 MHz repetition rate with  $\sim 20$  rad integrated phase noise (computed by upscaling the measured 50 mrad phase noise of the frequency-divided CEO beat by the division factor of 400) [34].

### 4.1.3 Conclusion

We have demonstrated what is, to the best of our knowledge, the first CEO frequency stabilization of a modelocked semiconductor laser. The 1.8 GHz VECSEL is amplified and spectrally-broadened in a double clad fiber amplifier, enabling 120-fs pulses and the generation of a coherent octave-spanning SC spectrum. The CEO frequency is detected with an  $f$ -to- $2f$  interferometer at an SNR of  $\sim 30$  dB (300 kHz RBW), which is sufficient for stabilization. Although the VECSEL is pumped by a highly multimode ( $M^2 = 43$ ) fiber-coupled diode laser, we were able to stabilize

the CEO beat note via modulation of the pump laser current with a residual integrated phase noise of 4.5 rad [1 Hz - 10 MHz].

The high frequency noise of the CEO beat that prevents the achievement of a better lock was shown to originate from the AM noise of the pump diode. Therefore, reducing this noise would lower the CEO noise. This could be achieved by investigating the use of other pump sources or by implementing an amplitude stabilization of the pump that might significantly reduce the noise level. Combining two feedback loops to the pump current acting in different bandwidths on the pump power and CEO frequency could be a way to reduce the CEO phase noise and improve the lock performance.

Finally, another alternative to increase the bandwidth of the CEO corrections and reduce the residual CEO noise would be to implement a feedforward loop using a frequency shifter acousto-optic modulator, as previously demonstrated with a Ti:sapphire comb [35] instead of the feedback loop used here.

Moreover, the ultrafast VECSEL technology is steadily evolving, and recently 101 fs pulses with 1 kW peak power were demonstrated [36]. This peak power level and pulse duration appear sufficient to suppress the amplification stage and generate the octave-spanning SC directly in millimeter-long silicon nitride waveguides [28].

**Funding.** Nano-Tera.ch MIXSEL II (20NA21\_145932).

#### 4.1.4 References

- [1] H. R. Telle, G. Steinmeyer, A. E. Dunlop, J. Stenger, D. H. Sutter, and U. Keller, "Carrier-envelope offset phase control: A novel concept for absolute optical frequency measurement and ultrashort pulse generation," *Appl. Phys. B* **69**(4), 327–332 (1999).
- [2] D. J. Jones, S. A. Diddams, J. K. Ranka, A. Stentz, R. S. Windeler, J. L. Hall, and S. T. Cundiff, "Carrier-Envelope Phase Control of

- Femtosecond Mode-Locked Lasers and Direct Optical Frequency Synthesis," *Science* **288**(5466), 635–639 (2000).
- [3] A. Apolonski, A. Poppe, G. Tempea, C. Spielmann, T. Udem, R. Holzwarth, T. W. Hänsch, and F. Krausz, "Controlling the Phase Evolution of Few-Cycle Light Pulses," *Phys. Rev. Lett.* **85**(4), 740–743 (2000).
- [4] A. Bartels, D. Heinecke, and S. A. Diddams, "10-GHz self-referenced optical frequency comb," *Science* **326**(5953), 681 (2009).
- [5] M. E. Fermann and I. Hartl, "Ultrafast Fiber Laser Technology," *IEEE J. Sel. Top. Quantum Electron.* **15**(1), 191–206 (2009).
- [6] S. Hakobyan, V. J. Wittwer, P. Brochard, K. Gürel, S. Schilt, A. S. Mayer, U. Keller, and T. Südmeyer, "Full stabilization and characterization of an optical frequency comb from a diode-pumped solid-state laser with GHz repetition rate," *Opt. Express* **25**(17), 20437–20453 (2017).
- [7] K. Gürel, V. J. Wittwer, S. Hakobyan, S. Schilt, and T. Südmeyer, "Carrier envelope offset frequency detection and stabilization of a diode-pumped mode-locked Ti:sapphire laser," *Opt. Lett.* **42**(6), 1035–1038 (2017).
- [8] S.-H. Park, J. Kim, H. Jeon, T. Sakong, S.-N. Lee, S. Chae, Y. Park, C.-H. Jeong, G.-Y. Yeom, and Y.-H. Cho, "Room-temperature GaN vertical-cavity surface-emitting laser operation in an extended cavity scheme," *Appl. Phys. Lett.* **83**(11), 2121–2123 (2003).
- [9] M. Rahim, M. Arnold, F. Felder, K. Behfar, and H. Zogg, "Midinfrared lead-chalcogenide vertical external cavity surface emitting laser with 5  $\mu\text{m}$  wavelength," *Appl. Phys. Lett.* **91**(15), 151102 (2007).
- [10] C.-H. Li, A. J. Benedick, P. Fendel, A. G. Glenday, F. X. Kärtner, D. F. Phillips, D. Sasselov, A. Szentgyorgyi, and R. L. Walsworth, "A laser

- frequency comb that enables radial velocity measurements with a precision of 1 cm s<sup>-1</sup>," *Nature* **452**(7187), 610–612 (2008).
- [11] T. Steinmetz, T. Wilken, C. Araujo-Hauck, R. Holzwarth, T. W. Hänsch, L. Pasquini, A. Manescau, S. D’Odorico, M. T. Murphy, T. Kentischer, W. Schmidt, and T. Udem, "Laser Frequency Combs for Astronomical Observations," *Science* **321**(5894), 1335–1337 (2008).
- [12] T. M. Fortier, M. S. Kirchner, F. Quinlan, J. Taylor, J. C. Bergquist, T. Rosenband, N. Lemke, A. Ludlow, Y. Jiang, C. W. Oates, and S. A. Diddams, "Generation of ultrastable microwaves via optical frequency division," *Nat. Photonics* **5**(7), 425–429 (2011).
- [13] X. Xie, R. Bouchand, D. Nicolodi, M. Giunta, W. Hänsel, M. Lezius, A. Joshi, S. Datta, C. Alexandre, M. Lours, P.-A. Tremblin, G. Santarelli, R. Holzwarth, and Y. L. Coq, "Photonic microwave signals with zeptosecond-level absolute timing noise," *Nat. Photonics* **11**(1), 44–47 (2017).
- [14] S. Schiller, "Spectrometry with frequency combs," *Opt. Lett.* **27**(9), 766–768 (2002).
- [15] S. M. Link, D. J. H. C. Maas, D. Waldburger, and U. Keller, "Dual-comb spectroscopy of water vapor with a free-running semiconductor disk laser," *Science* **356**(6343), 1164–1168 (2017).
- [16] O. G. Okhotnikov, *Semiconductor Disk Lasers: Physics and Technology* (John Wiley & Sons, 2010).
- [17] B. Rudin, V. J. Wittwer, D. J. H. C. Maas, M. Hoffmann, O. D. Sieber, Y. Barbarin, M. Golling, T. Südmeyer, and U. Keller, "High-power MIXSEL: an integrated ultrafast semiconductor laser with 6.4 W average power," *Opt. Express* **18**(26), 27582–27588 (2010).
- [18] D. Waldburger, S. M. Link, M. Mangold, C. G. E. Alfieri, E. Gini, M. Golling, B. W. Tilma, and U. Keller, "High-power 100 fs semiconductor disk lasers," *Optica* **3**(8), 844–852 (2016).

- [19] U. Keller, K. J. Weingarten, F. X. Kärtner, D. Kopf, B. Braun, I. D. Jung, R. Fluck, C. Hönninger, N. Matuschek, and J. Aus der Au, "Semiconductor Saturable Absorber Mirrors (SESAM's) for Femtosecond to Nanosecond Pulse Generation in Solid-State Lasers," *IEEE J. Sel. Top. Quantum Electron.* **2**(3), 435–453 (1996).
- [20] B. W. Tilma, M. Mangold, C. A. Zaugg, S. M. Link, D. Waldburger, A. Klenner, A. S. Mayer, E. Gini, M. Golling, and U. Keller, "Recent advances in ultrafast semiconductor disk lasers," *Light Sci. Appl.* **4**(7), e310 (2015).
- [21] D. Lorensen, D. J. H. C. Maas, H. J. Unold, A.-R. Bellancourt, B. Rudin, E. Gini, D. Ebling, and U. Keller, "50-GHz Passively Mode-Locked Surface-Emitting Semiconductor Laser With 100-mW Average Output Power," *IEEE J. Quantum Electron.* **42**(8), 838–847 (2006).
- [22] D. J. H. C. Maas, A.-R. Bellancourt, B. Rudin, M. Golling, H. J. Unold, T. Südmeyer, and U. Keller, "Vertical integration of ultrafast semiconductor lasers," *Appl. Phys. B* **88**(4), 493–497 (2007).
- [23] V. J. Wittwer, R. van der Linden, B. W. Tilma, B. Resan, K. J. Weingarten, T. Südmeyer, and U. Keller, "Sub-60-fs Timing Jitter of a SESAM Modelocked VECSEL," *IEEE Photonics J.* **5**(1), 1400107 (2013).
- [24] C. A. Zaugg, A. Klenner, M. Mangold, A. S. Mayer, S. M. Link, F. Emaury, M. Golling, E. Gini, C. J. Saraceno, B. W. Tilma, and U. Keller, "Gigahertz self-referenceable frequency comb from a semiconductor disk laser," *Opt. Express* **22**(13), 16445–16455 (2014).
- [25] P. Brochard, N. Jornod, S. Schilt, V. J. Wittwer, S. Hakobyan, D. Waldburger, S. M. Link, C. G. E. Alfieri, M. Golling, L. Devenoges, J. Morel, U. Keller, and T. Südmeyer, "First investigation of the noise and modulation properties of the carrier-envelope offset in a modelocked semiconductor laser," *Opt. Lett.* **41**(14), 3165 (2016).

- [26] N. Jornod, V. J. Wittwer, C. Kränkel, D. Waldburger, U. Keller, T. Südmeyer, and T. Calmano, "High-power amplification of a femtosecond vertical external-cavity surface-emitting laser in an Yb:YAG waveguide," *Opt. Express* **25**(14), 16527–16533 (2017).
- [27] K. G. Wilcox, A. C. Tropper, H. E. Beere, D. A. Ritchie, B. Kunert, B. Heinen, and W. Stolz, "4.35 kW peak power femtosecond pulse mode-locked VECSEL for supercontinuum generation," *Opt. Express* **21**(2), 1599–1605 (2013).
- [28] A. R. Johnson, A. S. Mayer, A. Klenner, K. Luke, E. S. Lamb, M. R. E. Lamont, C. Joshi, Y. Okawachi, F. W. Wise, M. Lipson, U. Keller, and A. L. Gaeta, "Octave-spanning coherent supercontinuum generation in a silicon nitride waveguide," *Opt. Lett.* **40**(21), 5117–5120 (2015).
- [29] S. Schilt, N. Bucalovic, L. Tombez, V. Dolgovskiy, C. Schori, G. Di Domenico, M. Zaffalon, and P. Thomann, "Frequency discriminators for the characterization of narrow-spectrum heterodyne beat signals: Application to the measurement of a sub-hertz carrier-envelope-offset beat in an optical frequency comb," *Rev. Sci. Instrum.* **82**(12), 123116 (2011).
- [30] G. Di Domenico, S. Schilt, and P. Thomann, "Simple approach to the relation between laser frequency noise and laser line shape," *Appl. Opt.* **49**(25), 4801–4807 (2010).
- [31] T. D. Shoji, W. Xie, K. L. Silverman, A. Feldman, T. Harvey, R. P. Mirin, and T. R. Schibli, "Ultra-low-noise monolithic mode-locked solid-state laser," *Optica* **3**(9), 995 (2016).
- [32] T. J. Yu, K.-H. Hong, H.-G. Choi, J. H. Sung, I. W. Choi, D.-K. Ko, J. Lee, J. Kim, D. E. Kim, and C. H. Nam, "Precise and long-term stabilization of the carrier-envelope phase of femtosecond laser pulses using an enhanced direct locking technique," *Opt. Express* **15**(13), 8203–8211 (2007).

- [33] W. Hänsel, M. Giunta, K. Beha, M. Lezius, M. Fischer, and R. Holzwarth, "Ultra-low phase noise all-PM Er:fiber optical frequency comb," in *Advanced Solid State Lasers (2015), Paper ATh4A.2* (Optical Society of America, 2015), p. ATh4A.2.
- [34] B. R. Washburn, S. A. Diddams, N. R. Newbury, J. W. Nicholson, M. F. Yan, and C. G. Jrgensen, "Phase-locked, erbium-fiber-laser-based frequency comb in the near infrared," *Opt. Lett.* **29**(3), 250–252 (2004).
- [35] S. Koke, A. Anderson, H. Frei, A. Assion, and G. Steinmeyer, "Noise performance of a feed-forward scheme for carrier-envelope phase stabilization," *Appl. Phys. B* **104**(4), 799–804 (2011).
- [36] D. Waldburger, C. G. E. Alfieri, S. M. Link, E. Gini, M. Golling, and U. Keller, "High-Power Semiconductor Disk Lasers with Record-Short Pulse Durations," in *European Conference on Lasers and Electro-Optics - European Quantum Electronics Conference* (Optical Society of America, 2017), p. CB-8.1.

# Chapter 5

## Towards longer wavelengths

The development of spectroscopy for the diagnosis of environmental factors such as pollutants detection or atmospheric analysis has strengthened the request for laser sources emitting in the mid-infrared (mid-IR, 2-12  $\mu\text{m}$ ). The mid-IR spectral region gathers two main advantages: first it corresponds to the so-called molecular fingerprint region, where numerous strong molecular rotational-vibrational absorption lines appear, as pictured in Figure 5.1.

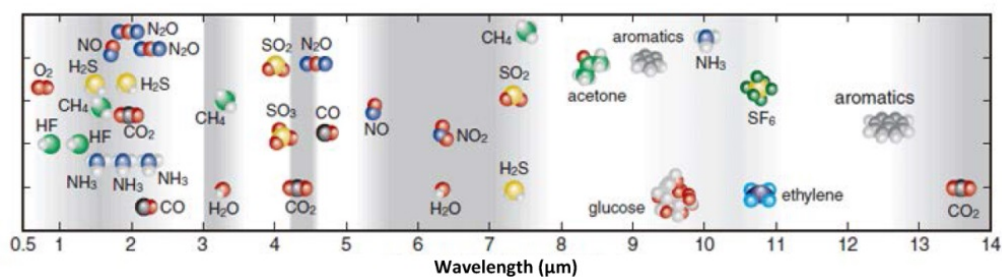


Figure 5.1: Molecular fingerprint region. Figure taken from [www.hamamatsu.com](http://www.hamamatsu.com).

Secondly the mid-IR contains several transparent windows of the atmosphere. The development of frequency combs emitting at these

wavelengths enables an improvement in precision, sensitivity, recording time and spectral bandwidth of molecular spectroscopy.

The SDL technology studied in this thesis is currently limited to emission at 2  $\mu\text{m}$  in the pulsed regime<sup>107</sup>. Several well developed visible and IR sources are difficult to extend to the longer wavelength region. Solid-state technology is pretty rare above 3  $\mu\text{m}$ , even though recent development of solid-state lasers has demonstrated emission between 4  $\mu\text{m}$  and 5  $\mu\text{m}$ <sup>122</sup>. A promising technology is the quantum cascade laser (QCL), which has a good wavelength versatility thanks to engineering of the semiconductor layer structure<sup>123</sup>. Another solution to reach longer wavelengths is parametric conversion of a laser source using nonlinear optics. This is the solution chosen in this work to extend a 1- $\mu\text{m}$  SDL towards the 1.4-3.5  $\mu\text{m}$  region using an optical parametric oscillator (OPO).

OPOs are an elegant source of tunable wavelength emission. Various nonlinear crystals enable expanding parametric generation over a very wide span from the visible to the mid-IR. For example lithium triborate (LBO) crystals have a transparency range extending from 170 nm to 2.2  $\mu\text{m}$ , lithium niobate demonstrates transparency from 330 nm to 4.5  $\mu\text{m}$  and semiconductor-based orientation-patterned GaAs and GaP support emission from 1  $\mu\text{m}$  to 12  $\mu\text{m}$ . The latter has recently demonstrated the impressive development of a single fs-OPO covering a spectral range from 5  $\mu\text{m}$  to 12  $\mu\text{m}$  and its application in molecular spectroscopy experiments<sup>124</sup>.

In addition to the aforementioned spectroscopic applications, a stabilized frequency comb based on an OPO also finds applications in metrology. For example, we demonstrated in a collaborative work the metrology experiment, where the absolute optical frequency of a frequency-doubled 1560-nm Rb-stabilized reference laser was measured using a fully stabilized OPO comb<sup>125</sup>.

This chapter presents the parametric conversion of a pulsed SDL towards IR and mid-IR regions. In section 5.1, the basic operation principle of parametric conversion in an OPO is introduced. The demonstration of an OPO synchronously pumped by a SDL is presented in section 5.2.

## 5.1 Basic principle of OPOs

OPOs are light sources which can provide coherent radiation with properties similar to lasers, both in CW and pulsed regime, but using parametric amplification as optical gain instead of stimulated emission. They are based on the second-order nonlinearity response of a nonlinear medium, characterized by the  $\chi^{(2)}$  coefficient, to transfer energy from a given pump frequency to two signals with variable frequencies. Like lasers, OPOs rely on an optical cavity to provide optical feedback and get amplification of the resonating signal. The two generated waves are linked to the pump wave by the conservation of energy and their frequency is determined by the phase-matching condition. However the parametric gain requires a coherent pump source with high intensity. Therefore most OPOs are pumped by a laser. The following section summarizes the theoretical description of nonlinear parametric conversion. It is mainly based on the description presented in the two textbooks by Boyd<sup>126</sup> and Powers<sup>127</sup>.

### 5.1.1 Energy conservation

The nonlinear process in OPOs involves the mixing of three electromagnetic waves. Thinking in terms of particles, a pump photon with frequency  $\nu_p$  enters the nonlinear crystal and is converted into two new photons, the signal and idler photons with frequencies  $\nu_s$  and  $\nu_i$ , respectively. The conservation of energy implies that the signal and idler photons frequencies satisfy

$$\nu_p = \nu_s + \nu_i. \quad (5.1)$$

Assuming that a signal photon is resonating in the OPO cavity, it will stimulate emission at the same frequency. It results that two signal and one idler photons exit the crystal generating an amplified signal wave as pictured in Figure 5.2.

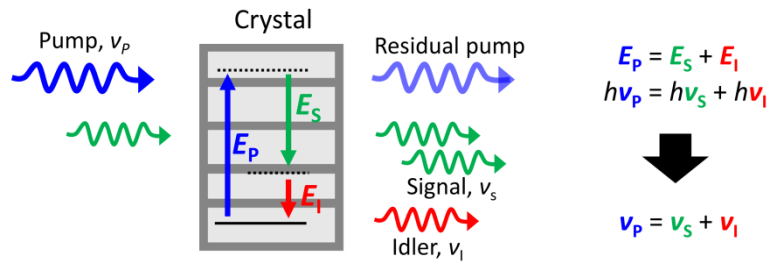


Figure 5.2: Schematic of the parametric frequency conversion in a nonlinear crystal satisfying the conservation of energy.

In contrary to lasers, the interacting frequencies do not depend on a fixed atomic or interband transition. The tunable conversion spectral range can cover a huge bandwidth only limited by the crystal. In addition, there is also no energy exchange with the crystal and therefore no heating of the medium.

### 5.1.2 Phase matching and conservation of momentum

During propagation in the crystal, chromatic dispersion causes a delay between the three propagating fields. This change in phase relation generates destructive interferences and the energy oscillates between the waves instead of being transferred in a constant direction. This phenomenon is illustrated by the violet curve in Figure 5.3(a) that represents the generated signal power as a function of the distance through the crystal. To avoid this interference and ensure an efficient energy transfer during the parametric interaction, a phase-matching condition, corresponding to the conservation of momentum, has to be respected

$$k_P = k_S + k_I, \quad (5.2)$$

where  $k_i$  are the pump, signal and idler wavenumber for  $i = P, S, I$ , respectively.

Several techniques have been developed to guarantee the phase-matching inside the crystal. Traditional phase-matching uses the natural birefringence of the nonlinear material to compensate the dispersion. This method is very efficient [see black curve in Figure 5.3(a)] but implies constraints on the choice of the polarizations and propagation directions in the birefringent nonlinear crystal. For a given pump wavelength, the available crystals and their bandwidth are limited.

### 5.1.3 Quasi-phase matching

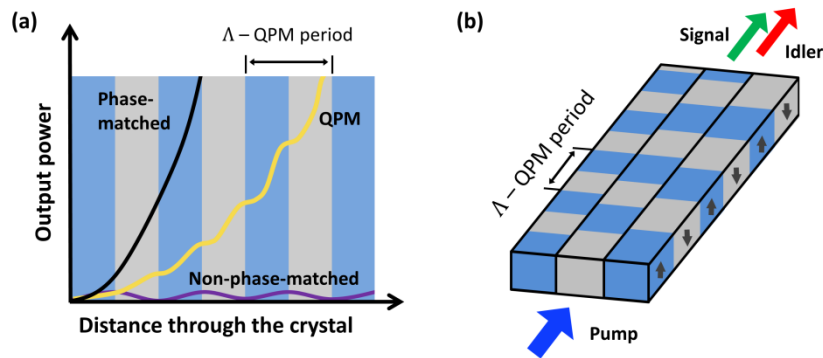


Figure 5.3: (a) Conversion efficiency as a function of the distance through the crystal for no phase-matching (violet), perfect phase-matching (black) and quasi-phase-matching (yellow). (b) Schematic structure of a periodically poled crystal with three different grating periods.

An alternative solution is to compensate the phase mismatch in the crystal by having micro-structured crystals with periodically inverted polarity of crystal domains (periodically poled crystals). Such a structure allows some mismatch over a certain length and inverts the sign of the nonlinear coefficient  $d_{\text{eff}}$  when the conversion is at its maximum. Here  $d_{\text{eff}}$  quantifies the strength of the nonlinear interaction<sup>126,127</sup>. The newly generated

photons are thus shifted by  $180^\circ$  and continue to interfere constructively with the previously generated photons. This conversion is called quasi-phase matching (QPM) and enables the appearance of a new term in the momentum conservation that compensates for the mismatch

$$k_p = k_s + k_i + \frac{2\pi}{\Lambda}. \quad (5.3)$$

It is illustrated by the yellow curve in Figure 5.3(a). The period of inversion in the crystal  $\Lambda$  depends on the interacting wavelengths and on the crystal temperature. Using the relation  $k_i = 2\pi \frac{n(\lambda_i)}{\lambda_i} = 2\pi \frac{n_i}{\lambda_i}$  for  $i = P, S, I$  and the Sellmeier equation<sup>128,129</sup> for the computation of  $n_i$ , equation (5.3) provides the requested poling period  $\Lambda$  as a function of temperature. For example, the results of simulations for a pump at  $1 \mu\text{m}$  in lithium niobate for different crystal temperatures of  $50^\circ\text{C}$ ,  $100^\circ\text{C}$  and  $150^\circ\text{C}$  are plotted in Figure 5.4. Periods between  $27 \mu\text{m}$  and  $30 \mu\text{m}$  are suitable for the generation of signal and idler waves in the range of  $1.4\text{--}3.5 \mu\text{m}$ .

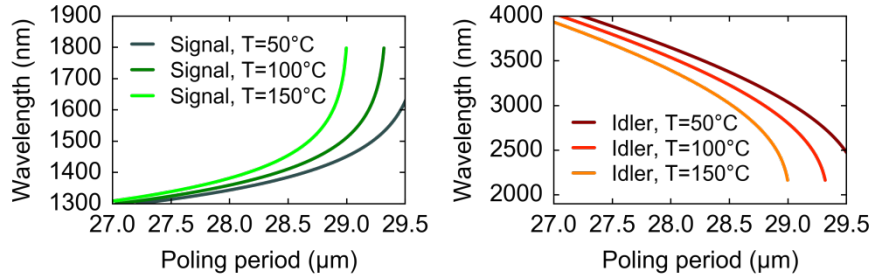


Figure 5.4: Quasi-phase matched signal and idler wavelengths as a function of the lithium niobate crystal poling period with a pump wavelength of  $1 \mu\text{m}$  and crystal temperatures of  $50^\circ\text{C}$ ,  $100^\circ\text{C}$  and  $150^\circ\text{C}$ .

The conversion efficiency with QPM is reduced by a factor of  $2/\pi$  compared to perfect phase-matching given a similar nonlinear coefficient. However, in a QPM crystal, the three waves can operate in the same polarization state, which enables accessing more efficient nonlinear

coefficients and can result in conversion efficiencies even higher than for perfect phase-matching<sup>126</sup>. The three waves also propagate in the same direction, which cancels spatial walk-off. Furthermore, a good choice of the poling period makes it possible to operate the crystal at room temperature. This phase matching technique enables a wide freedom in the nonlinear interaction as the generated wavelengths can be chosen by crystal engineering.

One of the first crystals used for nonlinear optics was lithium niobate<sup>130</sup>. It is nowadays one of the favorite materials for quasi-phase-matching thanks to its very high nonlinear coefficient value and its transparency window that covers 330 nm to 5.5  $\mu\text{m}$ <sup>127</sup>. The ferroelectric properties of lithium niobate make it suitable for periodic poling inversion using strong electric field application<sup>131</sup>. The processed crystal is called periodically poled lithium niobate or PPLN. It is the one chosen for the nonlinear wavelength conversion experiment described in section 5.2.

#### 5.1.4 Parametric gain

The single pass power gain in the crystal can be computed from solving the coupled wave equations in the nonlinear material<sup>126,127</sup>. Assuming no pump depletion, no initial idler beam and a perfect phase-matching, the parametric gain is given by

$$G_S = \frac{|E_S(L_{cr})|^2}{|E_S(0)|^2} - 1 = \sinh^2(\Gamma L_{cr}). \quad (5.4)$$

In this equation,  $L_{cr}$  is the length of the nonlinear crystal and  $\Gamma$  is the gain factor defined as

$$\Gamma^2 = \frac{2^3 \pi^2 d_{\text{eff}}^2}{c \epsilon_0 n_p n_s n_i \lambda_s \lambda_i} I_p, \quad (5.5)$$

where  $n_i$  are the frequency dependent refractive indices of the different waves and  $I_p$  is the pump intensity. The gain increases with  $I_p$ , therefore a higher conversion efficiency is obtained for a focused pump beam.

However, if the pump is focused too tightly, the intensity is only high near to the beam waist and falls rapidly off outside of the Rayleigh range  $Z_R$  (assuming here and in the following text that the waves are Gaussian beams). A good compromise is to operate the OPO with a confocal focusing condition, which means that the crystal length equals two times the Rayleigh length<sup>132</sup>

$$L_{cr} = 2Z_R = 2 \frac{n_p \pi w_p^2}{\lambda_p}. \quad (5.6)$$

The last equality results from the definition of the Rayleigh length of a Gaussian beam, where  $w_p$  is the pump beam waist defined as the  $1/e$  field radius at the focus. This condition gives a good estimate of the required pump waist.

### 5.1.5 Synchronous pumping

For a pulsed OPO, the pump and resonating signal pulses also have to temporally overlap in the crystal. When the period of the pulse train  $T_p = \frac{1}{f_{rep}}$  of the pump laser matches exactly the roundtrip time of the signal in the OPO cavity, it is called synchronous pumping. A small round-trip time mismatch can induce a huge loss of power. It is also possible to have differences in the OPO and pump laser cavity length in order to get an OPO repetition frequency that is a harmonic of the pump repetition frequency<sup>133</sup>. This is called harmonic pumping.

Typical properties of pulsed SDLs prevented so far the demonstration of parametric conversion in OPOs. The more recent development of low repetition frequency SDL by the company M Squared Lasers Ltd<sup>134</sup> enables reaching higher peak power and higher intensity, sufficient for nonlinear conversion. In the following section, an OPO synchronously pumped by a ps-SDL prototype with a repetition frequency of  $\sim 200$  MHz is presented. The reported results are a reprint of an Optics Express journal publication<sup>135</sup>.

## 5.2 Ultrafast optical parametric oscillator pumped by a vertical external-cavity surface-emitting laser

*N. Jornod,<sup>1</sup> V. J. Wittwer,<sup>1</sup> M. Gaponenko,<sup>1</sup> M. Hoffmann,<sup>1</sup> N. Hempler,<sup>2</sup> G. P. A. Malcolm,<sup>2</sup> G. T. Maker,<sup>2</sup> and T. Südmeyer<sup>1</sup>*

<sup>1</sup>Laboratoire Temps-Fréquence, Université de Neuchâtel, Avenue de Bellevaux 51, 2000 Neuchâtel, Switzerland

<sup>2</sup>M Squared Lasers Ltd, 1 Kelvin Campus, West of Scotland Science Park, Maryhill Road, Glasgow, G20 0SP, Scotland

**We report the first optical parametric oscillator synchronously pumped by a SESAM modelocked vertical external-cavity surface-emitting laser (VECSEL). As nonlinear medium, we use a periodically poled MgO:PPLN crystal. The VECSEL operates at a wavelength of 982 nm and a repetition rate of 198 MHz. The pump radiation is converted to signal and idler wavelengths tunable in the ranges of 1.4-1.8  $\mu\text{m}$  and 2.2-3.5  $\mu\text{m}$ , respectively, simply by a change of the poling period and crystal temperature. The signal pulses have a duration between 2 ps to 4 ps and an average output power up to 100 mW.**

### 5.2.1 Introduction

Optically-pumped vertical external-cavity surface-emitting lasers (VECSELs) [1] are a rapidly evolving technology which exhibits a wide spectral coverage in an inexpensive and compact setup [2-5]. Their foundation on semiconductor technology has the major advantage of emission wavelength flexibility which is easily achieved by bandgap engineering. They support emission wavelengths from the ultraviolet (391 nm) [6] up to the mid-infrared (mid-IR) spectral region (5.3  $\mu\text{m}$ ) [7]. Such semiconductor lasers secured their position in the continuous-wave

(CW) laser market [8–10], providing high power levels in fundamental transverse mode [9,11–13].

Pulsed operation of VECSELs can be obtained in the femtosecond and picosecond regime [3,4,14]. Typically, a semiconductor saturable absorber mirror (SESAM) [15] is used for pulse formation. This concept enabled impressive progress over the last years [16–20]. For example, a SESAM-modelocked VECSEL generated 5.1 W average power at 1030 nm in pulses with 682 fs duration [21]. Furthermore, operation with sub-100 fs pulse duration has been achieved for 100 mW of output power [22].

However, in contrast to the demonstrated spectral coverage of VECSELs in the CW regime, pulsed operation has been so far limited to wavelengths up to the 2  $\mu\text{m}$  range [23] and the best performance is obtained in the spectral region between 800–1200 nm [3]. This limitation in emission wavelength can be remedied by nonlinear frequency down-conversion. An effective approach is the use of an optical parametric oscillator (OPO) [24–26].

Ultrafast OPOs are usually synchronously pumped at the same repetition rate as the driving laser. During the last decades, synchronously-pumped OPOs have been pumped by different ultrafast laser types, including Ti:sapphire lasers [27], Yb-fiber lasers [28,29], Nd- and Yb-based solid-state lasers [30], Tm-lasers [31], and thin-disk lasers [32].

VECSELs can serve as a cost-efficient, versatile and compact alternative pump source for OPOs. However, so far the use of semiconductor lasers to pump OPOs has been limited to the CW-regime [33]. In this work we present the first ultrafast synchronously VECSEL-pumped OPO. We use a compact 982-nm modelocked VECSEL and a periodically poled MgO:PPLN crystal with different poling periods. We evaluate pulse duration, power levels, and tuning range.

## 5.2.2 Experiment

### 5.2.2.1 Pump laser: VECSEL prototype from M Squared Lasers

The pump laser source is a modelocked VECSEL developed by M Squared Lasers Ltd [34]. The laser has a central emission wavelength of 982 nm [Figure 5.5 (a)] and operates at a fundamental repetition rate of 197.6 MHz [Figure 5.5 (b)].

Low repetition frequencies are usually challenging to achieve with ultrafast VECSELs due to their relatively short gain carrier lifetime which typically leads to multi-pulsing in the cavity [35]. The pulse break-up is strongly influenced by the cavity design, the pump power, the semiconductor gain and saturable absorber characteristics. A careful selection of these parameters offers the window of operation where the laser can operate without modulation instabilities or harmonic mode-locking. The laser used in this experiment has a cavity designed without multiple passes through the gain and is passively modelocked with a SESAM [34]. It keeps a large intracavity dispersion which results in strongly chirped long pulses of a duration in the order of 60 ps. This mode of operation intends to keep the peak power low and avoid excessive nonlinear effects inside the cavity. A subsequent external compression in transmission gratings is implemented to efficiently compensate the chirp.

In Figure 5.5(c), we show the autocorrelation trace of the compressed output pulses with a typical pulse duration around 3 ps full width at half maximum (FWHM) assuming a  $\text{sech}^2$  pulse shape (intensity SHG-autocorrelator: Femtochrome FR-103). To confirm the single-pulse operation, we performed a sampling oscilloscope characterization of the laser pulse train [Figure 5.5(d)]. The laser pulses are equally separated by a time delay of 5.06 ns which corresponds to the 197.6 MHz fundamental repetition rate. The ringing of the signal measured with the sample oscilloscope is an electrical artefact. The compressed VECSEL generates up to 580 mW average output power, leading to a corresponding maximum

pulse energy of 2.9 nJ and a peak power of  $\sim 0.8$  kW (assuming a  $\text{sech}^2$  pulse shape). A beam quality measurement provided an  $M^2$  factor of 1.16, close to the diffraction-limit.

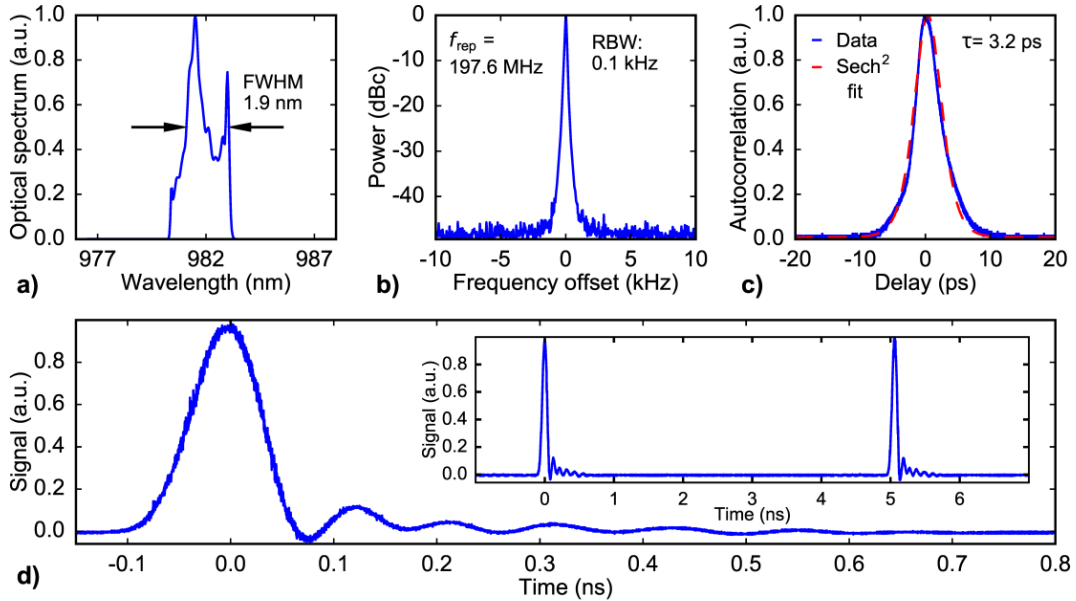


Figure 5.5: Pulse characterization of the pump laser. a) Optical spectrum with a peak intensity at 981.5 nm and estimated full width at half maximum of 1.9 nm. b) RF spectrum centered at 197.6 MHz at a resolution bandwidth (RBW) of 0.1 kHz. c) Autocorrelation trace (blue) and  $\text{sech}^2$  fit of the autocorrelation of the pulses (dashed red), corresponding to a pulse duration of 3.2 ps (FWHM). d) Sampling oscilloscope measurement with 1 ns and 8 ns (inset) span, confirming the single-pulse operation of the VECSEL. The weak ringing that follows the pulse signal trace is an artefact due to the electronics of the detection setup.

### 5.2.2.2 Optical parametric oscillator setup

Two different periodically-poled magnesium-doped lithium niobate (MgO:PPLN) crystals were used in the experiment. Their parameters are summarized in Table 5.1. Crystal #1 is a commercially available crystal from Covision Ltd. with multiple poling periods and dimensions of 10 mm  $\times$  10 mm  $\times$  0.5 mm. Four poling periods were used in our OPO

configuration: 27.91  $\mu\text{m}$ , 28.28  $\mu\text{m}$ , 28.67  $\mu\text{m}$  and 29.08  $\mu\text{m}$ . Input and output facets have an anti-reflection (AR) coating optimized for 1064 nm and 1.4-1.8  $\mu\text{m}$  wavelengths. Crystal #2 was custom made by the company Raicol Crystals. It has a single poling period of 29.15  $\mu\text{m}$  and a length of 5 mm. Both facets are AR-coated for 980 nm and 1520 nm wavelengths. The transmission of the pump through the crystals has been characterized using a CW diode (3S PHOTONICS 1999CHP) emitting at 976 nm. We measured a transmission of 96.3% for crystal #1 and 98.9% for crystal #2 at 100 mW of pump power. We operated both crystals at elevated temperatures between 50°C and 150°C in a crystal oven for temperature tuning.

	Length [mm]	Poling periods [ $\mu\text{m}$ ]	AR coating (from the datasheets)	Transmission at 976 nm
Crystal #1	10	27.91, 28.28, 28.67, 29.08	1064 nm ( R<1.5% ); 1400-1800 nm ( R<1% ); 2600-4800 nm ( R~6%-3% )	96.3%
Crystal #2	5	29.15	980 nm & 1520 nm	98.9%

Table 5.1: Crystals parameters

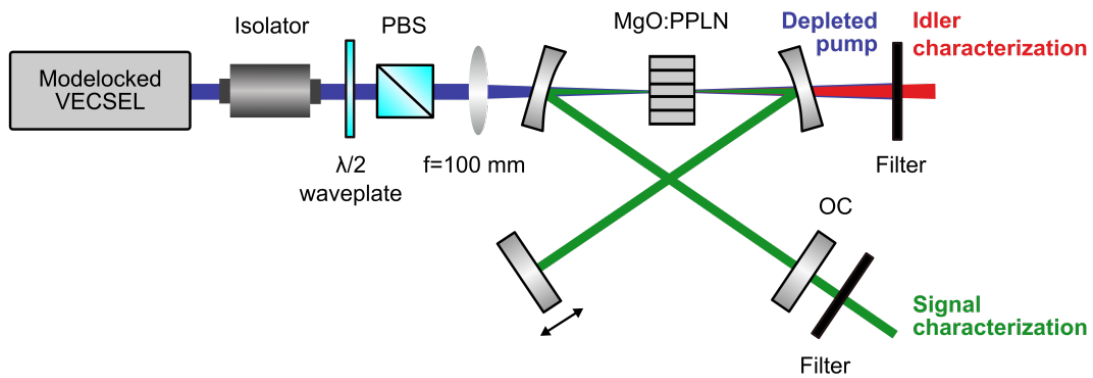


Figure 5.6: Experimental setup of the VECSEL-pumped OPO.

The experimental setup of the VECSEL-pumped OPO is shown schematically in Figure 5.6. The resonator is a standing-wave cavity, designed for the signal wave. The three highly reflective (HR) mirrors and

the output coupler (OC) are broadband coated to cover a signal wavelength range from 1.40  $\mu\text{m}$  to 1.75  $\mu\text{m}$ . The two curved HR mirrors have a radius-of-curvature of 150 mm and are separated by approximately 170 mm. From simulations, it results in a waist with a radius of 75  $\mu\text{m}$  for the signal beam in the crystal (software: RP Resonator). The curved mirrors have an AR coating for the pump wavelength on the backside and a high transmission at 980 nm on the front side in order to minimize the losses before the crystal and to eliminate the residual pump rapidly after the parametric conversion. An important part of the idler radiation exits the cavity through the curved mirror, where the idler spectral characterization is performed after a long pass filter with a cutoff wavelength of 1000 nm, used to remove residual pump and nonlinear frequency mixing signals. The idler output power cannot be directly measured due to the wavelength dependent absorption of the fused silica substrate of the curved mirror in the 2-3.5  $\mu\text{m}$  range. In the following we state the idler power computed from the signal output power times the ratio of the signal wavelength to the idler wavelength. A flat HR mirror is used as one end mirror of the cavity, while the other cavity end is formed by an OC with 1.5% transmission at the signal wavelength. The signal output power is measured after a long pass filter with a cutoff wavelength of 1000 nm. We corrected the output power for the losses in this filter (20%). The cavity length is  $\sim 750$  mm, corresponding to a total round trip length for the pulses of  $\sim 1500$  mm that matches the pump laser repetition rate. We did not use active stabilization of the cavity length, but adjusted the HR-end-mirror position manually with a standard mechanical translation stage.

An isolator is placed at the output of the pump laser to prevent disturbance of the VECSEL by back reflections from the OPO. A half-wave plate and a polarizing beam splitter (PBS) are used as polarization selective elements and for a continuous adjustment of the pump power. The pump beam is focused into the crystal with a lens of 100 mm focal

length resulting in a waist with a radius of 60  $\mu\text{m}$  in air, which optimizes the matching of the pump and signal spot size in the crystal according to the simulations.

### 5.2.3 Results

When operated with crystal #1, the typical cavity configuration for the maximum OPO output power generates a signal at wavelength between 1410 nm and 1550 nm. Using the poling period of 28.28  $\mu\text{m}$ , a maximum signal output power of 60 mW (48 mW measured with the power meter at the OC after the filter) is reached at 1413 nm for a pump power of 540 mW. The signal power conversion efficiency is 11%.

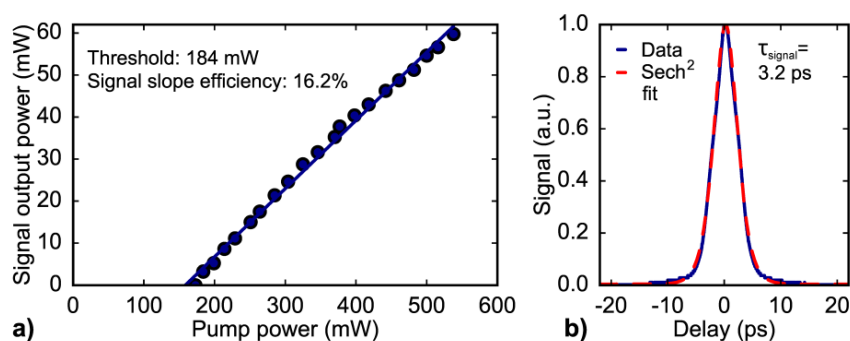


Figure 5.7: a) OPO signal output power as a function of the pump power and b) signal autocorrelation trace (blue) and sech<sup>2</sup> fit of the autocorrelation of the pulses (dashed red), corresponding to a pulse duration of 3.2 ps (FWHM) for a cavity configuration with the 10 mm-long crystal #1, period of 28.28  $\mu\text{m}$ , crystal temperature of 120°C and signal wavelength of 1413 nm

The corresponding computed idler power is 26 mW at 3214 nm. Figure 5.7 presents the signal output power as a function of the pump power. The OPO has a threshold at a pump power of 184 mW and operates with a signal slope efficiency of 16.2%. The signal emission wavelength is tuned by changing the temperature of the oven from 50°C to 150°C and using the four different poling periods of the crystal. Thereby it is possible to generate a signal wavelength covering a bandwidth of

420 nm from 1360 nm to 1780 nm with a corresponding idler wavelength varying from 2190 nm to 3530 nm.

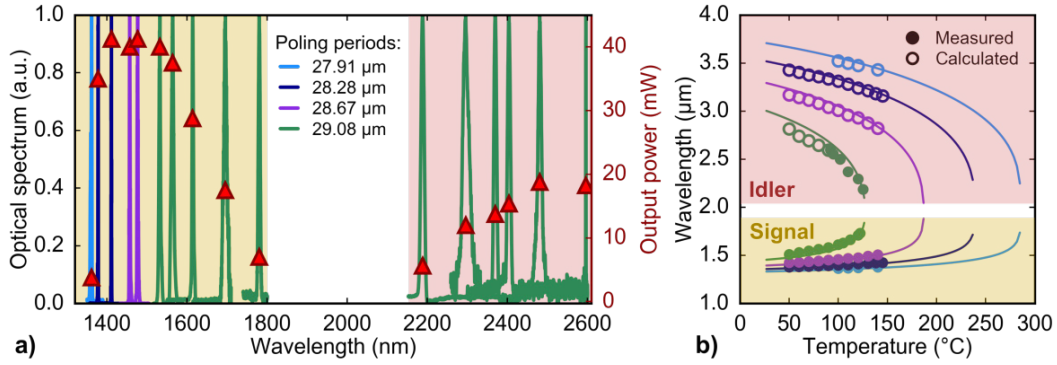


Figure 5.8: Characterization of signal and idler wavelengths with crystal #1 for the four different poling periods 27.91 μm (light blue), 28.28 μm (dark blue), 28.67 μm (violet), 29.08 μm (green). a) Signal and idler optical spectrum normalized (left axis) and the output power for a pump power of 450 mW (red triangles, right axis). b) Measured (filled dots) and computed (empty dots) signal and idler wavelengths as functions of the crystal temperature and the theoretical expected values (solid lines).

Figure 5.8(a) presents a selection of optical spectra of signal and idler waves measured with an optical spectrum analyzer (Anritsu MS9710B for the signal and A.P.E waveScan USB IR, which is limited to 2.6 μm, for the idler) and their corresponding output power (measured for the signal and computed for the idler) for a pump power of 450 mW with an optimization of the cavity length at every step. The limitation in the tunability of the generated signal is attributed mainly to the bandwidth of the HR coatings of the cavity mirrors which are limited to 1400-1750 nm. Figure 5.8(b) displays the signal and idler wavelengths as a function of the crystal temperature for the four different poling periods, illustrating the good fit between the measured and computed data. The signal pulse characterization was performed with the same autocorrelator as in Section 5.2.2.1, measuring pulse durations of 2-4 ps FWHM [see Figure 5.7(b)], determined by the duration of the input pulses.

Crystal #2 provided higher output powers with a maximum signal output power of 100 mW (80 mW measured with the power meter) at a pump power of 450 mW. In this configuration, the crystal is stabilized at a temperature of 85°C. The generated signal wavelength is 1630 nm with a computed idler power of 66 mW at a wavelength of 2467 nm. This corresponds to a signal power conversion efficiency of 22%, which is two times higher compared to crystal #1.

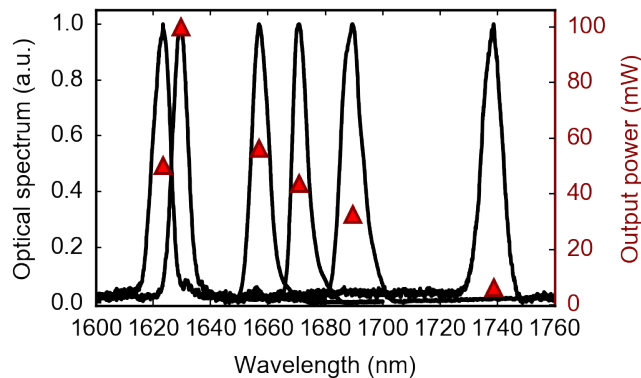


Figure 5.9: Characterization of operation with crystal #2. Signal optical spectra normalized (left axis) and output power for a pump power of 450 mW (red triangles, right axis).

A change of the crystal temperature from 80°C to 120°C tuned the signal from 1623 nm to 1739 nm, i.e. over a bandwidth of 116 nm (see Figure 5.9). The higher output power is surprising given that the crystal length is only 5 mm, i.e. half of the first crystal. An important effect that can reduce the conversion efficiency of longer crystals is the pump spectral acceptance bandwidth, which scales inversely proportional to the crystal length. However, the acceptance bandwidth of crystal #1 is stated above the 1.9 nm bandwidth of the pump VECSEL, suggesting only minor contribution to the conversion efficiency. We attribute the increase in efficiency with crystal #2 to the better quality of the AR coating for both the pump and signal wavelengths, minimizing the losses of the cavity.

## 5.2.4 Conclusion

We have demonstrated an OPO pumped by a picosecond VECSEL emitting at wavelength of 982 nm. We obtained signal and idler wavelengths tunable in the ranges of 1.4-1.8  $\mu\text{m}$  and 2.2-3.5  $\mu\text{m}$ , respectively, by changing the crystal temperature and poling periods. A maximum signal output power of 100 mW was generated from 450 mW of pump with a corresponding idler output power of 66 mW and a signal power conversion efficiency of 22%. This encouraging result paves the way for more compact and low-cost tunable ultrafast sources emitting in the IR and mid-IR spectral regions.

### **Funding**

European Community's Seventh Framework Programme (605057).

## 5.2.5 References and links

- [1] M. Kuznetsov, F. Hakimi, R. Sprague, and A. Mooradian, "High-Power (>0.5-W CW) Diode-Pumped Vertical-External-Cavity Surface-Emitting Semiconductor Lasers with Circular TEM<sub>00</sub> Beams," *IEEE Photonics Technol. Lett.* 9(8), 1063–1065 (1997).
- [2] O. G. Okhotnikov, *Semiconductor Disk Lasers: Physics and Technology* (John Wiley & Sons, 2010).
- [3] B. W. Tilma, M. Mangold, C. A. Zaugg, S. M. Link, D. Waldburger, A. Klenner, A. S. Mayer, E. Gini, M. Golling, and U. Keller, "Recent advances in ultrafast semiconductor disk lasers," *Light Sci. Appl.* 4(7), e310 (2015).
- [4] A. Rahimi-Iman, "Recent advances in VECSELs," *J. Opt.* 18(9), 093003 (2016).

- [5] M. Guina, A. Rantamäki, and A. Härkönen, "Optically pumped VECSELs: review of technology and progress," *J. Phys. Appl. Phys.* 50(38), 383001 (2017).
- [6] S.-H. Park and H. Jeon, "Microchip-Type InGaN Vertical External-Cavity Surface-Emitting Laser," *Opt. Rev.* 13(1), 20–23 (2006).
- [7] M. Rahim, M. Arnold, F. Felder, K. Behfar, and H. Zogg, "Midinfrared lead-chalcogenide vertical external cavity surface emitting laser with 5  $\mu\text{m}$  wavelength," *Appl. Phys. Lett.* 91(15), 151102 (2007).
- [8] "Verdi G-Series | Coherent," <https://www.coherent.com/lasers/laser/verdi-g-series>.
- [9] J. Chilla, Q.-Z. Shu, H. Zhou, E. Weiss, M. Reed, and L. Spinelli, "Recent Advances in Optically Pumped Semiconductor Lasers," *Proc. SPIE* 6451645109 (2007).
- [10] Y. Bai, J. Wisdom, J. Charles, P. Hyland, C. Scholz, Z. Xu, Y. Lin, E. Weiss, J. Chilla, and A. Lepert, "Advances in optically pumped semiconductor lasers for blue emission under frequency doubling," *Proc. SPIE* 973497340Q (2016).
- [11] F. Zhang, B. Heinen, M. Wichmann, C. Möller, B. Kunert, A. Rahimi-Iman, W. Stolz, and M. Koch, "A 23-watt single-frequency vertical-external-cavity surface-emitting laser," *Opt. Express* 22(11), 12817 (2014).
- [12] A. Rantamäki, A. Chamorovskiy, J. Lyytikäinen, and O. Okhotnikov, "4.6-W Single Frequency Semiconductor Disk Laser With <75-kHz Linewidth," *IEEE Photonics Technol. Lett.* 24(16), 1378–1380 (2012).
- [13] J. D. Berger, D. W. Anthon, A. Caprara, J. L. Chilla, S. V. Govorkov, A. Y. Lepert, W. Mefferd, Q.-Z. Shu, and L. Spinelli, "20 Watt CW TEM00 intracavity doubled optically pumped semiconductor laser at 532 nm," *Proc. SPIE* 8242824206 (2012).

- [14] M. A. Gaafar, A. Rahimi-Iman, K. A. Fedorova, W. Stolz, E. U. Rafailov, and M. Koch, "Mode-locked semiconductor disk lasers," *Adv. Opt. Photonics* 8(3), 370–400 (2016).
- [15] U. Keller, K. J. Weingarten, F. X. Kärtner, D. Kopf, B. Braun, I. D. Jung, R. Fluck, C. Hönninger, N. Matuschek, and J. Aus der Au, "Semiconductor Saturable Absorber Mirrors (SESAM's) for Femtosecond to Nanosecond Pulse Generation in Solid-State Lasers," *IEEE J. Sel. Top. Quantum Electron.* 2(3), 435–453 (1996).
- [16] S. Hoogland, S. Dhanjal, A. C. Tropper, J. S. Roberts, R. Häring, R. Paschotta, F. Morier-Genoud, and U. Keller, "Passively Mode-Locked Diode-Pumped Surface-Emitting Semiconductor Laser," *IEEE Photonics Technol. Lett.* 12(9), 1135–1137 (2000).
- [17] P. Klopp, U. Griebner, M. Zorn, and M. Weyers, "Pulse repetition rate up to 92 GHz or pulse duration shorter than 110 fs from a mode-locked semiconductor disk laser," *Appl. Phys. Lett.* 98(7), 071103 (2011).
- [18] M. Butkus, E. A. Viktorov, T. Erneux, C. J. Hamilton, G. Maker, G. P. A. Malcolm, and E. U. Rafailov, "85.7 MHz repetition rate mode-locked semiconductor disk laser: fundamental and soliton bound states," *Opt. Express* 21(21), 25526 (2013).
- [19] K. G. Wilcox, A. C. Tropper, H. E. Beere, D. A. Ritchie, B. Kunert, B. Heinen, and W. Stolz, "4.35 kW peak power femtosecond pulse mode-locked VECSEL for supercontinuum generation," *Opt. Express* 21(2), 1599–1605 (2013).
- [20] D. Lorensen, D. J. H. C. Maas, H. J. Unold, A.-R. Bellancourt, B. Rudin, E. Gini, D. Ebling, and U. Keller, "50-GHz Passively Mode-Locked Surface-Emitting Semiconductor Laser With 100-mW Average Output Power," *IEEE J. Quantum Electron.* 42(8), 838–847 (2006).

- [21] M. Scheller, T.-L. Wang, B. Kunert, W. Stolz, S. W. Koch, and J. V. Moloney, "Passively modelocked VECSEL emitting 682 fs pulses with 5.1 W of average output power," *Electron. Lett.* 48(10), 588–589 (2012).
- [22] D. Waldburger, S. M. Link, M. Mangold, C. G. E. Alfieri, E. Gini, M. Golling, B. W. Tilma, and U. Keller, "High-power 100 fs semiconductor disk lasers," *Optica* 3(8), 844–852 (2016).
- [23] A. Härkönen, J. Rautiainen, L. Orsila, M. Guina, K. Rössner, M. Hümmer, T. Lehnhardt, M. Müller, A. Forchel, M. Fischer, J. Koeth, and O. G. Okhotnikov, "2- $\mu\text{m}$  Mode-Locked Semiconductor Disk Laser Synchronously Pumped Using an Amplified Diode Laser," *IEEE Photonics Technol. Lett.* 20(15), 1332–1334 (2008).
- [24] J. A. Giordmaine and R. C. Miller, "Tunable Coherent Parametric Oscillation in LiNbO<sub>3</sub> at Optical Frequencies," *Phys. Rev. Lett.* 14(24), 973–976 (1965).
- [25] M. Ebrahimzadeh, "Mid-Infrared Ultrafast and Continuous-Wave Optical Parametric Oscillators," in *Solid-State Mid-Infrared Laser Sources*, I. T. Sorokina and K. L. Vodopyanov, eds. (Springer-Verlag Berlin Heidelberg, 2003).
- [26] K. Vodopyanov, "Pulsed Mid-IR Optical Parametric Oscillators," in *Solid-State Mid-Infrared Laser Sources*, I. T. Sorokina and K. L. Vodopyanov, eds. (Springer-Verlag Berlin Heidelberg, 2003).
- [27] J. H. Sun, B. J. S. Gale, and D. T. Reid, "Composite frequency comb spanning 0.4–2.4  $\mu\text{m}$  from a phase-controlled femtosecond Ti:sapphire laser and synchronously pumped optical parametric oscillator," *Opt. Lett.* 32(11), 1414–1416 (2007).
- [28] O. Kokabee, A. Esteban-Martin, and M. Ebrahim-Zadeh, "Efficient, high-power, ytterbium-fiber-laser-pumped picosecond optical parametric oscillator," *Opt. Lett.* 35(19), 3210–3212 (2010).

- [29] F. Adler, K. C. Cossel, M. J. Thorpe, I. Hartl, M. E. Fermann, and J. Ye, "Phase-stabilized, 1.5 W frequency comb at 2.8–4.8  $\mu\text{m}$ ," *Opt. Lett.* 34(9), 1330–1332 (2009).
- [30] C. W. Hoyt, M. Sheik-Bahae, and M. Ebrahimzadeh, "High-power picosecond optical parametric oscillator based on periodically poled lithium niobate," *Opt. Lett.* 27(17), 1543 (2002).
- [31] N. Leindecker, A. Marandi, R. L. Byer, K. L. Vodopyanov, J. Jiang, I. Hartl, M. Fermann, and P. G. Schunemann, "Octave-spanning ultrafast OPO with 2.6-6.1  $\mu\text{m}$  instantaneous bandwidth pumped by femtosecond Tm-fiber laser," *Opt. Express* 20(7), 7046–7053 (2012).
- [32] T. Petersen, J. D. Zuegel, and J. Bromage, "High-average-power, 2- $\mu\text{m}$  femtosecond optical parametric oscillator synchronously pumped by a thin-disk, mode-locked laser," *Opt. Express* 25(8), 8840 (2017).
- [33] D. J. M. Stothard, J.-M. Hopkins, D. Burns, and M. H. Dunn, "Stable, continuous-wave, intracavity, optical parametric oscillator pumped by a semiconductor disk laser (VECSEL)," *Opt. Express* 17(13), 10648–10658 (2009).
- [34] N. Hempler, B. Bialkowski, C. J. Hamilton, G. T. Maker, and G. P. A. Malcolm, "Development and commercialization of mode-locked VECSELs," *Proc. SPIE* 934993490K (2015).
- [35] C. A. Zaugg, M. Hoffmann, W. P. Pallmann, V. J. Wittwer, O. D. Sieber, M. Mangold, M. Golling, K. J. Weingarten, B. W. Tilma, T. Südmeyer, and U. Keller, "Low repetition rate SESAM modelocked VECSEL using an extendable active multipass-cavity approach," *Opt. Express* 20(25), 27915–27921 (2012).

# Chapter 6

## Conclusion and Outlook

The experiments presented in this thesis show for the first time that the SDL technology is suitable for the generation of optical frequency combs. This is an important step towards simpler and more cost-efficient frequency combs for industrial and scientific applications in various fields such as metrology or spectroscopy.

As an initial step, an indirect CEO frequency noise characterization method was used, demonstrating the first CEO frequency noise analysis of a SDL. The measured free-running CEO frequency noise spectrum and the CEO dynamic response to pump power modulation suggested the feasibility of a self-referenced stabilization, if the CEO frequency can be detected with a sufficient signal-to-noise ratio. Usually, the detection of the CEO frequency of GHz lasers with the standard nonlinear interferometry is challenging due to the strong request of high peak power and short pulse duration for the coherent octave-spanning SC generation. The here demonstrated alternative technique that necessitates only a low noise CW laser at the same emission wavelength as the modelocked laser is an efficient solution for the characterization of high repetition rate

modelocked lasers. A recent publication presents its application to a 25-GHz DPSSL with only 4 mW of output power<sup>136</sup>.

As next step, different methods of amplification were studied to enable standard nonlinear interferometry for CEO characterization and stabilization. The amplification in an 8.3-mm long Yb-doped waveguide demonstrated an efficient amplification of the laser output power from 60 mW to 2.9 W. In the amplification, the 300-fs pulses were temporally broadened to more than 600 fs due to gain narrowing. The optical spectrum of the pulses was reduced, meaning that a temporal compression would first require a spectral broadening stage. Switching to an Yb:CALGO-based waveguide that supports broader gain would allow getting around this issue. Such waveguides should even be able to operate with shorter pulse durations, constituting a compact way to reach high power levels and short pulse duration with a GHz VECSEL.

Another way to circumvent these difficulties is to combine the amplification with the spectral broadening stage. To achieve this, the development of an Yb-doped fiber amplifier based on a small-core fiber is presented. The nonlinearity in the gain medium directly provides the spectral broadening necessary for a temporal compression. The compressed pulses enabled the generation of a coherent octave-spanning SC in a commercial PCF. A standard  $f$ -to- $2f$  interferometer was used for the detection of a CEO signal with a sufficient SNR to demonstrate the first self-referenced CEO frequency stabilization of a SDL. The CEO frequency noise was efficiently reduced, but no tight lock could be obtained at this point. The free-running noise properties of the laser showed that a tight lock would require a broad modulation bandwidth of  $\sim 600$  kHz, difficult to implement with a direct modulation of the pump current. A deeper study of the origin of the noise of the free-running CEO frequency revealed that the noise plateau observed at high Fourier frequencies matches well the noise of the pump diode and therefore originates from the AM noise of the pump. In order to improve the

---

stabilization, work can be done to lower the free-running noise by reducing the noise of the pump source. This can be performed for example by implementing an amplitude stabilization of the pump.

An important advantage of the SDL technology compared to other modelocked technologies is the wafer-scale producibility associated with a multimode diode-pumping scheme that reduces the complexity and costs of the system. The external amplification approach demonstrated in this thesis brings additional difficulties compared to a simple laser technology and an ideal long term solution should avoid the amplifier stage. Silicon nitride waveguides have recently demonstrated their potential for efficient coherent SC generation with a lowered requested peak power<sup>137</sup>. Their application in the development of a DPSSL frequency comb even showed lower CEO noise than with a PCF<sup>138</sup>. The replacement of the PCF by a silicon nitride waveguide combined with the latest improved pulse duration and output power of modelocked VECSELS recently enabled the demonstration of a coherent octave-spanning SC without the need of external amplification<sup>139</sup>. In the redaction time of this thesis, the presentation of the full-stabilization of a SESAM-modelocked VECSEL using a silicon nitride waveguide for SC generation has been presented at the SPIE Photonics West conference (2018)<sup>140</sup>.

Longer wavelength emission towards the mid-IR is of great interest for remote trace gas sensing or molecular spectroscopy. Even though efforts are invested to push their limit to longer emission wavelengths, modelocked VECSELS are currently limited to 2  $\mu\text{m}$ <sup>107</sup>. Alternatively, nonlinear conversion techniques can be used to extend the accessible wavelength coverage. In the last chapter of this thesis, an approach using an ultrafast 200-MHz SDL-pumped OPO has been described. The nonlinear conversion produced a continuously tunable signal wave at 1.4-1.8  $\mu\text{m}$  and an idler wave at 2.2-3.5  $\mu\text{m}$ . Although no stabilization was implemented here, the experiment demonstrates new fields of applications of modelocked VECSELS with exciting possible outcome.

Frequency combs based on mid-IR OPOs add even more flexibility in the emitted spectral range and open new doors in Fourier transform spectroscopy and dual-comb spectroscopy enabling the fast acquisition speed and high resolution detection of a wide range of molecules<sup>141,142</sup>.

The results presented in this thesis together with the recent demonstration of low power octave-spanning SC generation in silicon nitride waveguide bring the ultrafast SDL technology in a very promising position in the family of stabilized optical frequency combs and its wide range of possible applications.

# Bibliography

1. C. W. Chou, D. B. Hume, J. C. J. Koelemeij, D. J. Wineland, and T. Rosenband, "Frequency Comparison of Two High-Accuracy  $\text{Al}^+$  Optical Clocks," *Phys. Rev. Lett.* **104**, 233903 (2010).
2. T. H. Maiman, "Stimulated Optical Radiation in Ruby," *Nature* **187**, 493–494 (1960).
3. T. W. Hänsch, "Nobel Lecture: Passion for precision," *Rev. Mod. Phys.* **78**, 1297–1309 (2006).
4. J. L. Hall, "Nobel Lecture: Defining and measuring optical frequencies," *Rev. Mod. Phys.* **78**, 1279–1295 (2006).
5. M. J. W. Rodwell, K. J. Weingarten, D. M. Bloom, T. Baer, and B. H. Kolner, "Reduction of timing fluctuations in a mode-locked Nd: YAG laser by electronic feedback," *Opt. Lett.* **11**, 638–640 (1986).
6. H. R. Telle, G. Steinmeyer, A. E. Dunlop, J. Stenger, D. H. Sutter, and U. Keller, "Carrier-envelope offset phase control: A novel concept for absolute optical frequency measurement and ultrashort pulse generation," *Appl. Phys. B* **69**, 327–332 (1999).
7. J. K. Ranka, R. S. Windeler, and A. J. Stentz, "Visible continuum generation in air-silica microstructure optical fibers with anomalous dispersion at 800 nm," *Opt. Lett.* **25**, 25–27 (2000).
8. D. J. Jones, S. A. Diddams, J. K. Ranka, A. Stentz, R. S. Windeler, J. L. Hall, and S. T. Cundiff, "Carrier-Envelope Phase Control of

- Femtosecond Mode-locked Lasers and Direct Optical Frequency Synthesis," *Science* **288**, 635–639 (2000).
9. A. Apolonski, A. Poppe, G. Tempea, C. Spielmann, T. Udem, R. Holzwarth, T. W. Hänsch, and F. Krausz, "Controlling the Phase Evolution of Few-Cycle Light Pulses," *Phys. Rev. Lett.* **85**, 740–743 (2000).
  10. S. Schilt and T. Südmeyer, "Carrier-Envelope Offset Stabilized Ultrafast Diode-Pumped Solid-State Lasers," *Appl. Sci.* **5**, 787–816 (2015).
  11. W. Hänsel, M. Giunta, K. Beha, M. Lezius, M. Fischer, and R. Holzwarth, "Ultra-low phase noise all-PM Er:fiber optical frequency comb," in *Advanced Solid State Lasers* (Optical Society of America, 2015), p. ATh4A.2.
  12. L. C. Sinclair, I. Coddington, W. C. Swann, G. B. Rieker, A. Hati, K. Iwakuni, and N. R. Newbury, "Operation of an optically coherent frequency comb outside the metrology lab," *Opt. Express* **22**, 6996–7006 (2014).
  13. I. Hartl, H. A. McKay, R. Thapa, B. K. Thomas, A. Ruehl, L. Dong, and M. E. Fermann, "Fully stabilized GHz Yb-fiber laser frequency comb," in *Advanced Solid-State Photonics* (Optical Society of America, 2009), p. MF9.
  14. A. Klenner, S. Schilt, T. Südmeyer, and U. Keller, "Gigahertz frequency comb from a diode-pumped solid-state laser," *Opt. Express* **22**, 31008–31019 (2014).
  15. S. Hakobyan, V. J. Wittwer, P. Brochard, K. Gürel, S. Schilt, A. S. Mayer, U. Keller, and T. Südmeyer, "Full stabilization and characterization of an optical frequency comb from a diode-pumped solid-state laser with GHz repetition rate," *Opt. Express* **25**, 20437–20453 (2017).

- 
16. S. Hakobyan, V. J. Wittwer, K. Gürel, A. S. Mayer, S. Schilt, and T. Südmeyer, "Carrier-envelope offset stabilization of a GHz repetition rate femtosecond laser using opto-optical modulation of a SESAM," *Opt. Lett.* **42**, 4651–4654 (2017).
  17. K. Gürel, V. J. Wittwer, S. Hakobyan, S. Schilt, and T. Südmeyer, "Carrier envelope offset frequency detection and stabilization of a diode-pumped mode-locked Ti:sapphire laser," *Opt. Lett.* **42**, 1035–1038 (2017).
  18. R. N. Hall, G. E. Fenner, J. D. Kingsley, T. J. Soltys, and R. O. Carlson, "Coherent Light Emission From GaAs Junctions," *Phys. Rev. Lett.* **9**, 366–368 (1962).
  19. M. Kuznetsov, F. Hakimi, R. Sprague, and A. Mooradian, "High-power (>0.5-W CW) Diode-Pumped Vertical-External-Cavity Surface-Emitting Semiconductor Lasers with Circular TEM<sub>00</sub> Beams," *IEEE Photonics Technol. Lett.* **9**, 1063–1065 (1997).
  20. S. Hoogland, S. Dhanjal, A. C. Tropper, J. S. Roberts, R. Häring, R. Paschotta, F. Morier-Genoud, and U. Keller, "Passively Mode-Locked Diode-Pumped Surface-Emitting Semiconductor Laser," *IEEE Photonics Technol. Lett.* **12**, 1135–1137 (2000).
  21. M. Scheller, T.-L. Wang, B. Kunert, W. Stolz, S. W. Koch, and J. V. Moloney, "Passively modelocked VECSEL emitting 682 fs pulses with 5.1 W of average output power," *Electron. Lett.* **48**, 588 (2012).
  22. D. Waldburger, S. M. Link, M. Mangold, C. G. E. Alfieri, E. Gini, M. Golling, B. W. Tilma, and U. Keller, "High-power 100 fs semiconductor disk lasers," *Optica* **3**, 844–852 (2016).
  23. C. W. Baker, M. Scheller, A. Laurain, A. Ruiz-Perez, W. Stolz, S. Addamane, G. Balakrishnan, S. W. Koch, R. J. Jones, and J. V. Moloney, "Multi-Angle VECSEL Cavities for Dispersion Control and Peak-Power Scaling," *IEEE Photonics Technol. Lett.* **29**, 326–329 (2017).

24. D. Lorentz, D. J. H. C. Maas, H. J. Unold, A.-R. Bellancourt, B. Rudin, E. Gini, D. Ebling, and U. Keller, "50-GHz Passively Mode-Locked Surface-Emitting Semiconductor Laser With 100-mW Average Output Power," *IEEE J. Quantum Electron.* **42**, 838-847 (2006).
25. K. G. Wilcox, A. H. Quarterman, V. Apostolopoulos, H. E. Beere, I. Farrer, D. A. Ritchie, and A. C. Tropper, "175 GHz, 400-fs-pulse harmonically mode-locked surface emitting semiconductor laser," *Opt. Express* **20**, 7040-7045 (2012).
26. D. J. H. C. Maas, A.-R. Bellancourt, B. Rudin, M. Golling, H. J. Unold, T. Südmeyer, and U. Keller, "Vertical integration of ultrafast semiconductor lasers," *Appl. Phys. B* **88**, 493-497 (2007).
27. M. Mangold, C. A. Zaugg, S. M. Link, M. Golling, B. W. Tilma, and U. Keller, "Pulse repetition rate scaling from 5 to 100 GHz with a high-power semiconductor disk laser," *Opt. Express* **22**, 6099-6107 (2014).
28. K. G. Wilcox, A. C. Tropper, H. E. Beere, D. A. Ritchie, B. Kunert, B. Heinen, and W. Stolz, "4.35 kW peak power femtosecond pulse mode-locked VECSEL for supercontinuum generation," *Opt. Express* **21**, 1599-1605 (2013).
29. A. H. Quarterman, L. E. Hooper, P. J. Mosley, and K. G. Wilcox, "Gigahertz pulse source by compression of mode-locked VECSEL pulses coherently broadened in the normal dispersion regime," *Opt. Express* **22**, 12096-12101 (2014).
30. A. Chamorovskiy, J. Kerttula, J. Rautiainen, and O. G. Okhotnikov, "Supercontinuum generation with amplified 1.57  $\mu\text{m}$  picosecond semiconductor disk laser," *Electron. Lett.* **48**, 1010-1012 (2012).
31. C. A. Zaugg, A. Klenner, M. Mangold, A. S. Mayer, S. M. Link, F. Emaury, M. Golling, E. Gini, C. J. Saraceno, B. W. Tilma, and U.

- 
- Keller, "Gigahertz self-referenceable frequency comb from a semiconductor disk laser," *Opt. Express* **22**, 16445–16455 (2014).
32. D. C. Heinecke, A. Bartels, and S. A. Diddams, "Offset frequency dynamics and phase noise properties of a self-referenced 10 GHz Ti:sapphire frequency comb," *Opt. Express* **19**, 18440–18451 (2011).
  33. A. Bartels, R. Gebs, M. S. Kirchner, and S. A. Diddams, "Spectrally resolved optical frequency comb from a self-referenced 5 GHz femtosecond laser," *Opt. Lett.* **32**, 2553–2555 (2007).
  34. A. Bartels, T. Dekorsy, and H. Kurz, "Femtosecond Ti:sapphire ring laser with a 2-GHz repetition rate and its application in time-resolved spectroscopy," *Opt. Lett.* **24**, 996–998 (1999).
  35. S.-W. Chu, T.-M. Liu, C.-K. Sun, C.-Y. Lin, and H.-J. Tsai, "Real-time second-harmonic-generation microscopy based on a 2-GHz repetition rate Ti:sapphire laser," *Opt. Express* **11**, 933–938 (2003).
  36. T. M. Fortier, A. Bartels, and S. A. Diddams, "Octave-spanning Ti:sapphire laser with a repetition rate >1 GHz for optical frequency measurements and comparisons," *Opt. Lett.* **31**, 1011–1013 (2006).
  37. G. T. Nogueira, B. Xu, Y. Coello, M. Dantus, and F. C. Cruz, "Broadband 2.12 GHz Ti:sapphire laser compressed to 5.9 femtoseconds using MIIPS," *Opt. Express* **16**, 10033–10038 (2008).
  38. R. A. McCracken, É. Depagne, R. B. Kuhn, N. Erasmus, L. A. Crause, and D. T. Reid, "Wavelength calibration of a high resolution spectrograph with a partially stabilized 15-GHz astrocomb from 550 to 890 nm," *Opt. Express* **25**, 6450–6460 (2017).
  39. I. Hartl, H. A. McKay, R. Thapa, B. K. Thomas, L. Dong, and M. E. Fermann, "GHz Yb-femtosecond-fiber laser frequency comb," in *Conference on Lasers and Electro-Optics (Optical Society of America, 2009)*, p. CMN1.

40. D. Chao, M. Y. Sander, G. Chang, J. L. Morse, J. A. Cox, G. S. Petrich, L. A. Kolodziejski, F. X. Kärtner, and E. P. Ippen, "Self-referenced Erbium Fiber Laser Frequency Comb at a GHz Repetition Rate," in *Optical Fiber Communication Conference and Exposition and The National Fiber Optic Engineers Conference* (Optical Society of America, 2012), p. OW1C.2.
41. H.-W. Chen, G. Chang, S. Xu, Z. Yang, and F. X. Kärtner, "3 GHz, fundamentally mode-locked, femtosecond Yb-fiber laser," *Opt. Lett.* **37**, 3522–3524 (2012).
42. C. Li, Y. Ma, X. Gao, F. Niu, T. Jiang, A. Wang, and Z. Zhang, "1 GHz repetition rate femtosecond Yb: fiber laser for direct generation of carrier-envelope offset frequency," *Appl. Opt.* **54**, 8350–8353 (2015).
43. H. Cheng, W. Wang, Y. Zhou, T. Qiao, W. Lin, S. Xu, and Z. Yang, "5 GHz fundamental repetition rate, wavelength tunable, all-fiber passively mode-locked Yb-fiber laser," *Opt. Express* **25**, 27646–27651 (2017).
44. A. Martinez and S. Yamashita, "Multi-gigahertz repetition rate passively modelocked fiber lasers using carbon nanotubes," *Opt. Express* **19**, 6155–6163 (2011).
45. S. Yamashita, Y. Inoue, K. Hsu, T. Kotake, H. Yaguchi, D. Tanaka, M. Jablonski, and S. Y. Set, "5-GHz Pulsed Fiber Fabry-Pérot Laser Mode-Locked Using Carbon Nanotubes," *IEEE Photonics Technol. Lett.* **17**, 750–752 (2005).
46. A. Martinez and S. Yamashita, "10 GHz fundamental mode fiber laser using a graphene saturable absorber," *Appl. Phys. Lett.* **101**, 041118 (2012).
47. A. Klenner, M. Golling, and U. Keller, "Compact gigahertz frequency combs," in *Advanced Solid State Lasers* (Optical Society of America, 2013), p. ATh3A-1.

- 
48. A. Klenner, M. Golling, and U. Keller, "Gigahertz diode-pumped Yb: CALGO laser with 60-fs pulses and an average output power of 3.5 W," in *Conference on Lasers and Electro-Optics* (Optical Society of America, 2014), p. SM4F-6.
  49. A. Klenner and U. Keller, "All-optical Q-switching limiter for high-power gigahertz modelocked diode-pumped solid-state lasers," *Opt. Express* **23**, 8532 (2015).
  50. A. S. Mayer, C. R. Phillips, and U. Keller, "Watt-level 10-gigahertz solid-state laser enabled by self-defocusing nonlinearities in an aperiodically poled crystal," *Nat. Commun.* **8**, 1673 (2017).
  51. P. Wasylczyk, P. Wnuk, and C. Radzewicz, "Passively modelocked, diode-pumped Yb:KYW femtosecond oscillator with 1 GHz repetition rate," *Opt. Express* **17**, 5630-5636 (2009).
  52. T. C. Schratwieser, C. G. Leburn, and D. T. Reid, "Highly efficient 1 GHz repetition-frequency femtosecond Yb<sup>3+</sup>: KY(WO<sub>4</sub>)<sub>2</sub> laser," *Opt. Lett.* **37**, 1133-1135 (2012).
  53. S. Pekarek, C. Fiebig, M. C. Stumpf, A. E. H. Oehler, K. Paschke, G. Erbert, T. Südmeyer, and U. Keller, "Diode-pumped gigahertz femtosecond Yb:KGW laser with a peak power of 3.9 kW," *Opt. Express* **18**, 16320-16326 (2010).
  54. S. Pekarek, T. Südmeyer, S. Lecomte, S. Kundermann, J. M. Dudley, and U. Keller, "Self-referenceable frequency comb from a gigahertz diode-pumped solid-state laser," *Opt. Express* **19**, 16491-16497 (2011).
  55. A. Klenner, M. Golling, and U. Keller, "A gigahertz multimode-diode-pumped Yb:KGW enables a strong frequency comb offset beat signal," *Opt. Express* **21**, 10351 (2013).
  56. S. Pekarek, M. C. Stumpf, S. Lecomte, S. Kundermann, A. Klenner, T. Südmeyer, J. M. Dudley, and U. Keller, "Compact gigahertz

- frequency comb generation: how short do the pulses need to be?," in *Advanced Solid-State Photonics* (Optical Society of America, 2012), p. AT5A-2.
57. S. Yamazoe, M. Katou, T. Adachi, and T. Kasamatsu, "Palm-top-size, 1.5 kW peak-power, and femtosecond (160 fs) diode-pumped mode-locked Yb<sup>+3</sup>:KY(WO<sub>4</sub>)<sub>2</sub> solid-state laser with a semiconductor saturable absorber mirror," *Opt. Lett.* **35**, 748–750 (2010).
  58. M. Endo, A. Ozawa, and Y. Kobayashi, "Kerr-lens mode-locked Yb:KYW laser at 4.6-GHz repetition rate," *Opt. Express* **20**, 12191–12197 (2012).
  59. S. Pekarek, A. Klenner, T. Südmeyer, C. Fiebig, K. Paschke, G. Erbert, and U. Keller, "Femtosecond diode-pumped solid-state laser with a repetition rate of 4.8 GHz," *Opt. Express* **20**, 4248–4253 (2012).
  60. M. Endo, A. Ozawa, and Y. Kobayashi, "6-GHz, Kerr-lens mode-locked Yb:Lu<sub>2</sub>O<sub>3</sub> ceramic laser for comb-resolved broadband spectroscopy," *Opt. Lett.* **38**, 4502–4505 (2013).
  61. M. Endo, I. Ito, and Y. Kobayashi, "Direct 15-GHz mode-spacing optical frequency comb with a Kerr-lens mode-locked Yb:Y<sub>2</sub>O<sub>3</sub> ceramic laser," *Opt. Express* **23**, 1276–1282 (2015).
  62. L. Krainer, R. Paschotta, S. Lecomte, M. Moser, K. J. Weingarten, and U. Keller, "Compact Nd:YVO<sub>4</sub> Lasers With Pulse Repetition Rates up to 160 GHz," *IEEE J. Quantum Electron.* **38**, 1331–1338 (2002).
  63. L. Krainer, R. Paschotta, J. Aus der Au, C. Hönninger, U. Keller, M. Moser, D. Kopf, and K. J. Weingarten, "Passively mode-locked Nd:YVO<sub>4</sub> laser with up to 13 GHz repetition rate," *Appl. Phys. B* **69**, 245–247 (1999).
  64. S. Lecomte, M. Kalisch, L. Krainer, G. J. Spühler, R. Paschotta, M. Golling, D. Ebling, T. Ohgoh, T. Hayakawa, S. Pawlik, B. Schmidt, and U. Keller, "Diode-Pumped Passively Mode-Locked Nd:YVO<sub>4</sub>

- 
- Lasers With 40-GHz Repetition Rate," *IEEE J. Quantum Electron.* **41**, 45–52 (2005).
65. A. E. H. Oehler, M. C. Stumpf, S. Pekarek, T. Südmeyer, K. J. Weingarten, and U. Keller, "Picosecond diode-pumped 1.5  $\mu\text{m}$  Er:Yb:glass lasers operating at 10–100 GHz repetition rate," *Appl. Phys. B* **99**, 53–62 (2010).
  66. G. J. Spühler, P. S. Golding, L. Krainer, I. J. Kilburn, P. A. Crosby, M. Brownell, K. J. Weingarten, R. Paschotta, M. Haiml, R. Grange, and U. Keller, "Multi-wavelength source with 25 GHz channel spacing tunable over C-band," *Electron. Lett.* **39**, 778 (2003).
  67. S. C. Zeller, L. Krainer, G. J. Spühler, K. J. Weingarten, R. Paschotta, and U. Keller, "Passively mode-locked 40-GHz Er:Yb:glass laser," *Appl. Phys. B* **76**, 787–788 (2003).
  68. S. C. Zeller, L. Krainer, G. J. Spühler, R. Paschotta, M. Golling, D. Ebling, K. J. Weingarten, and U. Keller, "Passively modelocked 50 GHz Er:Yb:glass laser," *Electron. Lett.* **40**, 875–877 (2004).
  69. S. C. Zeller, T. Südmeyer, K. J. Weingarten, and U. Keller, "Passively modelocked 77 GHz Er: Yb: glass laser," *Electron. Lett.* **43**, 32–33 (2007).
  70. A. E. Oehler, T. Südmeyer, K. J. Weingarten, and U. Keller, "100 GHz passively mode-locked Er:Yb:glass laser at 1.5  $\mu\text{m}$  with 1.6-ps pulses," *Opt. Express* **16**, 21930–21935 (2008).
  71. D. Li, U. Demirbas, J. R. Birge, G. S. Petrich, L. A. Kolodziejski, A. Sennaroglu, F. X. Kärtner, and J. G. Fujimoto, "Diode-pumped passively mode-locked GHz femtosecond Cr:LiSAF laser with kW peak power," *Opt. Lett.* **35**, 1446–1448 (2010).
  72. K. G. Wilcox, Z. Mihoubi, G. J. Daniell, S. Elsmere, A. Quarterman, I. Farrer, D. A. Ritchie, and A. Tropper, "Ultrafast optical Stark mode-locked semiconductor laser," *Opt. Lett.* **33**, 2797–2799 (2008).

73. K. G. Wilcox, A. H. Quarterman, H. Beere, D. A. Ritchie, and A. C. Tropper, "High Peak Power Femtosecond Pulse Passively Mode-Locked Vertical-External-Cavity Surface-Emitting Laser," *IEEE Photonics Technol. Lett.* **22**, 1021–1023 (2010).
74. A. Garnache, S. Hoogland, A. C. Tropper, I. Sagnes, G. Saint-Girons, and J. S. Roberts, "Sub-500-fs soliton-like pulse in a passively mode-locked broadband surface-emitting laser with 100 mW average power," *Appl. Phys. Lett.* **80**, 3892–3894 (2002).
75. D. Waldburger, M. Mangold, S. M. Link, M. Golling, E. Gini, B. W. Tilma, and U. Keller, "Sub-300-femtosecond Semiconductor Disk Lasers," in *Conference on Lasers and Electro-Optics (Optical Society of America, 2015)*, p. SM3F-2.
76. R. Häring, R. Paschotta, E. Gini, F. Morier-Genoud, D. Martin, H. Melchior, and U. Keller, "Picosecond surface-emitting semiconductor laser with > 200 mW average power," *Electron. Lett.* **37**, 766–767 (2001).
77. Y. F. Chen, Y. C. Lee, H. C. Liang, K. Y. Lin, K. W. Su, and K. F. Huang, "Femtosecond high-power spontaneous mode-locked operation in vertical-external cavity surface-emitting laser with gigahertz oscillation," *Opt. Lett.* **36**, 4581–4583 (2011).
78. M. Hoffmann, O. D. Sieber, W. P. Pallmann, V. J. Wittwer, Y. Barbarin, T. Südmeyer, U. Keller, I. L. Krestnikov, S. S. Mikhlin, A. R. Kovsh, G. Malcolm, and C. Hamilton, "All Quantum-Dot Based Femtosecond VECSEL," in *4th EPS-QEOD Europhoton Conference* (2010).
79. Z. Zhao, S. Bouchoule, J. Song, E. Galopin, J.-C. Harmand, J. Decobert, G. Aubin, and J.-L. Oudar, "Subpicosecond pulse generation from a 1.56  $\mu\text{m}$  mode-locked VECSEL," *Opt. Lett.* **36**, 4377–4379 (2011).

- 
80. M. Hoffmann, Y. Barbarin, D. J. H. C. Maas, M. Golling, I. L. Krestnikov, S. S. Mikhrin, A. R. Kovsh, T. Südmeyer, and U. Keller, "Modelocked quantum dot vertical external cavity surface emitting laser," *Appl. Phys. B* **93**, 733–736 (2008).
  81. C. R. Head, H.-Y. Chan, J. S. Feehan, D. P. Shepherd, S. Alam, A. C. Tropper, J. H. V. Price, and K. G. Wilcox, "Supercontinuum Generation With GHz Repetition Rate Femtosecond-Pulse Fiber-Amplified VECSELS," *IEEE Photonics Technol. Lett.* **25**, 464–467 (2013).
  82. P. Klopp, F. Saas, M. Zorn, M. Weyers, and U. Griebner, "290-fs pulses from a semiconductor disk laser," *Opt. Express* **16**, 5770–5775 (2008).
  83. P. Klopp, U. Griebner, M. Zorn, A. Klehr, A. Liero, M. Weyers, and G. Erbert, "Mode-locked InGaAs-AlGaAs disk laser generating sub-200-fs pulses, pulse picking and amplification by a tapered diode amplifier," *Opt. Express* **17**, 10820–10834 (2009).
  84. A. Ashwanden, D. Lorenser, H. J. Unold, R. Paschotta, E. Gini, and U. Keller, "2.1-W picosecond passively mode-locked external-cavity semiconductor laser," *Opt. Lett.* **30**, 272–274 (2005).
  85. M. Hoffmann, O. D. Sieber, V. J. Wittwer, I. L. Krestnikov, D. A. Livshits, Y. Barbarin, T. Südmeyer, and U. Keller, "Femtosecond high-power quantum dot vertical external cavity surface emitting laser," *Opt. Express* **19**, 8108–8116 (2011).
  86. P. Klopp, U. Griebner, M. Zorn, and M. Weyers, "Pulse repetition rate up to 92 GHz or pulse duration shorter than 110 fs from a mode-locked semiconductor disk laser," *Appl. Phys. Lett.* **98**, 071103 (2011).
  87. M. Hoffmann, O. D. Sieber, V. J. Wittwer, W. P. Pallmann, I. Krestnikov, S. S. Mikhrin, D. A. Livshits, M. Golling, Y. Barbarin, and T. Südmeyer, "Femtosecond VECSELS with up to 1-W Average

- Output Power," in *Conference on Lasers and Electro-Optics* (Optical Society of America, 2011), p. CThG4.
88. R. Häring, M. Paschotta, A. Aschwanden, E. Gini, F. Morier-Genoud, and U. Keller, "High-power Passively Mode-Locked Semiconductor Lasers," *IEEE J. Quantum Electron.* **38**, 1268–1275 (2002).
  89. O. D. Sieber, V. J. Wittwer, M. Mangold, M. Hoffmann, M. Golling, T. Südmeyer, and U. Keller, "Femtosecond VECSEL with tunable multi-gigahertz repetition rate," *Opt. Express* **19**, 23538–23543 (2011).
  90. B. Rudin, V. J. Wittwer, D. J. H. C. Maas, M. Hoffmann, O. D. Sieber, Y. Barbarin, M. Golling, T. Südmeyer, and U. Keller, "High-power MIXSEL: an integrated ultrafast semiconductor laser with 6.4 W average power," *Opt. Express* **18**, 27582–27588 (2010).
  91. A. Aschwanden, D. Lorensen, H. J. Unold, R. Paschotta, E. Gini, and U. Keller, "10 GHz passively mode-locked external-cavity semiconductor laser with 1.4 W average output power," *Appl. Phys. Lett.* **86**, 131102 (2005).
  92. B. Rudin, D. J. Maas, D. Lorensen, A.-R. Bellancourt, H. J. Unold, U. Keller, E. Gini, and D. Ebling, "High-Performance Mode-Locking with up to 50 GHz Repetition Rate from Integrable VECSELs," in *Conference on Lasers and Electro-Optics* (Optical Society of America, 2006), p. CThM2.
  93. M. Mangold, V. J. Wittwer, C. A. Zaugg, S. M. Link, M. Golling, B. W. Tilma, and U. Keller, "Femtosecond pulses from a modelocked integrated external-cavity surface emitting laser (MIXSEL)," *Opt. Express* **21**, 24904–24911 (2013).
  94. C. G. E. Alfieri, D. Waldburger, S. M. Link, E. Gini, M. Golling, G. Eisenstein, and U. Keller, "Optical efficiency and gain dynamics of modelocked semiconductor disk lasers," *Opt. Express* **25**, 6402–6420 (2017).

- 
95. M. Mangold, M. Golling, E. Gini, B. W. Tilma, and U. Keller, "Sub-300-femtosecond operation from a MIXSEL," *Opt. Express* **23**, 22043–22059 (2015).
  96. C. G. E. Alfieri, D. Waldburger, M. Golling, and U. Keller, "High-power Sub-300-Femtosecond Quantum Dot Semiconductor Disk Lasers," *IEEE Photonics Technol. Lett.* 1–1 (2018).
  97. K. G. Wilcox, H. D. Foreman, J. S. Roberts, and A. C. Tropper, "Timing jitter of 897 MHz optical pulse train from actively stabilised passively modelocked surface-emitting semiconductor laser," *Electron. Lett.* **42**, 159–160 (2006).
  98. A. H. Quarterman, K. G. Wilcox, S. P. Elsmere, Z. Mihoubi, and A. C. Tropper, "Active stabilisation and timing jitter characterisation of sub-500 fs pulse passively modelocked VECSEL," *Electron. Lett.* **44**, 1135–1137 (2008).
  99. V. J. Wittwer, C. A. Zaugg, W. P. Pallmann, A. E. H. Oehler, B. Rudin, M. Hoffmann, M. Golling, Y. Barbarin, T. Südmeyer, and U. Keller, "Timing Jitter Characterization of a Free-Running SESAM Mode-locked VECSEL," *IEEE Photonics J.* **3**, 658–664 (2011).
  100. V. J. Wittwer, R. van der Linden, B. W. Tilma, B. Resan, K. J. Weingarten, T. Südmeyer, and U. Keller, "Sub-60-fs Timing Jitter of a SESAM Modelocked VECSEL," *IEEE Photonics J.* **5**, 1400107 (2013).
  101. M. Mangold, S. M. Link, A. Klenner, C. A. Zaugg, M. Golling, B. W. Tilma, and U. Keller, "Amplitude Noise and Timing Jitter Characterization of a High-Power Mode-Locked Integrated External-Cavity Surface Emitting Laser," *IEEE Photonics J.* **6**, 1500309 (2014).
  102. A. Schlatter, B. Rudin, S. C. Zeller, R. Paschotta, G. J. Spühler, L. Krainer, N. Haverkamp, H. R. Telle, and U. Keller, "Nearly quantum-noise-limited timing jitter from miniature Er:Yb:glass lasers," *Opt. Lett.* **30**, 1536–1538 (2005).

103. S. Schilt, N. Bucalovic, V. Dolgovskiy, C. Schori, M. C. Stumpf, G. Di Domenico, S. Pekarek, A. E. H. Oehler, T. Südmeyer, U. Keller, and P. Thomann, "Fully stabilized optical frequency comb with sub-radian CEO phase noise from a SESAM-modelocked 1.5- $\mu\text{m}$  solid-state laser," *Opt. Express* **19**, 24171–24181 (2011).
104. S.-H. Park, J. Kim, H. Jeon, T. Sakong, S.-N. Lee, S. Chae, Y. Park, C.-H. Jeong, G.-Y. Yeom, and Y.-H. Cho, "Room-temperature GaN vertical-cavity surface-emitting laser operation in an extended cavity scheme," *Appl. Phys. Lett.* **83**, 2121–2123 (2003).
105. M. Rahim, M. Arnold, F. Felder, K. Behfar, and H. Zogg, "Midinfrared lead-chalcogenide vertical external cavity surface emitting laser with 5  $\mu\text{m}$  wavelength," *Appl. Phys. Lett.* **91**, 151102 (2007).
106. R. Bek, G. Kersteen, H. Kahle, T. Schwarzbäck, M. Jetter, and P. Michler, "All quantum dot mode-locked semiconductor disk laser emitting at 655 nm," *Appl. Phys. Lett.* **105**, 082107 (2014).
107. A. Härkönen, J. Rautiainen, L. Orsila, M. Guina, K. Rössner, M. Hümmer, T. Lehnhardt, M. Müller, A. Forchel, M. Fischer, J. Koeth, and O. G. Okhotnikov, "2- $\mu\text{m}$  Mode-Locked Semiconductor Disk Laser Synchronously Pumped Using an Amplified Diode Laser," *IEEE Photonics Technol. Lett.* **20**, 1332–1334 (2008).
108. A. L. Schawlow and C. H. Townes, "Infrared and Optical Masers," *Phys. Rev.* **112**, 1940–1949 (1958).
109. D. S. Elliott, R. Roy, and S. J. Smith, "Extracavity laser band-shape and bandwidth modification," *Phys. Rev. A* **26**, 12–18 (1982).
110. G. Di Domenico, S. Schilt, and P. Thomann, "Simple approach to the relation between laser frequency noise and laser line shape," *Appl. Opt.* **49**, 4801–4807 (2010).

- 
111. D. Von der Linde, "Characterization of the Noise in Continuously Operating Mode-Locked Lasers," *Appl. Phys. B* **39**, 201–217 (1986).
  112. Wittwer, Valentin Johannes, "New Frontiers of Ultrafast Semiconductor Disk Lasers: High Power MIXSELS and Low Noise VECSELS," (2012).
  113. R. Ell, U. Morgner, F. X. Kärtner, J. G. Fujimoto, E. P. Ippen, V. Scheuer, G. Angelow, T. Tschudi, M. J. Lederer, A. Boiko, and B. Luther-Davies, "Generation of 5-fs pulses and octave-spanning spectra directly from a Ti: sapphire laser," *Opt. Lett.* **26**, 373–375 (2001).
  114. L. Matos, D. Kleppner, O. Kuzucu, T. R. Schibli, J. Kim, E. P. Ippen, and F. X. Kaertner, "Direct frequency comb generation from an octave-spanning, prismless Ti:sapphire laser," *Opt. Lett.* **29**, 1683–1685 (2004).
  115. P. Brochard, S. Schilt, V. J. Wittwer, and T. Südmeyer, "Characterizing the carrier-envelope offset in an optical frequency comb without traditional  $f$ -to- $2f$  interferometry," *Opt. Lett.* **40**, 5522–5525 (2015).
  116. P. Brochard, N. Jornod, S. Schilt, V. J. Wittwer, S. Hakobyan, D. Waldburger, S. M. Link, C. G. E. Alfieri, M. Golling, L. Devenoges, J. Morel, U. Keller, and T. Südmeyer, "First investigation of the noise and modulation properties of the carrier-envelope offset in a modelocked semiconductor laser," *Opt. Lett.* **41**, 3165–3168 (2016).
  117. J. M. Dudley, G. Genty, and S. Coen, "Supercontinuum generation in photonic crystal fiber," *Rev. Mod. Phys.* **78**, 1135–1184 (2006).
  118. N. Jornod, V. J. Wittwer, C. Kränkel, D. Waldburger, U. Keller, T. Südmeyer, and T. Calmano, "High-power amplification of a femtosecond vertical external-cavity surface-emitting laser in an Yb:YAG waveguide," *Opt. Express* **25**, 16527–16533 (2017).

119. J. M. Dudley and J. R. Taylor, *Supercontinuum Generation in Optical Fibers* (Cambridge University Press, 2010).
120. G. Genty, S. Coen, and J. M. Dudley, "Fiber supercontinuum sources (Invited)," *J. Opt. Soc. Am. B* **24**, 1771–1785 (2007).
121. N. Jornod, K. Gürel, V. J. Wittwer, P. Brochard, S. Hakobyan, S. Schilt, D. Waldburger, U. Keller, and T. Südmeyer, "Carrier-envelope offset frequency stabilization of a gigahertz semiconductor disk laser," *Optica* **4**, 1482–1487 (2017).
122. S. Mirov, V. Fedorov, I. Moskalev, D. Martyshkin, and C. Kim, "Progress in Cr<sup>2+</sup> and Fe<sup>2+</sup> doped mid-IR laser materials," *Laser Photonics Rev.* **4**, 21–41 (2010).
123. F. Capasso, "High-performance midinfrared quantum cascade lasers," *Opt. Eng.* **49**, 111102 (2010).
124. L. Maidment, P. G. Schunemann, and D. T. Reid, "Molecular fingerprint-region spectroscopy from 5 to 12  $\mu\text{m}$  using an orientation-patterned gallium phosphide optical parametric oscillator," *Opt. Lett.* **41**, 4261–4264 (2016).
125. K. Balskus, S. Schilt, V. J. Wittwer, P. Brochard, T. Ploetzing, N. Jornod, R. A. McCracken, Z. Zhang, A. Bartels, D. T. Reid, and T. Südmeyer, "Frequency comb metrology with an optical parametric oscillator," *Opt. Express* **24**, 8370–8381 (2016).
126. R. W. Boyd, *Nonlinear Optics*, 3rd ed (Academic Press, 2008).
127. P. E. Powers, *Fundamentals of Nonlinear Optics* (CRC Press, 2011).
128. W. Sellmeier, "Zur Erklärung der abnormen Farbenfolge im Spectrum einiger Substanzen," *Ann. Phys. Chem.* **219**, 272–282 (1871).
129. D. H. Jundt, "Temperature-dependent Sellmeier equation for the index of refraction,  $n_e$ , in congruent lithium niobate," *Opt. Lett.* **22**, 1553–1555 (1997).

- 
130. J. A. Giordmaine and R. C. Miller, "Tunable Coherent Parametric Oscillation in LiNbO<sub>3</sub> at Optical Frequencies," *Phys. Rev. Lett.* **14**, 973–976 (1965).
  131. M. Yamada, N. Nada, M. Saitoh, and K. Watanabe, "First-order quasi-phase matched LiNbO<sub>3</sub> waveguide periodically poled by applying an external field for efficient blue second-harmonic generation," *Appl. Phys. Lett.* **62**, 435–436 (1993).
  132. G. D. Boyd and D. A. Kleinman, "Parametric Interaction of Focused Gaussian Light Beams," *J. Appl. Phys.* **39**, 3597–3639 (1968).
  133. R. A. McCracken, K. Balskus, Z. Zhang, and D. T. Reid, "Observations of complex frequency comb structure in a harmonically-pumped femtosecond optical parametric oscillator," *J. Phys. Conf. Ser.* **594**, 012004 (2015).
  134. N. Hempler, B. Bialkowski, C. J. Hamilton, G. T. Maker, and G. P. A. Malcolm, "Development and commercialization of mode-locked VECSELs," *Proc. SPIE* **9349**, 93490K (2015).
  135. N. Jornod, V. J. Wittwer, M. Gaponenko, M. Hoffmann, N. Hempler, G. P. A. Malcolm, G. T. Maker, and T. Südmeyer, "Ultrafast optical parametric oscillator pumped by a vertical external-cavity surface-emitting laser (VECSEL)," *Opt. Express* **25**, 28983–28989 (2017).
  136. P. Brochard, V. J. Wittwer, S. Bilicki, B. Resan, K. J. Weingarten, S. Schilt, and T. Südmeyer, "Frequency Noise Characterization of a 25-GHz Diode-Pumped Mode-Locked Laser With Indirect Carrier-Envelope Offset Noise Assessment," *IEEE Photonics J.* **10**, 3200110 (2018).
  137. A. R. Johnson, A. S. Mayer, A. Klenner, K. Luke, E. S. Lamb, M. R. E. Lamont, C. Joshi, Y. Okawachi, F. W. Wise, M. Lipson, U. Keller, and A. L. Gaeta, "Octave-spanning coherent supercontinuum generation in a silicon nitride waveguide," *Opt. Lett.* **40**, 5117–5120 (2015).

138. A. Klenner, A. S. Mayer, A. R. Johnson, K. Luke, M. R. E. Lamont, Y. Okawachi, M. Lipson, A. L. Gaeta, and U. Keller, "Gigahertz frequency comb offset stabilization based on supercontinuum generation in silicon nitride waveguides," *Opt. Express* **24**, 11043–11053 (2016).
139. D. Waldburger, A. S. Mayer, C. G. Alfieri, A. R. Johnson, X. Ji, A. Klenner, Y. Okawachi, M. Lipson, A. L. Gaeta, and U. Keller, "Self-referenced CEO Frequency Detection of a Semiconductor Disk Laser using a Silicon Nitride Waveguide," in *Advanced Solid State Lasers* (Optical Society of America, 2017), p. ATu6A-3.
140. D. Waldburger, A. S. Mayer, C. G. E. Alfieri, A. R. Johnson, X. Ji, A. Klenner, Y. Okawachi, M. Lipson, A. L. Gaeta, and U. Keller, "Octave-spanning supercontinuum generated in silicon nitride waveguide directly from a SESAM-modelocked VECSEL," in *SPIE Photonics West* (2018), pp. 10515–17.
141. F. Adler, P. Maślowski, A. Foltynowicz, K. C. Cossel, T. C. Briles, I. Hartl, and J. Ye, "Mid-infrared Fourier transform spectroscopy with a broadband frequency comb," *Opt. Express* **18**, 21861–21872 (2010).
142. O. Kara, L. Maidment, T. Gardiner, P. G. Schunemann, and D. T. Reid, "Dual-comb spectroscopy in the spectral fingerprint region using OPGaP optical parametric oscillators," *Opt. Express* **25**, 32713–32721 (2017).

# Curriculum Vitae

Name Nayara Jornod  
Date of Birth January 24, 1989 (Neuchâtel, Switzerland)  
Nationality Swiss

## Education

- 2014-2018 Doctoral studies, University of Neuchâtel, Switzerland.
- 2012-2014 Mathematics studies, University of Bern, Switzerland.
- 2010-2012 Master of Science in Physics with special qualification in Theoretical Physics, University of Bern, Switzerland.
- 2007-2010 Bachelor of Science in Physics, University of Bern, Switzerland.

## Research Experience

- 2014-2018 Doctoral studies at the Laboratoire Temps-Fréquence in the group of Prof. Thomas Südmeyer, University of Neuchâtel, Switzerland. *Semiconductor Disk Laser-Based Frequency Combs.*
- 2012 Master thesis under the supervision of Prof. Matthias Blau, University of Bern, Switzerland. *Comparison of Hawking radiation for different observers.*
- 2010 Bachelor thesis under the supervision of Prof. Jean-Pierre Derendinger, University of Bern, Switzerland. *Helium Abundance in the Universe.*



# Remerciements

J'aimerais exprimer ma gratitude à toutes les personnes qui ont été présentes, m'ont apporté leur support et soutien durant ces années de doctorat et ont participé à les rendre productives et amusantes.

Je remercie en premier lieu Thomas pour m'avoir donné la possibilité de faire mes études de doctorat dans son groupe. Sa passion, ses idées ainsi que la grande confiance et liberté qu'il nous a données ont contribué à créer un environnement de travail agréable et efficace.

Ce travail n'aurait pas été possible sans le support et la supervision de Valentin, toujours présent en cas de pépin. Son approche très technique et ses connaissances pointues dans tous les domaines ont été un précieux guide lors du travail de laboratoire et de rédaction.

Au même titre, un grand merci à Stéphane pour l'important partage de connaissances scientifiques. Sa patience dans les investigations pour « trouver l'erreur dans le setup » et les nombreuses relectures assidues des articles et de ce travail.

Je tiens également à remercier le Prof. Majid Ebrahim-Zadeh et le Dr. Keith Wilcox pour avoir accepté d'être membres externes du jury, pour avoir accordé leur temps précieux à l'évaluation de ce manuscrit et s'être déplacés jusqu'à Neuchâtel pour ma défense.

Le travail en laboratoire ne serait pas possible sans l'aide et l'expertise des techniciens et ingénieurs du LTF et du service technique de

---

l'université : Daniel, Christian, Dominique, Thierry, Patrick, Marc, Isidro et André.

Le groupe ne marcherait pas droit bien longtemps sans l'aide administrative. Un grand merci à Sandrine, Joelle, Patricia et Séverine pour leur aide précieuse pour tous les petits détails de dernière minute et des pensées émues à Natacha et ces belles années partagées.

Ces années n'auraient pas eu la même saveur et le même dynamisme sans l'ambiance agréable entretenue par de nombreuses personnes : Kutan, the splice-master, ses partages musicaux et culinaires; Pierre, son aide calme et efficace et sa connaissance parfaite de tous les composants RF du labo ; Martin, ses conseils avisés pour construire mon premier laser ; Loïc, son partage indéfectible de pain et son optimisme contagieux ; Sargis « I go to the gym, man » ; Clément « Là-bas, au laboratoire... » ; Norbert « Le saviez-vous ? » ; Maxim « Let's have an urgent meeting in five minutes » ; François « Tu me dois une chocolatine », Nil, William, Matthieu, Bertrand, Christoph et tous les autres membres du LTF.